

Unsaturated flow through permeable pavements: An experimental study

Hein Van Vuuren

U29221898

Submitted in partial requirement for the degree

M.Sc. Engineering and Environmental Geology

Geology Department, Faculty of Natural and Agricultural Sciences, University of Pretoria

Submitted 31 October 2019

DECLARATION OF ORIGINALITY / DECLARATION ON PLAGIARISM

The **Department of Geology (University of Pretoria)** places great emphasis upon integrity and ethical conduct in the preparation of all written work submitted for academic evaluation. While academic staff teaches you about referencing techniques and how to avoid plagiarism, you too have a responsibility in this regard. If you are at any stage uncertain as to what is required, you should speak to your lecturer before any written work is submitted.

You are guilty of plagiarism if you copy something from another author's work (e.g. a book, an article or a website) without acknowledging the source and pass it off as your own. In effect you are stealing something that belongs to someone else. This is not only the case when you copy work word-for-word (verbatim), but also when you submit someone else's work in a slightly altered form (paraphrase) or use a line of argument without acknowledging it. You are not allowed to use work previously produced by another student. You are also not allowed to let anybody copy your work with the intention of passing it off as his/her work.

Students who commit plagiarism will not be given any credit for plagiarised work. The matter may also be referred to the Disciplinary Committee (Students) for a ruling. Plagiarism is regarded as a serious contravention of the University's rules and can lead to expulsion from the University.

The declaration which follows must accompany all written work submitted while you are a student of the **Department of Geology (University of Pretoria)**. No written work will be accepted unless the declaration has been completed and attached.

I, the undersigned, declare that:

1. I understand what plagiarism is and am aware of the University's policy in this regard.
2. I declare that this assignment (e.g. essay, report, project, assignment, dissertation, thesis, etc) is my own original work. Where other people's work has been used (either from a printed source, Internet or any other source), this has been properly acknowledged and referenced in accordance with Departmental requirements.
3. I have not used work previously produced by another student or any other person to hand in as my own.
4. I have not allowed, and will not allow, anyone to copy my work with the intention of passing it off as his or her own work.

Full names of student: Johan Heinrich van Vuuren

Student number: 29221898

Date submitted: 30 October 2019

Topic of work: Unsaturated flow through permeable pavements: An experimental study

Signature: JH

Supervisor: M.A. Dippenaar

Acknowledgements:

D. Wertheim Aymes – C.E.O., Bosun Brick (Pty) Ltd. Midrand
R. van Biljon – Technical Specifier, Bosun Brick (Pty) Ltd. Midrand
H. Jonker – Technical Manager, Bosun Brick (Pty) Ltd. Midrand
Prof. L. van Rooy – H.O.D., Dept. Geology, University of Pretoria
Dr. M.A. Dippenaar – Senior Lecturer, Dept. Geology, University of Pretoria
Dr. R. Diamond – Senior Lecturer, Dept. Geology, University of Pretoria
Wietsche Jacobs – Pr. Eng. JT Evolve (Pty) Ltd. Kempton Park
O. B. Barker – Managing Member, Banzi Geotechnics cc.
P. J. van Vuuren
R. E. van Vuuren
N. I. van Vuuren
J. Lyle
&
R. A. Ludick – my loving partner, without whom, this would not be possible.

ABSTRACT

Permeable Interlocking Concrete Pavements (PICP) have seen increased popularity in the principles of Water Sensitive Urban Design and Sustainable Drainage Systems in recent years. To address certain design queries that still existed in industry, a two-year experimental study was conducted. It entailed the construction of an Infiltration Table Apparatus and subjecting a representative volume of PICP to hydraulic testing within it. The study aimed at determining the controls of the flow of water into and through these pavements, the effect of variations in construction materials and incline on them, the validity of the hydraulic testing methods currently being applied to them in industry and lastly, to inform on their infiltration rates. A host of permeability data for PICP was gained and it was found that both the choice of materials and the incline on which PICP are constructed, can change their hydraulic properties drastically. In general, the selection of lower permeability materials in the surface portion of the layer works decreased the overall permeability of the pavement, while increases in inclines did the same. In addition, it was found that field investigation techniques require revision and further innovation before they can be effectively applied to PICP.

Keywords: Permeable pavements, permeability, hydraulic conductivity, stormwater runoff.

TABLE OF CONTENTS

Abstract.....	4
List of Figures	7
List of Tables.....	11
1 Introduction.....	14
1.1 Rationale.....	14
1.2 Aims and Objectives	17
2 Anatomy of Pavements	18
2.1 Conventional Pavements	18
2.1.1 LBP Structure.....	19
2.1.2 LBP Materials and Standards.....	21
2.1.3 NLBP Structure.....	25
2.1.4 NLBP Materials and Standards.....	27
2.2 Permeable Interlocking Concrete Pavements	28
2.2.1 PICP Structure	28
2.2.2 Unsaturated Flow in Urban Developments.....	33
2.2.3 Current PICP Evaluation and Performance	35
3 Apparatus	41
3.1 Field Testing.....	41
3.2 Basic Model.....	43
3.3 Full-Scale Model.....	45
3.3.1 Model Water Cycle.....	47
3.4 Additional Apparatus.....	49
4 Materials and Methods	50
4.1 Field Testing.....	50
4.2 Basic Model.....	51
4.2.1 Preliminary Testing	53
4.2.2 Sub-surface Testing.....	53
4.2.3 Surface Testing.....	54
4.3 Full-scale Model	56
4.3.1 Model Design	56
4.3.2 Model Design: Influx	59

4.3.3	Model Design: Layer Works.....	59
4.3.4	Model Design: Bricks	61
4.3.5	Model Design: Bedding and Jointing Sand	62
4.3.6	Model Design: Incline	68
4.3.7	Model Testing Procedure	68
4.3.8	Additional Model Testing.....	69
5	Results and Discussion	70
5.1	Field Testing.....	70
5.2	Basic Model.....	72
5.2.1	Preliminary Testing	72
5.2.2	Sub-surface Testing.....	73
5.2.3	Surface Testing.....	74
5.2.4	Additional Observations	76
5.3	Full-scale Model	78
5.3.1	Model Design	78
5.3.2	The Effect of Surface Materials.....	83
5.3.3	The Effect of Incline	86
5.3.4	Additional Observations	90
6	Conclusion.....	94
6.1	Key Findings	94
6.2	Limitations and Assumptions.....	95
6.3	Way Forward.....	96
	References	97
	Appendix A	101
	Technical and design drawings of the Basic Model Apparatus (BMA) and Infiltration Table Apparatus (ITA)	101
	Appendix B	113
	Additional photography of the Infiltration Table Apparatus (ITA).....	113
	Appendix C.....	118
	Geotechnical logs of the test pits at the Brooks Street Site.....	118
	Appendix D.....	121
	Absorption data of interlocking concrete brick products.....	121
	Appendix E	127

Data obtained from the Basic Model	127
Appendix F	129
Data obtained from Model Design testing on the Generic Layer Works.....	129
Appendix G.....	132
Data obtained from the Full-scale Model.....	132

LIST OF FIGURES

Fig. 1: An example of erosional damage to a retaining wall (a), damage to an interlocking pavement due to poor drainage (b) and two stormwater drains clogged by silts and organic matter (c) and (d) in Gauteng province respectively.....	15
Fig. 2: The general structure of a sealed pavement (TRH14, 1980).....	19
Fig. 3: A typical Interlocking Concrete Pavement layer works (Bosun – Midrand, 2018)	25
Fig. 4: An example of different concrete brick laying patterns for a simple interlocking concrete brick (Cairns, N.D.)	26
Fig. 5: A typical PICP layer works. (Adapted from Technicrete, 2017).....	30
Fig. 6: (a) Dispersion plume formation on a capillary boundary between soil and rock when wetting first occurs, (b) Breaching of the capillary boundary with variably saturated flow, (c) Invasion of a drying plume when the water supply was depleted and (d) Invasion of a rewetting plume with merging rivulets in the rock. (Brouwers and Dippenaar, 2018).....	34
Fig. 7: A Double-ring Infiltrometer Test modified for use on ICP. (Beeldens and Herrier, 2006) 38	
Fig. 8: The Double-Ring Infiltrometer constructed for field tests conducted on the Brooks St. site.....	42
Fig. 9: The custom Single Ring Infiltrometer constructed for field tests of already installed PICP.	43
Fig. 10: The apparatus constructed to perform tests on the representative volume for the basic flow model.	44
Fig. 11: A schematic diagram of the Infiltration Table Apparatus.	46
Fig. 12: An image of the Infiltration Table Apparatus in the quality control laboratories at Bosun Brick Midrand. (2018)	46
Fig. 13: The 1000 ℓ water tank that provided water to the ITA for testing (Bosun – Midrand, 2018).....	47
Fig. 14: The outlet system of the Infiltration Table Apparatus (Bosun – Midrand, 2019).....	48
Fig. 15: The joint-focused Double Ring Infiltrometer constructed for use within the ITA.	49
Fig. 16: (a) The selected brick paving unit, Product 55: Bevelled and (b) the selected arrangement of bricks for the surface layer. (Supplied by MVA Bricks Pta. West).....	52
Fig. 17: A step-by-step illustration of the testing procedure used for the sub-surface layers of a concrete brick paving system.....	54
Fig. 18: A step-by-step illustration of the testing procedure used for the surface and sub-surface layers of a concrete brick paving system.	55
Fig. 19: A schematic diagram of the concrete brick orientations used in the surface of the Generic Layer Works during the Model Design Testing	58

Fig. 20: Typical rainfall design parameters for the Pretoria area, South Africa – Courtesy of PVA Consulting Engineers cc.	59
Fig. 21: A cross-section of the layer works used inside the Infiltration table apparatus for the study.....	60
Fig. 22: Two of the permeable paving products available from Bosun.	61
Fig. 23: The two packing methods selected for use in the Infiltration Table Apparatus.	62
Fig. 24: The basic profile of what was termed a P-Type 1 sand for the purposes of this study..	63
Fig. 25: The basic profile of what was termed a P-Type 2 sand for the purposes of this study..	64
Fig. 26: The basic profile of what was termed a P-Type 3 sand for the purposes of this study..	65
Fig. 27: The basic profile of what was termed a P-Type 4 sand for the purposes of this study..	66
Fig. 28: The basic profile of what was termed a P-Type 5 sand for the purposes of this study..	67
Fig. 29: A column graph showing the comparison of water volume percentages captured at each point for tests using a sub-surface layer works only, at various inclines.	74
Fig. 30: A column graph showing the comparison of water volume percentages captured at each point for tests using a surface and sub-surface layer, at various inclines.	75
Fig. 31: A comparison of the color of water captured from different exit points at (a) an incline of 0° and (b) an incline of 6°.	77
Fig. 32: A column graph showing the comparison of water volume changes at each point for model design tests using different layers of the GLW.	79
Fig. 33: A column graph showing discharges at different exit points of the Infiltration Table Apparatus as incline increased.	81
Fig. 34: A graph of the short interval discharges at different points of Full-scale Model with a Waterwise and P-Type 1 combination layer works.....	82
Fig. 35: A column graph comparing the percentages of the influx volume exiting each point for different surface material combinations in the Full-Scale Model at a 2.5° incline.	85
Fig. 36: A column graph showing the maximum mean discharge per linear meter of pavement for waterwise containing surface material combination layer works in the Full-scale Model at different inclines.....	87
Fig. 37: A column graph showing the maximum mean discharge per linear meter of pavement for waterwise containing surface material combination layer works in the Full-scale Model at different inclines.....	88
Fig. 38: A schematic diagram of the observed unsaturated flow velocity components in Permeable Interlocking Concrete Pavements at different inclines.	89
Fig. 39: Tendrils formed in the sub-base layers for Full-scale Model testing of a layer works containing a Citylock® and P-Type 3 sand surface combination at an incline of 2.5°	91
Fig. 40: A schematic representation of the flow mechanisms observed during testing of the Full-scale Model.	91
Fig. 41: The erosion of jointing material beneath the sealant of the inner ring of the double-ring infiltrometer constructed for this study	92
Fig. 42: A schematic diagram of the reason for the failure of ring infiltrometer tests in Permeable Interlocking Concrete Pavements.....	93
Fig. A-1: The top view of the Basic Model Apparatus design drawing.....	102
Fig. A-2: A section of the side view of the Basic Model Apparatus design drawing.	103

Fig. A-3: The side view of the Infiltration Table Apparatus design drawing. (Bosun Midrand, 2017)	104
Fig. A-4: The top view of the Infiltration Table Apparatus design drawing. (Bosun Midrand, 2017)	105
Fig. A-5: The front view of the Infiltration Table Apparatus design drawing. (Bosun Midrand, 2017)	106
Fig. A-6: The design drawing of the construction surface (deck) of the Infiltration Table Apparatus. (Bosun Midrand, 2017).....	107
Fig. A-7: The design drawing of the ITA reservoir (Inlet Boxes). (Bosun Midrand, 2017).....	108
Fig. A-8: The design drawing of the collection bins (catch tray(s)) of the Infiltration Table Apparatus. (Bosun Midrand, 2017).....	109
Fig. A-9: The design drawing of the supports under the construction surface of the Infiltration Table Apparatus. (Bosun Midrand, 2017)	110
Fig. A-10: The design drawing of additional components that retained the glass sides of the Infiltration Table Apparatus. (Bosun Midrand, 2017)	111
Fig. A-11: The design drawing of additional components that allowed for the tilting of the Infiltration Table Apparatus. (Bosun Midrand, 2017)	112
Fig. B-1: An image of the Infiltration Table Apparatus showing the guide rods welded to the construction surface (deck).	114
Fig. B-2: An image of the bibum being cut to size for use in the Full-scale Model Testing.	114
Fig. B-3: An image of the way the Waterwise® concrete bricks were laid during construction of the Full-scale Model layer works.	115
Fig. B-4: An image of P-Type 1 jointing material being added to a Waterwise®-containing layer works in the Model Design Testing.....	115
Fig. B-5: An image showing the completed construction of a Citylock® and P-Type 1 sand containing layer works in the Full-scale Model shortly before testing.....	116
Fig. B-6: An image showing the side view of a completed construction of a Citylock® and P-Type 1 sand containing layer works in the Full-scale Model shortly before testing. Here, the filter media can be seen in the collection bins below the ITA and the block and tackle used to change the incline above.	116
Fig. B-7: An image showing the testing of a Waterwise® and P-Type 5 sand containing layer works during the Model Design testing. Here, the wetting front can be seen traversing the full length of the pavement.....	117
Fig. D-1: Absorption test results for MVA bricks product 50 with black colouring. (MVA Bricks, 2016)	122
Fig. D-2: Absorption test results for MVA bricks product 50 with red colouring. (MVA Bricks, 2016)	123
Fig. D-3: Absorption test results for MVA bricks product 50 with clay (terracotta) colouring. (MVA Bricks, 2016)	124
Fig. D-4: Absorption test results for MVA bricks product 50 with clay (terracotta) colouring. (MVA Bricks, 2016)	125

Fig. D-5: Absorption test results for MVA bricks product 50 with plum colouring. (MVA Bricks, 2016) 126

Fig. G-1: A graph of discharge per unit time for the Full-scale Model with a Waterwise and P-Type 1 surface combination layer works at 0° incline. 133

Fig. G-2: A graph of discharge per unit time for the Full-scale Model with a Waterwise and P-Type 1 surface combination layer works at 2.5° incline. 134

Fig. G-3: A graph of discharge per unit time for the Full-scale Model with a Waterwise and P-Type 1 surface combination layer works at 5° incline. 135

Fig. G-4: A graph of discharge per unit time for the Full-scale Model with a Waterwise and P-Type 2 surface combination layer works at 0° incline. 136

Fig. G-5: A graph of discharge per unit time for the Full-scale Model with a Waterwise and P-Type 2 surface combination layer works at 2.5° incline. 137

Fig. G-6: A graph of discharge per unit time for the Full-scale Model with a Waterwise and P-Type 2 surface combination layer works at 5° incline. 138

Fig. G-7: A graph of discharge per unit time for the Full-scale Model with a Waterwise and P-Type 3 surface combination layer works at 0° incline. 139

Fig. G-8: A graph of discharge per unit time for the Full-scale Model with a Waterwise and P-Type 3 surface combination layer works at 2.5° incline. 140

Fig. G-9: A graph of discharge per unit time for the Full-scale Model with a Waterwise and P-Type 3 surface combination layer works at 5° incline. 141

Fig. G-10: A graph of discharge per unit time for the Full-scale Model with a Waterwise and P-Type 4 surface combination layer works at 0° incline. 142

Fig. G-11: A graph of discharge per unit time for the Full-scale Model with a Waterwise and P-Type 4 surface combination layer works at 2.5° incline. 143

Fig. G-12: A graph of discharge per unit time for the Full-scale Model with a Waterwise and P-Type 4 surface combination layer works at 5° incline. 144

Fig. G-13: A graph of discharge per unit time for the Full-scale Model with a Waterwise and P-Type 5 surface combination layer works at 0° incline. 145

Fig. G-14: A graph of discharge per unit time for the Full-scale Model with a Waterwise and P-Type 5 surface combination layer works at 2.5° incline. 146

Fig. G-15: A graph of discharge per unit time for the Full-scale Model with a Waterwise and P-Type 5 surface combination layer works at 5° incline. 147

Fig. G-16: A graph of discharge per unit time for the Full-scale Model with a Citylock and P-Type 1 surface combination layer works at 0° incline. 148

Fig. G-17: A graph of discharge per unit time for the Full-scale Model with a Citylock and P-Type 1 surface combination layer works at 2.5° incline. 149

Fig. G-18: A graph of discharge per unit time for the Full-scale Model with a Citylock and P-Type 1 surface combination layer works at 5° incline. 150

Fig. G-19: A graph of discharge per unit time for the Full-scale Model with a Citylock and P-Type 2 surface combination layer works at 0° incline. 151

Fig. G-20: A graph of discharge per unit time for the Full-scale Model with a Citylock and P-Type 2 surface combination layer works at 2.5° incline. 152

Fig. G-21: A graph of discharge per unit time for the Full-scale Model with a Citylock and P-Type 2 surface combination layer works at 5° incline 153

Fig. G-22: A graph of discharge per unit time for the Full-scale Model with a Citylock and P-Type 3 surface combination layer works at 0° incline	154
Fig. G-23: A graph of discharge per unit time for the Full-scale Model with a Citylock and P-Type 3 surface combination layer works at 2.5° incline	155
Fig. G-24: A graph of discharge per unit time for the Full-scale Model with a Citylock and P-Type 3 surface combination layer works at 5° incline	156
Fig. G-25: A graph of discharge per unit time for the Full-scale Model with a Citylock and P-Type 5 surface combination layer works at 0° incline	157
Fig. G-26: A graph of discharge per unit time for the Full-scale Model with a Citylock and P-Type 5 surface combination layer works at 2.5° incline.	158
Fig. G-27: A graph of discharge per unit time for the Full-scale Model with a Citylock and P-Type 5 surface combination layer works at 5° incline.	159
Fig. G-28: A column graph of volume percentages exiting the Full-scale Model with a Waterwise and P-Type 1 surface combination layer works, at various points and various inclines.	160
Fig. G-29: A column graph of volume percentages exiting the Full-scale Model with a Waterwise and P-Type 2 surface combination layer works, at various points and various inclines.	160
Fig. G-30: A column graph of volume percentages exiting the Full-scale Model with a Waterwise and P-Type 3 surface combination layer works, at various points and various inclines.	161
Fig. G-31: A column graph of volume percentages exiting the Full-scale Model with a Waterwise and P-Type 4 surface combination layer works, at various points and various inclines.	161
Fig. G-32: A column graph of volume percentages exiting the Full-scale Model with a Waterwise and P-Type 5 surface combination layer works, at various points and various inclines.	162
Fig. G-33: A column graph of volume percentages exiting the Full-scale Model with a Citylock and P-Type 1 surface combination layer works, at various points and various inclines.	162
Fig. G-34: A column graph of volume percentages exiting the Full-scale Model with a Citylock and P-Type 2 surface combination layer works, at various points and various inclines.	163
Fig. G-35: A column graph of volume percentages exiting the Full-scale Model with a Citylock and P-Type 3 surface combination layer works, at various points and various inclines.	163
Fig. G-36: A column graph of volume percentages exiting the Full-scale Model with a Citylock and P-Type 5 surface combination layer works, at various points and various inclines.	164

LIST OF TABLES

Table 1: Pavement layer material selection classification codes. (TRH 14, 1980)	22
Table 2: Pavement layer material specifications for material classification codes. (TRH 14, 1980)	22
Table 3: Common South African rock types and their appropriate LBP layer applications. Adapted from SAPEM, (2013) (Weinert, 1980)	24
Table 4: Permeability (K) value guidelines for different soils (Powers, 1992).....	37
Table 5: Typical Permeability and associated CBR values for different soils. Adapted from Woods-Ballard et al., (2007) (Interpave, 2005)	37
Table 6: A comparison of construction material and permeability data obtained in different studies.....	40
Table 7: Infiltrometer results for HA01.....	70

Table 8: Infiltrometer results for HA02.....	71
Table 9: The times taken for 5ℓ of water to migrate through the Basic Model.	72
Table 10: Average percentages of water volumes captured at each exit point for the elementary volume representing a sub-surface layer works only.	73
Table 11: Average percentages of water volumes captured at each exit point for an elementary volume consisting of a surface and sub-surface layer works.....	75
Table 12: Short interval test results for a Waterwise® and P-Type 1 combination layer works of the Full-scale Model.....	82
Table 13: Maximum discharge and permeability values per linear meter of pavement for different surface material combinations at 2.5° incline	84
Table 14: A data comparison of Full-scale Model layer works with surface combinations containing Waterwise® bricks at different inclines.....	86
Table 15: A data comparison of Full-scale Model layer works with surface combinations containing Citylock® bricks at different inclines	87
Table 16: Model Design testing volumes and discharges for different layers of the Generic Layer Works at 2.5°	130
Table 17: Model design testing volumes and discharges of the full Generic Layer Works at different inclines.....	131
Table C-1: The geotechnical log of test pit HA01	119
Table C-2: The geotechnical log of test pit HA02.....	120
Table E-1: Volumes of water exiting the Basic Model representing a sub-surface layer works only.....	128
Table E-2: Volumes of water exiting the full Basic Model layer works.....	128
Table G-1: Full-scale Model test data for a Waterwise® and P-Type 1 combination layer works at 0° incline.....	133
Table G-2: Full-scale Model test data for a Waterwise® and P-Type 1 combination layer works at 2.5° incline	134
Table G-3: Full-scale Model test data for a Waterwise® and P-Type 1 combination layer works at 5° incline.....	135
Table G-4: Full-scale Model test data for a Waterwise® and P-Type 2 combination layer works at 0° incline.....	136
Table G-5: Full-scale Model test data for a Waterwise® and P-Type 2 combination layer works at 2.5° incline	137
Table G-6: Full-scale Model test data for a Waterwise® and P-Type 2 combination layer works at 5° incline.....	138
Table G-7: Full-scale Model test data for a Waterwise® and P-Type 3 combination layer works at 0° incline.....	139
Table G-8: Full-scale Model test data for a Waterwise® and P-Type 3 combination layer works at 2.5° incline	140
Table G-9: Full-scale Model test data for a Waterwise® and P-Type 3 combination layer works at 5° incline.....	141

Table G-10: Full-scale Model test data for a Waterwise® and P-Type 4 combination layer works at 0° incline.....	142
Table G-11: Full-scale Model test data for a Waterwise® and P-Type 4 combination layer works at 2.5° incline	143
Table G-12: Full-scale Model test data for a Waterwise® and P-Type 4 combination layer works at 5° incline.....	144
Table G-13: Full-scale Model test data for a Waterwise® and P-Type 5 combination layer works at 0° incline.....	145
Table G-14: Full-scale Model test data for a Waterwise® and P-Type 5 combination layer works at 2.5° incline	146
Table G-15: Full-scale Model test data for a Waterwise® and P-Type 5 combination layer works at 5° incline.....	147
Table G-16: Full-scale Model test data for a Citylock® and P-Type 1 combination layer works at 0° incline	148
Table G-17: Full-scale Model test data for a Citylock® and P-Type 1 combination layer works at 2.5° incline.....	149
Table G-18: Full-scale Model test data for a Citylock® and P-Type 1 combination layer works at 5° incline	150
Table G-19: Full-scale Model test data for a Citylock® and P-Type 2 combination layer works at 0° incline	151
Table G-20: Full-scale Model test data for a Citylock® and P-Type 2 combination layer works at 2.5° incline.....	152
Table G-21: Full-scale Model test data for a Citylock® and P-Type 2 combination layer works at 2.5° incline.....	153
Table G-22: Full-scale Model test data for a Citylock® and P-Type 3 combination layer works at 0° incline	154
Table G-23: Full-scale Model test data for a Citylock® and P-Type 3 combination layer works at 2.5° incline.....	155
Table G-24: Full-scale Model test data for a Citylock® and P-Type 3 combination layer works at 5° incline	156
Table G-25: Full-scale Model test data for a Citylock® and P-Type 5 combination layer works at 0° incline	157
Table G-26: Full-scale Model test data for a Citylock® and P-Type 5 combination layer works at 2.5° incline.....	158
Table G-27: Full-scale Model test data for a Citylock® and P-Type 5 combination layer works at 5° incline	159

1 INTRODUCTION

1.1 RATIONALE

Interlocking concrete brick pavements (ICP) are fast becoming commonplace in today's urban environments due to their convenience, rapid construction time, load bearing capability and cost effectiveness. Common applications include interior and exterior parking, driveways, walkways, traffic barriers and several other engineering and civil applications. The civil industry however, is still faced with several geotechnical issues that accompany the use of pavements, primarily the gradual reduction of infiltration into the natural surface through continuous urban development which effectively "seals" the land on which it takes place. In addition, the industry is also faced with design issues such as stormwater management, due to modern legislative reform which dictate that stormwater be dealt with on site (Woods-Ballard et al., 2007), water conservation and groundwater pollution.

The issue of stormwater management centers around the reduction of peak flow. When peak flow is inadequately catered for, it can lead to ponding, downslope flooding, damage to drainage systems and severe erosional damage of the land surface (Fig. 1). It can be especially destructive to buildings and infrastructure and in some cases, can even prove fatal. An example can be seen in a study by Salberg (1997) who showed that there was a link between the number of motorist fatalities in Gauteng from 1995 to 1997 and improper stormwater drainage on roads. The improper drainage lead to a buildup of water on the road surface resulting in vehicles hydroplaning, colliding and in numerous deaths across the province. This was due to the breaking coefficient of a vehicle significantly decreasing when excess water on a road is present (Salberg, 1997).

The issue of water conservation and groundwater pollution is a complex one but centers around the attenuation and storage of water for irrigation or periods of drought as well as ensuring the safe recharge of natural groundwater reserves. An example of this can be seen in Cape Town where the city implemented Phase 1 of its Critical Water Shortages Disaster Plan in October 2017 and continued it throughout 2018 due to widespread drought in the Western Cape province (Bosman, 2017). Another example can be seen in the city of Sydney which implemented similar restrictions in May 2019 following a drought, where water reserves reached the lowest levels since 1940 (Pavey, 2019).



Fig. 1: An example of erosional damage to a retaining wall (a), damage to an interlocking pavement due to poor drainage (b) and two stormwater drains clogged by silts and organic matter (c) and (d) in Gauteng province respectively.

To combat these issues, a growing civil and geotechnical industry movement has begun toward designing and implementing greener alternatives for major processes and products, known as water sensitive urban design (WSUD) or sustainable drainage systems (SuDS). It focuses on decreasing the human-impact on the environment through intelligent, eco-friendly design that still meets the increasing demand for livable and workable space. One of the WSUD or SuDS products to see rising popularity in the last 30 years is permeable interlocking concrete pavements (PICP) (Lucke, et al., 2014). The reasons for their popularity in WSUD or SuDS are most notably their hydraulic properties, specifically their high permeability and hydraulic conductivity. They promote water ingress instead of forcing water to surface drainage systems, unlike sealed pavements and can also be designed to have specific hydraulic properties, providing several geotechnical and engineering benefits.

The first of these benefits is that PICP aid in managing stormwater and reduce peak flow. This is accomplished through two of their hydrological characteristics. Firstly, they have high permeabilities and infiltration rates, reportedly able to accommodate between 5000 and 10000 mm/hour (Ferguson, 2006). Technicrete, (2017) claims that PICP constructed with the Aqua Trojan Slab® or Aqua Zig-zag® can achieve a surface permeability of up to 9000 mm/hour but are unfortunately limited by the permeability of the geotextile used within the pavement to 4500 mm/hour. They also claim that in the worst-case scenario, where severe clogging has taken place, the same pavement will still achieve a permeability of 900 mm/hour. Secondly, PICP discharge water at a much slower rate, often much slower than the original rate of the natural surface (subgrade) in the predevelopment case (Fassman & Blackburn, 2010) which can be as low as 2.5 l/s/ha (Technicrete, 2017). This minimizes downslope flooding, erosional damage, ponding, blocked drainage systems.

Secondly, PICP function as reservoirs for water storage or attenuation schemes. In some cases, they are capable of attenuating more than 6mm of water within a small pavement surface area, freeing development space which would otherwise be utilized for on-surface storage tanks (Kelly et al., 2007). Most notably however, their large storage capacity and slow discharge allow for groundwater recharge through subgrades, previously considered impermeable. An example of this was demonstrated by Dreelin et al., (2006) where a permeable pavement allowed for the infiltration of 93% of the rainfall volume, occurring in events of less than 20 mm at a time.

Lastly, PICP are cited to act as filters and traps, capable of removing sediments and pollutants such as nitrates, phosphates and certain heavy metals from water infiltrating through them (Lucke et al., 2014). This is partly due to the gradual reduction in particle size within the pavement from its base to its surface and the affinity of these particles to attract those suspended in the infiltrating water. In some cases, a permeable pavement capable of removing up to 50% of the total suspended solids (TSS). (Morquecho et al. 2005) The other factor involved is the presence of naturally occurring microbes within permeable pavements. These microbes have been shown to be particularly effective at digesting pollutants such as oil spillage from vehicle traffic, in some cases as much as 70 g per m² of pavement per year. (Technicrete, 2017) The result is that water discharge from permeable pavements is clean and has a near neutral pH which is advantageous for sensitive groundwater resources and for use over dolomitic environments, reducing the risk of sinkhole development due to urban water drainage. This would also prevent the need for additional filtration steps in the water treatment process of an on-site attenuation scheme.

While there are a host of environmental and engineering benefits to the use of PICP which have made them a popular choice for WSUD or SUDS, they are a fairly new technology and as such, current literature is heavily focused on their mechanisms of failure, particularly the phenomenon of clogging. There is still very little data available which adequately describes their hydrological performance using different construction materials, the effect of the slope on which they are constructed and their implementation over different subgrades. Most designs are thus based on estimates gained from the experience of the design professional and gratuitous overcompensation in layer thicknesses.

1.2 AIMS AND OBJECTIVES

To illuminate the issues surrounding PICP in WSUD or SuDS, the University of Pretoria, in association with Bosun Brick (Pty) Ltd. Midrand, conducted a three-year experimental study. The aim of the investigation was threefold. Firstly, it aimed at determining the geotechnical controls of flow into and through PICP experimentally, using a specially designed Infiltration Table Apparatus (ITA). The apparatus allowed for investigation into the effect of using construction materials with different geological origins. It also allowed for the investigation of the effect of different environmental conditions, such as incline, on PICP systems – a factor which is poorly covered in literature but is often governed by the pavement site geology. Secondly, the study aimed at assessing the validity of hydraulic test methods currently being applied to PICP on site and in the laboratory to determine their hydraulic properties. Accurate and reliable permeability data is imperative for the design phase and long-term maintenance of any PICP, however, large disparity and variation exists in available data regarding their reported results. Lastly, this investigation aimed to further inform of the hydraulic properties of PICP, adding to the growing database available for permeable pavements and assisting practitioners in mitigating the risks presented by complex subgrades.

2 ANATOMY OF PAVEMENTS

Pavements have been utilized since before 1500 BC (Weinert, 1980) but since then, several technological developments have occurred, resulting in an immense variety of designs, methods and applications. To fully understand the implications of this study, it is pertinent to define precisely what is meant by the term 'pavements' in a modern context and their general structure. Pavements, as described by Technical Recommendations for Highways (TRH) 14 (1980) and 20 (1990), are a group of layers of different imported or local materials placed on the natural surface (Subgrade) to provide a stable platform on which to operate vehicles. With the growing number of pavement types and applications however, it is preferable that the term rather refers to any engineered surface, consisting of one or more layers of local or imported material above the subgrade, that is intended for human or vehicular traffic.

2.1 CONVENTIONAL PAVEMENTS

Modern pavement design for urban development, such as for the construction of national roads and interlocking concrete pavements (ICP) is a science unto its own. It requires intense planning, years of experience and rigorous application of quality control and well-established construction standards. As a science and an engineering practice, it is covered in excruciating detail in literature, especially in the field of heavily trafficked roads, being regulated locally and internationally by various agencies and professional organizations. This study is primarily concerned with the hydrological and geotechnical implications of PICP, and thus, fully describing modern pavement design does not lie within its scope. A brief overview with examples is provided in this section however, to convey a deeper understanding of PICP structure and design in relation to that of conventional pavements such as roads and ICP. Broadly speaking, conventional pavements can be grouped into two main types namely; Load-bearing Pavements (LBP) and Aesthetic or Non-load-bearing Pavements (NLBP).

Load-bearing pavements are some of the most highly engineered surfaces commonly found in urban developments today. Some examples include arterial roads, national freeways, loading areas and large aircraft runways. They are designed and constructed for high traffic volumes, in excess of 400 vehicles per day, and large bearing capacities, in excess of 80 kN axle loads. Most examples of LBP are sealed to prevent water ingress into their layer works which would cause instability, loss of strength and decrease their service lifetime. Although most examples of LBP are sealed, several unsealed and permeable options including porous asphalt and concrete

pavements as considered by Bean et al., (2007), have been developed in recent years and are being evaluated for WSUD or SuDS applications. Non-load-bearing pavements, such as ICP and compacted turfs, are less engineered surfaces than those grouped in the LBP type. They are often temporary or aesthetic additions to urban developments, used for walkways, traffic barriers, driveways and parking surfaces and differ from LBP in several ways. Firstly, they are intended for much lower traffic volumes; less than 400 vehicles per day and/or low bearing capacities. Secondly, they are constructed with slightly less emphasis on the use of standards and specifications, however, a great deal of preparation is still involved in their construction. Permeable pavements exist on the verge between these two types of pavements, containing traits of both modern high-traffic roads and basic ICP which are discussed in greater detail in Section 2.2 but first, a greater understanding of the structure, construction materials and standards for both LBP and NLBP is required.

2.1.1 LBP Structure

In general, the structure of LBP remains consistent throughout the different branches of civil industry, from residential and industrial developments to the construction of national road networks and major catchment dams. From top to bottom, they consist of four primary layers built upon the subgrade as follows: (Fig. 2):

- 1) Surface;
- 2) Base;
- 3) Sub-base;
- 4) Selected Subgrade (if required)
- 5) Natural Subgrade.

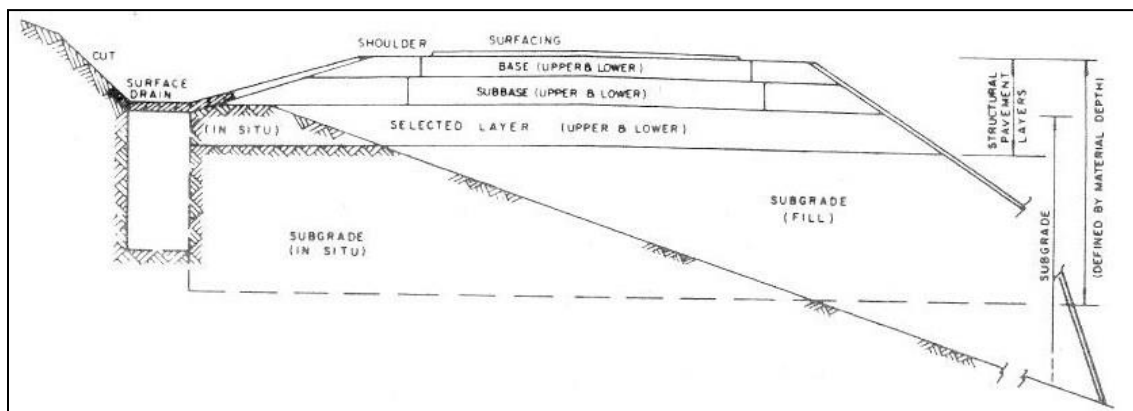


Fig. 2: The general structure of a sealed pavement (TRH14, 1980).

The layers of LBP can be grouped into three major components; the surface, the structural layers (consisting of the Base, Sub-base and Selected Subgrade) and the Natural Subgrade or foundation. The surface is often considered the most important portion of any load bearing pavement as it is the uppermost portion of the layer works and comes into direct contact with the intended traffic. As such, the surface must consist of materials with certain abrasion characteristics like crushed granite, andesite or even crushed concrete, adhered to each other and the rest of the pavement, by a binder like bitumen. While it is usually much thinner than the other layers, it protects the underlying ones from erosion, provides traction for vehicles and is the determining factor in whether the LBP is sealed or unsealed. (Weinert, 1980)

Directly below the surface is the base layer and it commonly consists of a controlled selection of gravel or crushed stone, that is compacted to a specific degree. The base provides a stable, level surface on which the surface layer can be constructed and forms part of the group of layers that distribute and carry any imparted loads. The base can vary in thickness, depending on intended use but is commonly much thinner than the layers that underly it. Below it are two additional layers of crushed and compacted stone/gravel namely; the sub-base and, if needed, the selected subgrade, respectively. The degree of compaction, thicknesses and grading of these layers is determined by the intended use of the pavement and together with the base, they form the structural layers of the pavement, with the foundation for the being provided by the subgrade or in-situ material. (TRH 14, 1980) The result is a flexible, yet durable surface that effectively distributes loads and has a long service lifetime.

2.1.2 LBP Materials and Standards

Given the function of each layer in LBP, it is understandable that there would be strict requirements on the physical and chemical properties associated with the materials selected for each of these layers. Considering firstly the surface layer, the aggregate required must have a certain minimum strength so that the particles are not crushed by the traversing traffic. The strength requirements for surfacing aggregates vary internationally, and in some cases locally, depending on the selected road agency but are commonly in the range of 150 to 210 kN. Another physical and chemical requirement of surfacing aggregate is their propensity for polishing, or polishing index (Weinert, 1980). Polishing occurs when the angular edges of the aggregate are uniformly worn down by passing traffic, reducing the friction coefficient of the surface. This commonly occurs when the parent material of the aggregate consists of only one (monomineralic), or two minerals of similar hardness. Quartzite, despite its high strength, is a prime example of monomineralic rock and is thus better suited for use in the lower layers of LBP such as the sub-base. Aggregates produced from parent material that contain two or more minerals of drastically varying hardness, wear differentially and polish the least. Thus, they are more favourable for use in the surface layer of a pavement. Examples of such parent materials are granite, tillite and quartzitic sandstone. (Weinert, 1980)

Considering the structural layers of LBP however, the characteristics of physical strength and interlock ability of the material as an aggregate, become more influential in governing their selection. Systems of specifications and standards detailing the preferred/required physical attributes of materials for these and other pavement layers have been developed around the globe for this purpose. An example of the standards used in such cases in South Africa, can be seen in TRH14 (1980) and TRH20 (1990). These documents detail the material characteristics as well as compactions, thicknesses and maintenance schedules of the layers in both sealed and unsealed LBP respectively (TRH14, 1980 & TRH20, 1990). In these documents, the materials permitted in each pavement layer are given a primary coded classification, as summarised in Tables 1 and 2 and with a set of physical requirements attached to them that the material must adhere to.

Table 1: Pavement layer material selection classification codes. (TRH 14, 1980)	
Road Layer	Material Classification Codes
Surfacing	AG, AC, AS, AO, S1, S2, S3, S4, PCC
Base	G1, G2, G3, G4, WM1, WM2, C1, C2, C3, C4, BC, BS, TC, TS, BT1, BT2, BT3, PM
Subbase	G5, G6, C1, C2, C3, C4, BT3
Selected Layer	G6, G7, G8, G9
Subgrade	G8, G9, G10

Table 2: Pavement layer material specifications for material classification codes. (TRH 14, 1980)	
Code	Material
AG	Asphalt Surfacing - gap-graded
AC	Asphalt Surfacing - continuous-graded
AS	Asphalt Surfacing - semi-gap-graded
AO	Asphalt Surfacing - open-graded
ST1	Surface Treatment - single seal
ST2	Surface Treatment - multiple seal
SS	Sand Seal
SC	Cape Seal
SL1	Slurry - fine grading
SL2	Slurry - coarse grading
G1	Graded crushed stone
G2	Graded crushed stone
G3	Dumprock
G4	Natural Gravel
G5	Natural Gravel
G6	Natural Gravel
G7	Gravel-soil
G8	Gravel-soil
G9	Gravel-soil
G10	Gravel-soil
WM	Waterbound Macadam
C1	Cemented crushed stone or gravel
C2	Cemented crushed stone or gravel
C3	Cemented natural gravel
C4	Cemented natural gravel
C5	Treated natural gravel
BC	Bitumen hot mix - continuously graded
BS	Bitumen hot mix - semi-gap-graded
TC	Tar hot mix - continuously graded
TS	Tar hot mix - semi-gap-graded
BT1	Bituminous treated crushed stone
BT2	Bituminous treated natural gravel
BT3	Bituminous treated cohesionless sand
PM	Penetration Macadam
PCC	Portland cement concrete
GWC	Gravel wearing course

A G2 material in TRH 14, (1980) for example, is designated by this system as “graded crushed stone” and is often sought for use in the base layer of LBP. For a material to be fit for the classification of G2 and thus permitted use in the base of LBP, it must comply to the associated requirements of the rest of the document summarised below (TRH 14, 1980):

- At least 50% of the G2 material retained on a 4.75 mm sieve should have at least one fractured face;
- The 10% Fines Aggregate Crushing Test (FACT) value of the material should be greater than 100 kN;
- The Aggregate Crushing Value (ACV) of the material should be less than 29%;
- The flakiness index of the material should be less than 35%;
- The material should have a California Bearing Ratio (CBR) after soaking of not less than 80% at 98% Mod. American Association of State Highway Officials (AASHTO) density;
- The material must have a maximum swell of 0.2% at 100% Mod. AASHTO density;
- The material should be investigated for the presence of deleterious minerals such as sulphide minerals, soluble salts and micas.

Lastly, consider the subgrade component of LBP structures. The commonly applied standards in this area of the pavement in South Africa are SANS 1200-DM, (1981) but ultimately, the encountered materials and preparation will be entirely dependent on their location and thus, geologic origin. Subgrades originating from igneous parent rock for example, such as soils formed over diabase dykes, granites and gneisses can be especially problematic. They often contain large amounts of clay minerals which can heave with water ingress, resulting in cracking, deformation and possible failure of the pavement. (SAPEM, 2013) In other cases, subgrades containing silts and chalks, rapidly loose stiffness and thus deform with a marginal increase in their moisture content. (Woods-Ballard et al., 2007) For this reason, each subgrade requires detailed investigation, planning and preparation before use in LBP. The required preparation can vary from simple chemical stabilization such as the addition of lime for clay-rich soils, to the excavation and re-compaction by dynamic roller for sandy, voided soils. There are however, a set of basic principles which guide the appropriate selection of subgrades, most notably that the natural or compacted CBR of the subgrade should be at least 15% for use in a load bearing pavement. (Technicrete, 2017 & TRH 14, 1980)

From this it is clear that one of the largest challenges faced by practitioners during LBP design is the sourcing and selection of the appropriate materials for a given application within the pavement and particularly in that of the subgrade. They must continuously give careful consideration to the availability, material quality, technical feasibility, environmental impact and commercial viability of the pavement (SAPEM, 2013) all of which, are governed by the geological origin of the materials. The South African Pavement Engineering Manual (SAPEM), (2013), summarizes the broad geological origin of most pavement construction materials as shown in Table 3.

Table 3: Common South African rock types and their appropriate LBP layer applications. Adapted from SAPEM, (2013) (Weinert, 1980)

Aggregate Materials		Appropriate Application		
Rock Type	Name	Surfacing	Base Layer	Sub-base Layer
Crystalline - Basic	Amphibolite	x	x	
	Andesite	x	x	x
	Anorthosite		x	
	Basalt	x	x	x
	Diabase	x	x	x
	Diorite	x		x
	Dolerite	x	x	x
	Gabbro	x		
	Greenschist	x	x	x
	Norite		x	x
	Peridotite		x	x
	Phonolite	x		
	Serpentinite	x	x	x
Crystalline - Acidic	Felsite	x	x	x
	Gneiss		x	
	Granite	x	x	x
	Pegmatite		x	x
	Rhyolite	x		
	Syenite	x	x	
Silica-rich	Chert		x	x
	Hornfels	x	x	
	Quartzite	x	x	x
	Vein Quartz	x	x	x
Arenaceous	Arkose	x	x	x
	Conglomerate		x	x
	Gritstone		x	x
	Mica Schist			x
	Sandstone	x	x	x
Argillaceous	Sericite Schist		x	x
	Phyllite		x	x
	Shale		x	x
	Mudstone		x	x
	Slate		x	x

2.1.3 NLBP Structure

The structure and purpose of the layers in Non-load-bearing Pavements are best described by example as it varies depending on the type of pavement and intended application. To facilitate this and provide further understanding of the place of PICP in modern pavement design, the example of ICP was selected. From top to bottom, most ICP consist of three primary layers as follows: (Fig. 3)

- 1) Surface;
- 2) Bedding;
- 3) Subgrade.

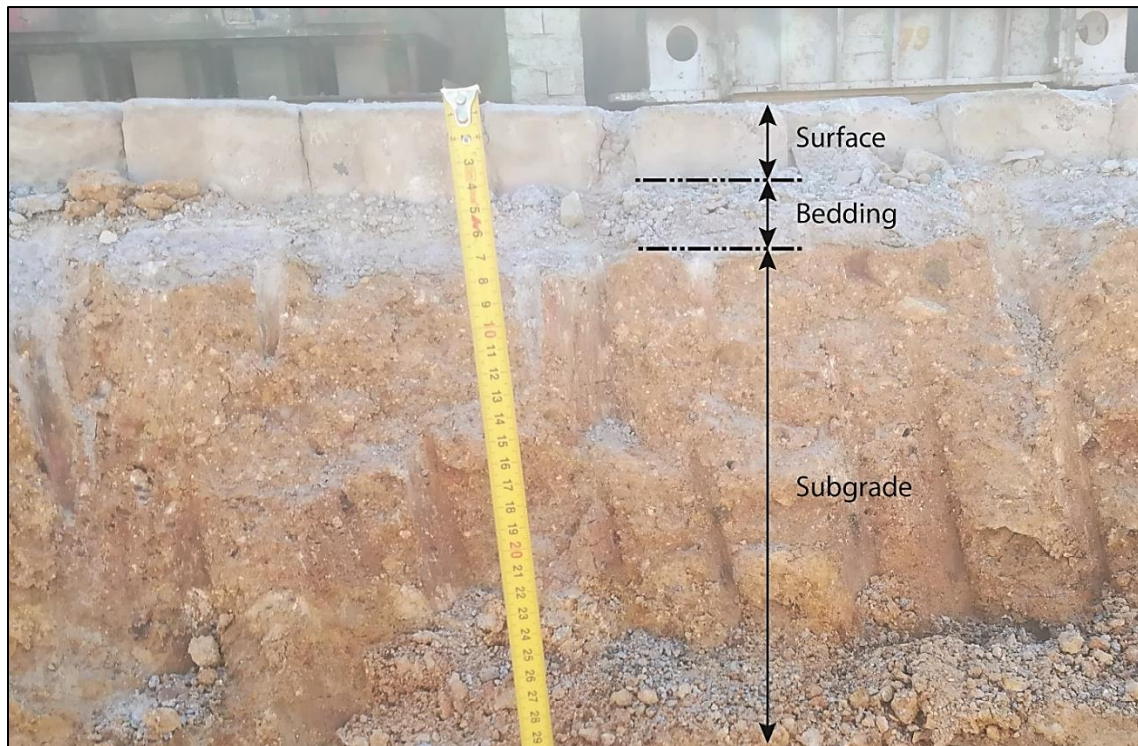


Fig. 3: A typical Interlocking Concrete Pavement layer works (Bosun – Midrand, 2018)

The structure of ICP is described by Cairns (N.D.), with detailed explanation of their construction which is divided into four basic steps. The structure of ICP is very similar to LBP but is often much thinner, more cost effective and contains substantially less layers. Just as with LBP however, the subgrade forms the foundation of the pavement and will again vary depending on the geological origin of the materials. As the layers above the subgrade in ICP are often not thick enough to compensate for deformation caused by heave in clay soils for example, the subgrade must often be prepared by compaction (Ferguson, 2006) and if needed, chemical stabilization.

Above the subgrade is the bedding course which averages 25-30mm in thickness and commonly consists of a well graded sand. The bedding course fills any depressions remaining in the prepared subgrade and provides a level surface on which the surface is constructed. Lastly, is the surface layer which consists of two components namely; the concrete masonry units (interlocking bricks) and the joint fill between them. The interlocking bricks form the interaction layer between the pavement and the intended traffic and distribute the imparted loads to the rest of the pavement while the joint fill prevents horizontal movement of the concrete bricks during use, which would otherwise damage the bricks and the rest of the pavement (SANS 1200-MJ, 1984). Interlocking concrete brick products are often designed with geometry that lends themselves to a set of specific laying patterns. Once a pattern is selected, it is recommended that it is kept consistent throughout the pavement for optimum performance (Fig. 4).

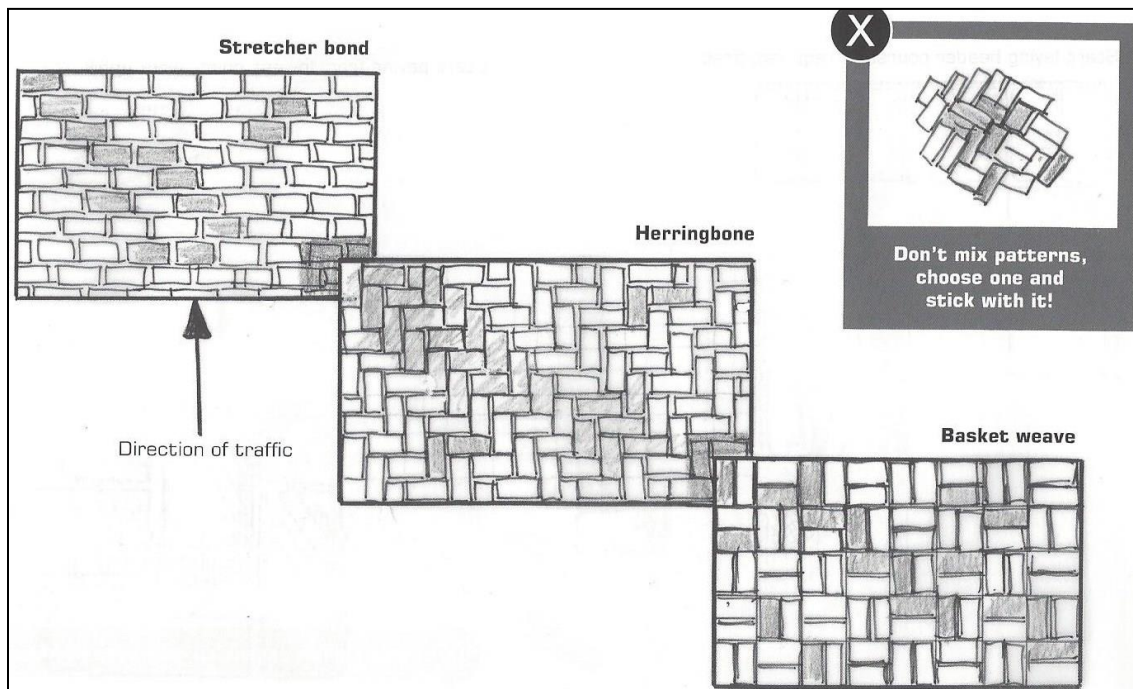


Fig. 4: An example of different concrete brick laying patterns for a simple interlocking concrete brick (Cairns, N.D.).

The result is also a flexible yet durable surface, that distributes imparted loads, is cost effective, aesthetically pleasing and can be rapidly constructed. In terms of hydrological performance, these pavements are considered largely sealed. They generally have a shorter lifespan than that of LBP and thus maintenance must be regularly performed. Interlocking concrete brick pavements can be constructed for high volumes of traffic by applying the techniques used for LBP, however, maintenance of the surface layer would have to be frequent making the pavement far less cost effective.

2.1.4 NLBP Materials and Standards

Just as with LBP, the material selection and construction of NLBP must comply to a rigorous set of standards. In the case of ICP, there are three primary documents to this effect. Firstly, the overall construction of ICP must adhere to South African National Standards (SANS) 1200-MJ (1984). The second document, SANS 927, (2007) regulates every aspect of the design and manufacture of concrete units such as kerb blocks and channels that are placed within or on the periphery of ICP. Lastly, SANS 1058, (2012), regulates the design and manufacture of the concrete units which comprise the surface of ICP.

As the surface layer of ICP must perform both load-bearing and tractional functions for the pavement, a large investment of time and effort is placed on the material selection, quality and design of the units or bricks that comprise it. The commonly applied standards specify the allowable materials, dimensions, appearance, abrasive resistance, absorbance and most importantly, the strength of each unit. For example, each unit must have a tensile strength of between 1.8 and 2.5 MPa and a wet compressive strength of at least 20 MPa to ensure adequate performance in the surface of the pavement (SANS 1038, 2014 and SANS 1200-MJ, 2014). In terms of the geological origin of the materials in the surface layer however, the aggregates in the concrete and joint fill are not dealt with in much detail. Their physical characteristics such as grading, flakiness index and chemical stability against Alkali-Silicate Reactions (ASR) are instead given preference because the surface of ICP is an agglomerate of manufactured components, with their materials specially sourced by the manufacturer, rather than a layer of appropriate locally sourced material.

The bedding course and subgrade of ICP bear significant similarity to those in LBP and are commonly treated in the same way, particularly in terms of the CBR requirement of at least 15% for the subgrade for heavy vehicle traffic (Technicrete, 2017). The geological origin will thus, once again determine their characteristics and required preparation, as described in Section 2.1.2. The documents SANS 1200-DM, (1981) and SANS 1200-MJ, (1984) do detail required compactions for the subgrade (between 90% and 100% Mod AASHTO) and gradings for the bedding course respectively.

2.2 PERMEABLE INTERLOCKING CONCRETE PAVEMENTS

As stated before, permeable interlocking concrete pavements are blend between LBP and ICP, with many differences and similarities to both. They are nearly identical to LBP in terms of their layer structure but are constructed according to the same “rules” as ICP, allowing for lower bearing capacity (Beeldens and Herrier, 2006). They form part of a group of WSUD and SuDS elements known as Permeable Pavements (PP) which consist of engineered surfaces such as porous asphalt, pervious concrete, single-sized aggregate, porous turf and many more (Woods-Ballard et al., 2007). At their core, PICP are modular, engineered surfaces that promote water ingress through their layer works to fulfil specific design requirements. To provide further understanding of the purpose and implications of this study, this section provides an in-depth review of PICP, their construction materials, current testing methods and hydrological performance.

2.2.1 PICP Structure

Just as with all other subsets of modern pavements, there are several variations in designs and structures of PICP applied around the world. Generally speaking, the structure of PICP closely resembles that of LBP but in all cases, consist of highly porous layers materials with finer particles sizes at the top, gradually becoming coarser toward the bottom to prevent silting (Beeldens and Herrier, 2006). There are three main types of PICP used in WSUD or SuDS namely, Type-A: Full Infiltration, Type-B: Partial Infiltration and Type-C: Tanked/No Infiltration pavements. Full Infiltration PICP primarily discharge water into the subgrade and groundwater system and are commonly constructed on free draining or high permeability soils. Partial Infiltration PICP discharge into the subgrade as well but contain a system of drains that remove the portion of water ingress that exceeds the subgrade’s infiltration rate. These types of PICP are mostly used where the subgrade has a moderate to low permeability and/or infiltration rate, reducing risks to soil stability caused by excess water build-up. Tanked Infiltration pavements prevent discharge into the subgrade completely and are commonly constructed with an impermeable membrane at the base. They are primarily used when one or more of the following issues exist (Woods-Ballard et al., 2007):

- The underlying groundwater must be protected;
- The sub-base is 1m or less from the water table;
- Water ingress into the pavement is being attenuated;
- Water ingress can cause instability in the subgrade or it has a low permeability;
- Contaminants in the subgrade can be mobilized by water ingress.

Examples of the standards used in the design and construction of PICP can be seen in the UK draft paper, National Standards for Sustainable Drainage Systems (DEFRA, 2011), The SuDS Manual CIRIA C697 (Woods-Ballard et al., 2007) and guidelines written by Technicrete (2017). These documents describe the recommended design performance, materials and maintenance of PICP but take cognizance of the variety of situations in which PICP can be applied, giving practitioners large amounts of freedom to tailor-make the pavements for their specific applications.

As this study is concerned with the hydrological performance of PICP, in an effort to better understand their relationship with complex subgrades, this section is presented in terms of a Type-A: Full Infiltration PICP. From top to bottom, the basic structure is as follows but bear in mind, different variations of this exist and are purely dependent on the application, type of subgrade, available materials and the design of the practitioner (Fig. 5). Additional components such as drainage pipes, meshes, silt traps and additional geotextile layers are placed throughout the layer works of the pavement construction as well, depending on the application (Technicrete, 2017):

- 1) Surface;
- 2) Bedding;
- 3) Geotextile;
- 4) Upper sub-base;
- 5) Lower sub-base;
- 6) Subgrade

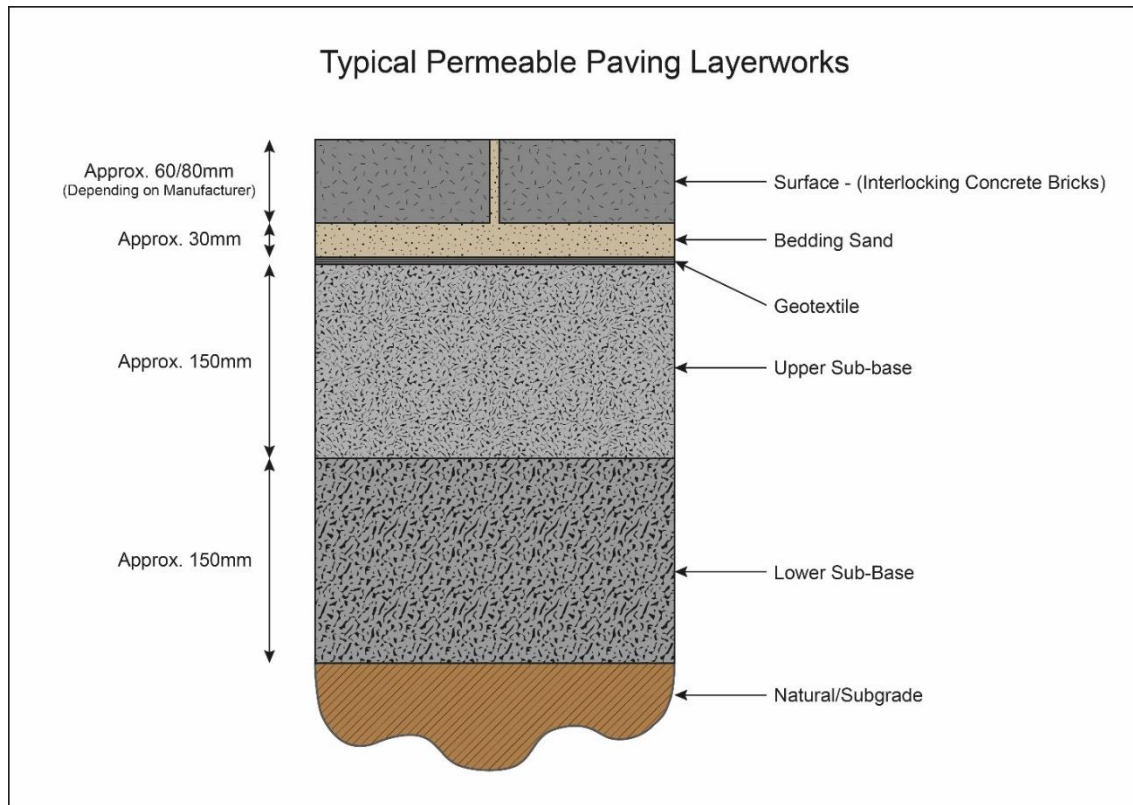


Fig. 5: A typical PICP layer works. (Adapted from Technicrete, 2017).

As with ICP, the surface of PICP consist of two parts, the interlocking concrete bricks (block or units) and the jointing material between them. The bricks in PICP are not in themselves porous but instead, their geometry results in them fitting together in such a way that their joint surfaces provide a conduit for the infiltration of water. Similarly to ICP the bricks used in the surface must also comply with SANS 1058, (2012). The jointing material is usually a sand or fine stone of which the particle size is highly controlled to eliminate the presence particles smaller than 0.425mm, or as they are commonly known the “fines” (USDA, 2012). The surface layer is likely the most influential portion of any PICP. Kumar et al., (2015) showed that the overall hydrological performance of a permeable pavement depends on the surface layer as a whole, even though variations in the actual concrete units make no remarkable difference to its permeability as described by Beeldens and Herrier, (2006). Using a standard, well graded sand however, can reportedly reduce the permeability by 50% (Technicrete, 2017). In a study by Pezzaniti et al., (2009) it was also shown that clogging at the surface, a common failure mechanism of PICP, had a greater impact on the permeability and performance of the pavement than if it occurred in the geotextile below it. For this reason, the materials used in the surface were deeply investigated in this study.

Directly below the surface is the bedding/laying course which commonly consists of a 50mm thick layer of 6.7 to 2.36 mm, poorly graded, clean crushed stone as described in SANS 1083, (2014). It is often very similar to the jointing material and aids in promoting water ingress into the layers below as well as to provide a level platform, upon which, the surface layer can be constructed. The aggregate materials in this layer and the surface should ideally have porosities of between 30% and 40%, providing surface infiltration rates of approximately 25 000 mm/h as shown in ASTM 57, 8 and 10 (Ferguson, 2006). As with other pavements and their course layers, the materials for the bedding layer will be subject again to their geological origin and must be carefully selected if the requirements of the relevant standards are to be met.

Below the surface and bedding layers, a synthetic material known as a geotextile is commonly placed. A geotextile is a thin, fibrous fabric which primarily prevents the migration of particles between unbound layers in PICIP (Woods-Ballard et al., 2007). They can also be placed at the base of PICIP, above inappropriate subgrades to prevent the movement of plastic soils such as clays, into the sub-base layers (Ferguson, 2006). They are generally made from polyethylene fiber to make them resistant to acidic environments and give them high tensile strengths which has the secondary effect of increasing the tensile strength of the pavement (Woods-Ballard et al., 2007). Caution must be applied to the specification of geotextiles between layers however, as they can act as a horizontal slip surfaces in the presence of excessive breaking forces (Beeldens and Herrier, 2006).

The final two layers at the base of PICIP, are the upper and lower sub-base layers. The two layer design is adopted for two reasons. Firstly, for structural performance as the upper sub-base layer is primarily only for light vehicular traffic and the lower is added for heavier axle loads (Fassman and Blackburn, 2010). The second is to increase the water storage capacity, which is governed by PICIP base layer thickness (Beeldens and Herrier, 2006). The typical upper sub-base layer in PICIP is approximately 100 mm thick and consists of between 4 mm and 20 mm clean crushed stone while the lower is usually around 250 mm thick and consists of 10 mm to 63 mm clean crushed stone (Technicrete, 2017). In cold climates however, it is recommended that the sub-base layers have a total thickness of at least 450 mm to accommodate for frost heave if the subgrade cannot do so itself (Woods-Ballard et al., 2007). An additional function of the sub-base layers is that they often provide rooting space for trees which is not present in conventional pavements, often resulting in deformation and subsequent failure of the pavement, making PICIP more attractive for application in urban developments with low available space budgets (Ferguson, 2006).

The aggregates selected for the sub-base layers should be open graded for good interlock during construction (Ferguson, 2006) must also comply with SANS 1083, (2014) just as in other pavements. According to Technicrete, (2017), the sub base layers should also be compacted to at least 97% lab bulk density by vibratory roller or plate compactors to ensure proper strength. Suitable material types for use in the sub-base layers include most gravels and crushed stone or concrete provided they are non-plastic, not friable and are free from clays (Technicrete, 2017) however, they will also be subject to their geological origin. Acceptable material origins include granite, basalt, gabbro and even some blast furnace slags provided they have adequate strength and more than 90% fracture surfaces (Woods-Ballard et al., 2007). Material specifications with further detail such as suitable gradings, fines content, durability and more can be seen in BS EN 13242, (2003).

Just as in conventional pavements, beneath all the other layers is the subgrade and it always has a major effect on the permeability and overall performance of PICP. It, along with the sub-base layers, will ultimately determine the storage capacity of the pavement (Beeldens and Herrier, 2006). Again, the geological origin of the subgrade will be the determining factor in the eventual success of PICP for example, PICP installed on sandy soils tend to maintain their performance, regardless of age (Bean et al., 2007). It is believed that PICP generally do not work on clay subgrades because the action of storing water within the pavement, will increase the moisture content of the subgrade if no impermeable liner at the base is present and as stated before, clays, silts and chalks loose stiffness if that occurs (Woods-Ballard et al., 2007). Compaction has been shown to be able to alleviate this and so can making the sub-base thicker (Ferguson, 2006). In any case, PICP must always be specifically designed for the subgrade on which it will be constructed (DEFRA, 2011 and Woods-Ballard et al., 2007).

2.2.2 Unsaturated Flow in Urban Developments

Type-A and B PICP will both discharge additional water volumes into the subgrade, albeit at a significantly lower rate than its initial infiltration or the natural permeability of that subgrade. So, in order to design PICP that will overly that subgrade, it is important to understand the natural flow mechanisms that occur within in as well as how the PICP may possibly influence it. As PICP are commonly implemented in areas above saturated or waterlogged ground i.e. where the groundwater table is expected to be well below the base of the pavement, this section will focus on unsaturated flow mechanisms that commonly occur in urban developments.

Dippenaar and van Rooy (2018) describe six possible instances of unsaturated flow in the natural and urban environment namely:

- 1) Normal Perching – where water is trapped above a low permeability unit as a result of the energy required to break the suction pressures within it caused by its reduced void sizes;
- 2) Capillary Barrired Perching – where water is trapped above a higher permeability unit as a result of strong adhesion and suction within the lower permeability, fine grained unit above;
- 3) Imbibition – where water is drawn into finer grained units with lower moisture contents through suction;
- 4) Shallow Interflow – where water in low permeability units is mobilized by cohesion alone.
- 5) Percolation – where water from a higher saturation is mobilized through cohesion and gravity, migrating to lower units;
- 6) Unsaturated fracture flow – where water migrates through fracture networks between units without completely wetting these fractures.

To fully understand how these flow mechanisms may occur in a subgrade, it is advantageous to group all possible subgrades for PICP into two broad categories, namely; high and low permeability subgrades. The high permeability category would include subgrades such as gravel, deep, sandy soils or shallow, permeable soils that overly a fractured rock mass. The low permeability category would contain subgrades such as hardpan ferricretes, clays and shallow, permeable soils overlying a unfractured rock mass.

In the case of the high permeability category, consider a shallow, permeable soil overlying a fractured rock mass as the intended subgrade. This is a common situation in South Africa, associated with plateaus, undulating topography and footslope development sites (Henning, 2015). In these cases, it is understandable to assume that the permeability of the subgrade as a whole, will be determined by that of the rock mass and not the thin soil above it but in truth, the shallow soil will still remain the controlling factor as flow, particularly into a vertical fracture is governed by the overlying material and its hydraulic conductivity (Brouwers & Dippenaar, 2018). Only if the hydraulic conductivity of the soil is higher than that of the rock mass will, fracture flow be the determining factor. Additionally, the way in which the rock mass is fractured will also determine flow regimes. In predominantly vertically fractured rock masses such as steeply dipping shales, only 30% of the fracture volume will be used for flow (Brouwers & Dippenaar, 2018). This is because flow in such fractures commonly occurs only in tendrils or “rivulets” in near surface conditions, never fully saturating the fracture (Fig. 6).

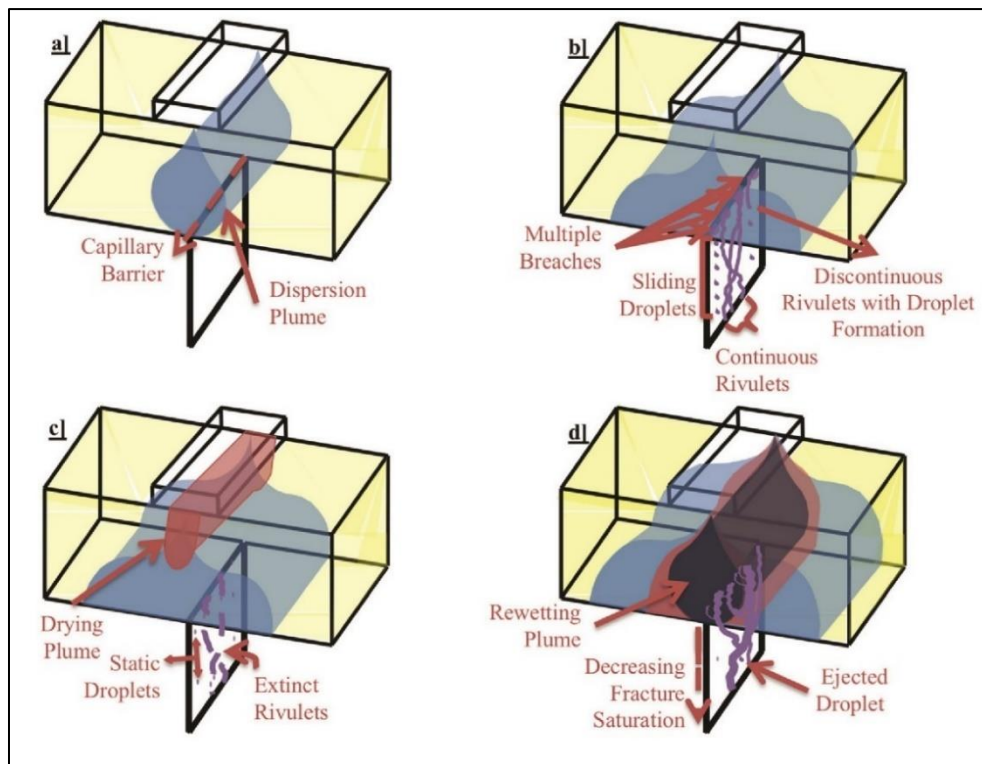


Fig. 6: (a) Dispersion plume formation on a capillary boundary between soil and rock when wetting first occurs, (b) Breaching of the capillary boundary with variably saturated flow, (c) Invasion of a drying plume when the water supply was depleted and (d) Invasion of a rewetting plume with merging rivulets in the rock. (Brouwers and Dippenaar, 2018)

In horizontally fractured rock masses or on the interface between soil and rock, unsaturated flow proves to have longer pathways than vertical flow. This is because water commonly flows in a “fill and spill” method in horizontal fractures due to the influence of gravity. Any depression or irregularity in the fracture surface or soil-rock interface, must be filled before water is able to exit over its outermost edges and flow into the next. This can further be influenced by contact obstacles which can increase the length of the flow path by up to 14% (Jones et al., 2018) further decreasing perceived hydraulic conductivity. For this reason, and others like it, it is of vital importance to the performance of any PICP that the subgrade on which it built be considered in the design phase and deeply investigated before construction takes place.

2.2.3 Current PICP Evaluation and Performance

As stated before, the primary goal of any PICP is to manage peak flow and thus improve the predevelopment characteristics of the subgrade on which it is built. To achieve that, a deep understanding of the hydrological characteristics of PICP is required, in addition an understanding of the subgrade. An effective PICP design should have a surface infiltration rate that is greater than that of the design rainfall intensity (Woods-Ballard et al., 2007). Several standards and guidelines are available to this effect but in short, an effective PICP should have a service lifetime of approximately 15 years with a overall permeability of 4500 l/s/ha that only decreases to 1250 l/s/ha over that period (Technicrete, 2017). Due to the wide variety of designs, construction materials and subgrades however, empirical prediction of PICP performance from its design alone is nearly impossible. The most effective method of determining their performance is thus still experimental evaluation. The following section details some notable studies to this effect.

Before describing the test methods and their results, it is pertinent to describe the hydraulic test methods commonly applied in industry to conventional pavement s and other surfaces such as ICP. Most of these testing procedures evaluate one or more of the following hydraulic properties (Kuosa et al., 2014):

- Void content;
- Porosity;
- Density;
- Permeability;
- Hydraulic conductivity;
- Water infiltration capacity.

The void content for both surface and sub-surface layers of ICP are commonly determined using two groups of standardized tests. The first group is described by EN 1097-3 (1998) and ASTM C29, (2009) which determine the void ratio and bulk density for aggregates less than 63 mm and 125 mm in diameter respectively. The second group determines the density and void content for concrete units such as those used in ICP. The first, ASTM C1688 (2013), measures the void content and density of the freshly mixed concrete while the second, the ASTM C1754 (2012), measures the same variables but for hardened concrete specimens. There are few limitations to these tests in terms of accuracy but they must be carried out in a laboratory and/or before the surface layer of the pavement system is constructed.

The porosity of hardened concrete units can be measured through a method described by Lian and Zhuge (2010), where specimens are dried, their dimensions are measured, they are soaked in a bucket with a specific amount of water for 24 hours and then the volume of water needed to refill the bucket to its original level is measured. The volumetric change caused by the water absorbed by the specimen is equated to its porosity by Equation 1. This test method must also be carried out in a laboratory and before the surface layer of the pavement system is constructed.

$$P(\%) = \left(\frac{V_T - V_C}{V_T} \right) 100\% \quad (1)$$

Where:

V_T = Total specimen volume when dry.

V_C = Volume required to refill bucket to original level.

While permeability and hydraulic conductivity are often used interchangeably, they are in reality two very different properties of a material. Kuosa et al., (2014) state that permeability (Darcy Permeability or Transmissivity “ k ” in m^2/s) is actually a measure of how well the medium transmits a fluid while the hydraulic conductivity (Permeability “ K ” in m/s) of that medium refers to how easy a fluid flows through it. Common permeability values for some natural and engineering materials are shown in Tables 4 and 5.

Table 4: Permeability (K) value guidelines for different soils (Powers, 1992)

Soil Types	Permeability (K) (cm/s)
Poorly graded gravel	≥ 1
Uniform gravel	1 – 0.2
Well-graded gravel	0.3 – 0.05
Uniform Sand	$0.2 - 5 \times 10^{-3}$
Well graded sand	$0.1 - 10^{-3}$
Silty sand	$5 \times 10^{-3} - 10^{-3}$
Clayey Sand	$10^{-3} - 10^{-4}$
Low-plasticity silt	$10^{-4} - 5 \times 10^{-5}$
Low-plasticity clay	$10^{-5} - 10^{-8}$

Table 5: Typical Permeability and associated CBR values for different soils. Adapted from Woods-Ballard et al., (2007) (Interpave, 2005)

Soil Classification	Typical Coefficient of Permeability k(m/s)	Typical CBR
Heavy clay	10^{-8} to 10^{-10}	2 to 5
Silty Clay	10^{-8} to 10^{-9}	3 to 6
Sandy Clay	10^{-6} to 10^{-9}	5 to 20
Poorly Graded Sand	5×10^{-6} to 5×10^{-7}	10 to 40
Well Graded Sand	10^{-4} to 5×10^{-6}	10 to 40
Well Graded Sandy Gravel	10^{-3} to 10^{-5}	30 to 80

When it comes to measuring the permeability or hydraulic conductivity of ICP in-situ, commonly used tests are the ASTM C1781, (2013) (single ring infiltrometer) and ASTM D3385, (2009) (double-ring infiltrometer) an example of which, modified by Beeldens and Herrier, (2006) is shown in Fig. 7. In addition to this, the hydraulic conductivity of the sub-surface layers of pavement system can be determined by using ASTM D5084, (2010) and ASTM D2434, (2006). The first of these tests uses a flexible wall permeameter to determine hydraulic conductivity and was originally intended for soil and rock while the second, makes use of a constant head test to determine permeability and was intended for laminar flow through granular soils. Newer tests are also being developed such as the ASTM C1701 (2009) and National Center for Asphalt Technology (NCAT) permeameter. Although both have been shown to yield satisfactory results, the ASTM C1701 produced results that were as much as 90% lower than the NCAT permeameter (Li et al., 2013).

The standardized tests do not appear without complications however. Bean et al., (2007) showed that the ASTM D3385, (2009) failed when applied to PICP due to horizontal migration and subsequent upward percolation of water outside the rings. These tests often do not account for spatial variances such as clogging or high traffic wear. In addition, they do not account for upslope water source influences, the effect of incline, only test small areas of pavements (Lucke et al., (2014) and rely on a volume of water being placed above the surface, creating an unnatural pressure head, resembling flood conditions instead of normal rainfall.



Fig. 7: A Double-ring Infiltrometer Test modified for use on ICP.

(Beeldens and Herrier, 2006)

As a result of the challenges presented when attempting to apply these standardized tests to PICP however, few of them are effective at determining their hydraulic properties. Experimental evaluation remains the best method of determining PICP hydraulic properties and as such, several experimental studies have been conducted. The methodologies for these tests vary greatly throughout literature with radical procedures and outcomes but rarely include the achieved permeability data and any information on the materials in the pavements apart from their thicknesses. Information regarding the subgrades on which the pavements tested lie are also rarely included.

The Stormwater Infiltration Field Test (SWIFT) by Lucke et al., (2015) was one such method, aimed primarily at evaluating the degree of clogging in PICP. It involved placing a 25 l bucket with a 40 mm diameter hole in the bottom, 60 mm above the surface of a pavement. The hole was plugged and the bucket filled with 6l of water. The plug was then removed and the bucket drained onto the test surface. The area wetted by the test was then related to permeability values obtained by the standardized Single-ring Infiltrometer test. In terms of the construction materials and subgrade of the pavements however, no mention is made apart from what bricks were used and the thickness of the sub-base layer.

Another method proposed was a full-scale constant and falling-head test by Lucke et al., (2014). It involved isolating an area of approximately 65 m² of a pavement and measuring the difference in head with transducers placed at strategic locations in constant and falling-head conditions. It was found to be extremely time consuming and difficult to obtain accurate readings as a result of the difficulty involved in sealing the boundaries of such a large area and again, no detailed information was provided on the subgrade and construction materials apart from their layer thicknesses. Infiltration rate information was provided in this case but the variation made any data difficult to apply in practice. The data obtained from Double-ring infiltrometer used for comparison varied between 90 mm/h and 760 mm/h while the actual test data varied between 46 mm/h and 259 mm/h.

Lastly, and most similar to the methodology of this study, was the use of an Infiltration Table Apparatus (ITA) by Lucke and Beecham, (2013). It involved constructing an apparatus in which 18 m² of pavement, permeable or otherwise, could be placed as it would in industry and be subjected to a realistic representation of rainfall and peak flow of approximately 0.0042 m³/min. In addition, the ITA was allowed to rotate in the horizontal axis between 0% and 30% so that the effect of incline could be analyzed. The entire pavement within the apparatus is subjected to flow from surface and the outflow beneath one portion of the downslope length of the pavement was measured at a time. Unfortunately, this was a qualitative analysis with no reported permeability data for the pavement constructed within their rig provided. In addition, no material data was given as well apart from basic schematic representations.

Some studies conducted in literature do supply permeability and construction material data however, a crucial part of understanding the hydraulic performance of PICP and their subgrades for more effective design. Table 6 gives a brief summary of these studies and their associated permeability and construction material data. From this data it can be seen that PICP generally

have far higher infiltration rates than their subgrades and thus, the predevelopment conditions of the site however, their hydraulic performance is generally only as good as the selection of materials used within them and the subgrades on which they are built.

Table 6: A comparison of construction material and permeability data obtained in different studies.

Study Authors	Design Influx			Geological Origin of Pavement Construction Material				Mean Performance K (m/s)
	Storm	Rainfall Quantity	Equivalent K (m/s)	Surface	Base & Sub-base	Subgrade	Subgrade K (m/s)	
Beeldens and Herrier (2006)	1/30 year	270 l/s/ha	5.4×10^{-5}	Porphyry (Granite or Rhyolite)		Silty	NM	3.8×10^{-6}
Beeldens and Herrier (2006)	1/30 year	271 l/s/ha	5.4×10^{-6}	Porphyry (Granite or Rhyolite)		Sandy	1.03×10^{-3}	4.0×10^{-4}
Fassman and Blackbourn (2010)	1/2-5 year	1200 mm/hr	NM	NM	NM	Clay	NM	8.64×10^{-1}
Bean et al. (2007)	NM	NM	NM	NM	NM	Sandy	NM	72×10^3
Kumar et al. (2016)	NM	NM	NM	NM	NM	NM	NM	2.54×10^{-2}

*NM = No Mention

Apart from the importance of the origin of construction materials and subgrades on the hydraulic performance of PICP, some interesting structural design effects were noted in literature as well. Incline was one such aspect as shown by Castro et al., (2007) who showed that a difference from 0% to 2% in the incline at which a pavement was constructed, resulted in a shift of infiltration into the pavement from 70% in the first half of the pavement to the middle and end of the pavement instead. Similar effects were observed by Kamali et al., (2016) where the ratio of horizontal to vertical hydraulic conductivity of the pavement shifted from nearly 0.5 to 3.5 with an increase of 2% in incline. This implies that site topography and slope of the pavement are also factors not to be overlooked in PICP design.

Lastly, despite their performance, PICP are not immune to failure. Common failure mechanisms of PICP include bad grading of their construction materials, clogging of either the surface or geotextile layers, adding fines to certain layers such as the bedding and sub-base layers to improve compaction, incorrect concrete brick selection and heavy silt loads (Technicrete, 2017). Thus, the design of PICP is a fine balancing act between the physical and hydraulic requirements of the pavement and the materials available for their construction.

3 APPARATUS

Due to the scale of variables involved, it was decided to evaluate flow through pavements in terms of two models. The first was the basic model, consisting of a small elementary volume with a simplified ICP layer works, aimed at determining the effect of incline on the hydraulic performance of pavements. This would illuminate considerations that had to be made on the larger scale and assist in the design of the full-scale apparatus and the methodology applied within it. Once the basic model was understood, the second, full-scale model was designed. It consisted of a large volume of PICP with a complex layer works tested in the Infiltration Table Apparatus (ITA). The full-scale model was used to determine the effect of the remaining variables on the flow through PICP such as the effect of different layer materials, their orientations and effect on one another. These results would then be compared to that of the field tests to assess their validity.

3.1 FIELD TESTING

It was decided to begin the study with a series of field tests to establish a baseline for the data obtained and to guide the design of later test apparatuses. A double ring infiltrometer was constructed for this purpose based on methods stipulated in ASTM D3385 (1994). This infiltrometer was of a slightly modified design to facilitate easier transport as well as to allow it to fit in the base of test pits in the field. The outer ring consisted of a steel tube with an inner diameter of 300 mm, a wall thickness of 4 mm and a height of 300 mm. The inner ring was made of clear acrylic and had an inner diameter of 140 mm, a wall thickness of 2 mm and a length of 500 mm. A tape measure was inserted into the inner ring in such a way that its zero mark was in contact with the testing surface to measure the change in head. (Fig. 8)



Fig. 8: The Double-Ring Infiltrometer constructed for field tests conducted on the Brooks St. site.

For field evaluation of already installed PICP, it was decided to construct an additional customised test apparatus, based on the principles of the ASTM C178 (2013), single ring infiltrometer. This was because of the issues highlighted in literature regarding their application on PICP. The customised apparatus would allow for faster on-site testing of PICP as well as infiltration testing of a single paving unit, which cannot be otherwise conducted with the standard ASTM C178 (2013), apparatus (Fig. 9). This apparatus consisted of a clear PVC tube with an inner diameter of 86 mm and a wall thickness of 2 mm. The tube was 495 mm in length and was marked incrementally at 10 mm intervals starting at a height of 100 mm from the test surface end. In addition, it was fitted with a rubber gasket and a weight bearing frame which created a seal on the test surface, allowing for rapid testing in multiple locations without the need for an adhesive. Downward force on the frame was supplied by an 8.4 kg sandbag.

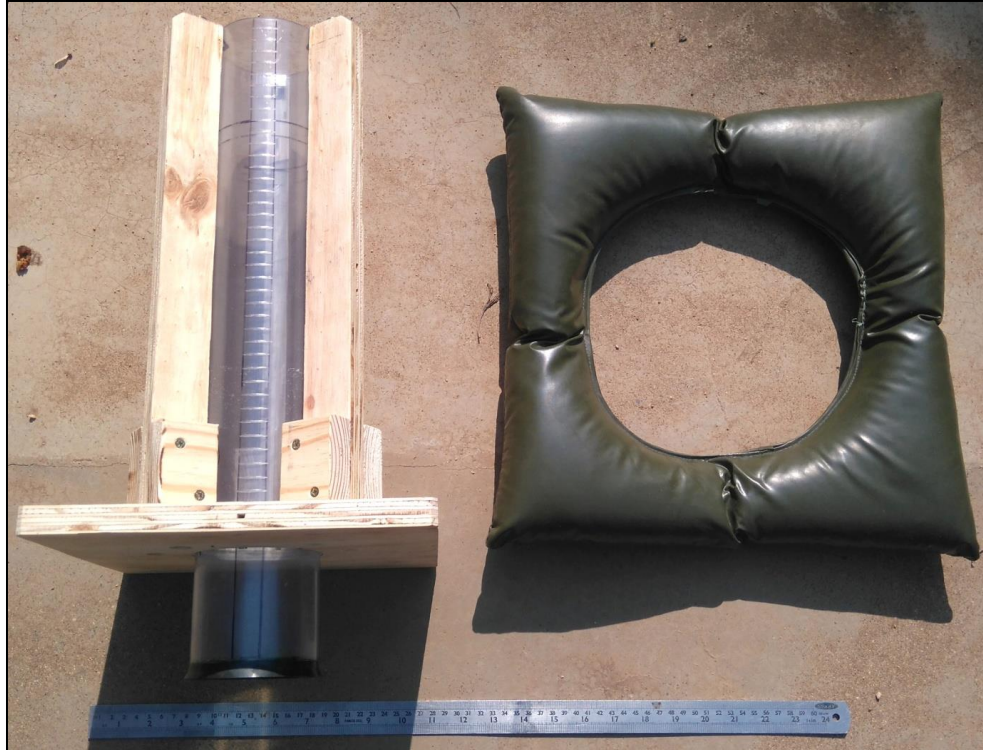


Fig. 9: The custom Single Ring Infiltrometer constructed for field tests of already installed PICP.

3.2 BASIC MODEL

Various test methods and apparatuses were considered for this part of the testing procedure and it was decided to construct a custom set of apparatus which will hereafter be referred to as the Basic Model Apparatus (BMA). The BMA along with all of its components, excluding the water source, is shown in Fig. 10. The part of the BMA shown in Fig. 10(a) consisted of 3mm steel plate, which could be inclined accurately in 1° intervals and in which the elementary volume of ICP could be constructed and tested. It measured 1000 mm long, 500 mm wide, 200 mm high and had drainage holes in the base for the measurement of five infiltration volume variables. The five volumes included surface runoff, horizontal subsurface flow (Point 4) and the volumes of vertical flow at 250 mm intervals (i.e. 250 mm, 500 mm and 750 mm from the elevated side, labelled point 1, 2 and 3 respectively). Detailed technical drawings used in the construction of the BMA are included in Appendix A. Controlled volumes of water were provided to the BMA by the wetting system shown in Fig. 10(b). It consisted of a wooden frame holding a length of perforated hose which was capped at one end, through which water entered the system, evenly wetting the surface of the elementary volume. The incline of the BMA was controlled by a jack placed at one end as shown in Fig. 10(c). The incline of the BMA was measured with a plumb-line and protractor which was attached to the side as shown in Fig. 10(d).



Fig. 10: The apparatus constructed to perform tests on the representative volume for the basic flow model.

3.3 FULL-SCALE MODEL

Based on information gained in literature, consultation with practitioners, field tests and the basic model, an Infiltration Table Apparatus (ITA) was designed and constructed to accommodate the Full-scale Model, using funding and laboratory facilities from Bosun Brick (Pty) Ltd. The designs of the ITA tabled are presented in Appendix: A. The ITA that was constructed for the study from these designs is represented schematically in Fig. 11 and shown in Fig. 12. The apparatus consisted primarily of 200 x 100 mm IPE beams, 2 mm stainless steel plate and 25 mm steel square tubing. Tempered glass measuring 9mm thick was used for the sides and front of the construction area of the apparatus.

The apparatus measured 6 m in length and 2 m in width, with 6 mm slots cut into the construction surface (deck), perpendicular to the flow direction within it, at 1 m intervals. The slots were cut in 191 mm and 132 mm intervals across the width of the ITA to direct flow past the structural beams. As a precaution against subsurface flow passing from one meter of PICP to the next between these slots, 10 mm steel rods were welded to the construction surface to direct the flow (Appendix B). The slots were directly above outflow collection bins (catch trays) under the construction surface (Q_1 - Q_4), which in-turn were connected to flow meters that measured the real-time outflow at each point. A water reservoir (inlet box) at the upper end of the apparatus provided the influx (Q_{IN}), while the tempered glass sides provided a view of what occurred within the subsurface layers during testing. A thick, steel divider retained the PICP constructed in the ITA at the 4 m mark, allowing any runoff to be measured in real time too (Q_S /RUNOFF).

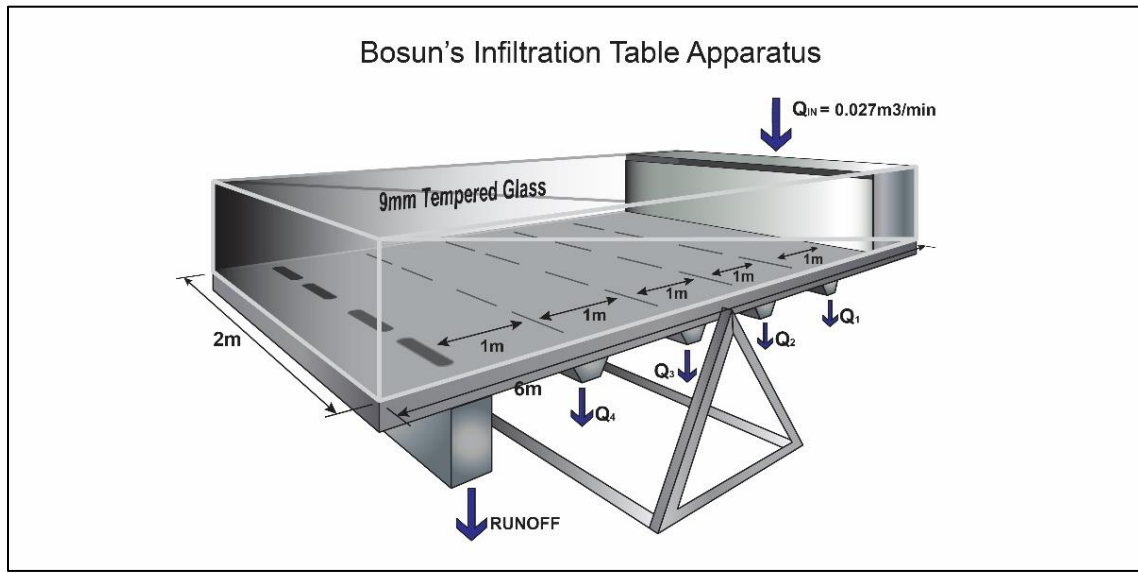


Fig. 11: A schematic diagram of the Infiltration Table Apparatus.



Fig. 12: An image of the Infiltration Table Apparatus in the quality control laboratories at Bosun Brick Midrand. (2018)

The ITA was designed to be tilted along its half-length axis from 0° to a maximum of 6° relative to horizontal. Tilting was supplied by scaffold jacks and a 4 Mg block-and-tackle at the front and rear of the apparatus. The ITA was designed to accept 8 m^2 of any PICP, constructed according to industry guidelines, provided the PICP did not exceed a total height of 420 mm.

3.3.1 Model Water Cycle

Water entering the ITA was supplied by a 1000 ℓ plastic tank, connected to the water mains, on a platform 2.3 m above the floor of the Bosun laboratory floor (Fig 13). This tank, the supply tank, supplied water to the ITA reservoir via 50 mm PVC pipe which in turn, were connected to 3 Elster Kent V100 PSM water meters. These meters supplied the Q_{IN} value and will furthermore be referred to as “Inlet Meters”. Three ball-cocks were installed directly after the inlet meters for two reasons. Firstly, closing the supply to the ITA reservoir after the inlet meters would ensure that they remain saturated when testing was not being conducted. This was an important step in ensuring the meters performed adequately, as if the meters were allowed to dry, the internal components would often become cemented together by calcium precipitates and stall, depending on the water quality. Secondly, the ball-cocks would allow for a variable Q_{IN} . By closing one or more of them completely or partially, the amount of water flowing into the reservoir and thus the amount of water entering the system could be controlled.



Fig. 13: The 1000 ℓ water tank that provided water to the ITA for testing (Bosun – Midrand, 2018).

The ITA reservoir had a slot cut into the top of its forward-facing side, 460 mm from the base, such that when the it was filled, any additional water entering it would exit the slot in sheet flow. Water flowing out of the ITA reservoir then ran onto the surface of the PICP that was constructed within the ITA for each test. Depending on the chosen PICP, water that flowed through it would exit through the slots in the construction surface to be caught in the collection bins below.

To prevent damage or clogging of downstream flow meters and other equipment, non-woven polyester filter media measuring 0.3 mm thick was placed into each of the bins. The filter media was selected to remove particles larger than 0.4 mm. Water collected in each bin was drained via 50 mm PVC pipe to 5 Madalena DS TRP flow meters and then into the bottom half of another 1000 l collection tank (Fig 14). These flow meters will hereafter be referred to as the “Outlet Meters”. Readings from the flow meters were taken in High Definition video with a GoPro® camera mounted above the meters to provide real-time data. Large taps were again added between the outlet meters and the collection tank to keep the meters saturated when not in use.



Fig. 14: The outlet system of the Infiltration Table Apparatus (Bosun – Midrand, 2019).

Once water had drained through the ITA into the collection tank, a submersible pump moved the water back to the raised supply tank for reuse. This meant that test durations could be lengthened to any requirement. Fines washed out of the PICP in the ITA were captured by the filters in the collection bins and by settling in the collection tank, ensuring that they would not be reintroduced to the PICP.

3.4 ADDITIONAL APPARATUS

A second smaller double ring infiltrometer was constructed for application within the ITA, again based on findings in literature and the methods stipulated in ASTM D3385 (1994). The design of this apparatus was also smaller than that stipulated by ASTM D3385 to focus infiltration upon the joints of the concrete bricks used in the surface layer, in an attempt to circumvent horizontal migration and upward percolation of water outside the ring as demonstrated by Bean et al., (2007) (Fig. 15). The inner ring in this case, consisted of the clear PVC tube used in the custom single ring infiltrometer used for field testing. The outer ring was made of polyethylene, had a height of 180 mm, a wall thickness of 1 mm and an inner diameter of 175 mm. The outer and inner ring were sealed to the PICP with adhesive putty before each test.

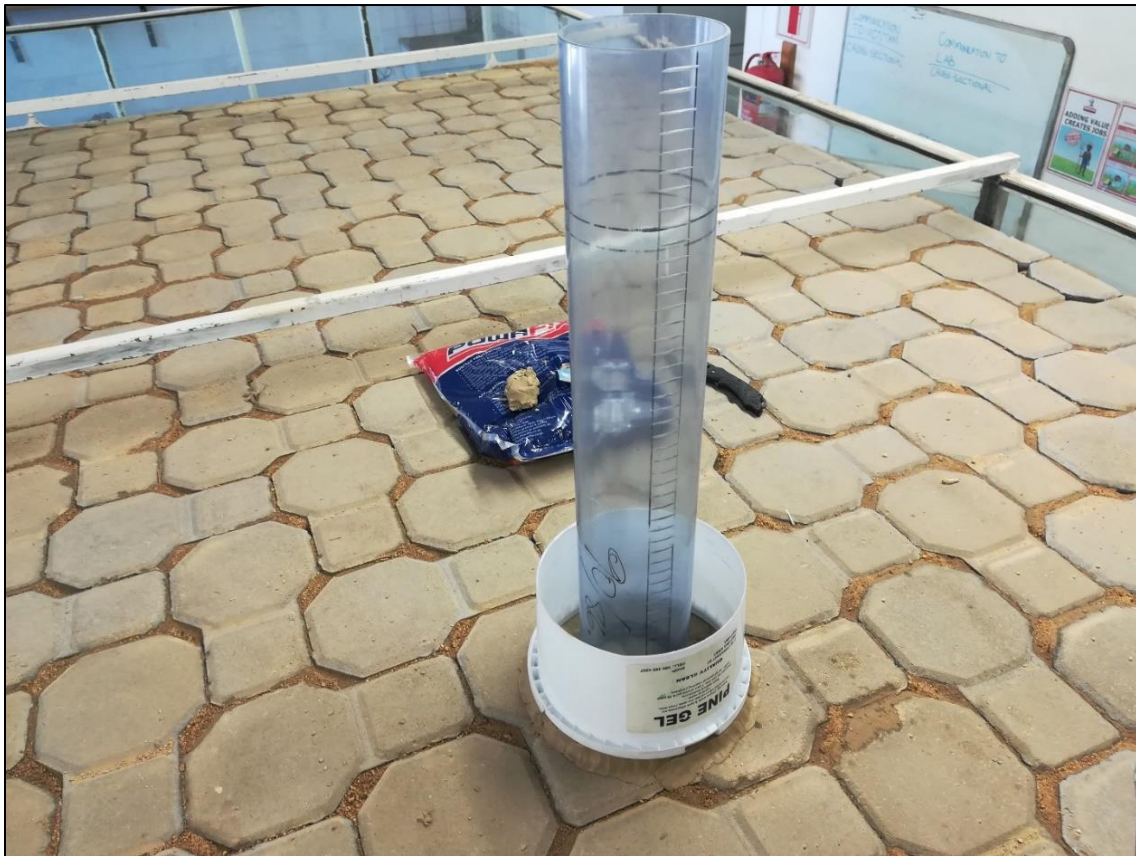


Fig. 15: The joint-focused Double Ring Infiltrator constructed for use within the ITA.

4 MATERIALS AND METHODS

4.1 FIELD TESTING

Permission was obtained from the owners of a property on Brooks Street, Brooklyn, Pretoria to carry out infiltrometer tests on the in-situ material there. All testing on this site was conducted with the custom double ring infiltrometer apparatus described in Section 5.1. The site was selected because the in-situ material consisted primarily of silty-sand and highly weathered quartzite gravel, a common subgrade for pavements throughout South Africa. As stated in literature, the subgrade is often prepared for the construction of a pavement by scraping off or excavating the upper layer of soil, removing deleterious materials, organic matter and exposing the more stable portions of the underlying soil profile. Thus, the infiltrometer tests were carried out in the base of test pits on the site to resemble the slightly excavated conditions upon which pavements are commonly constructed.

Fifteen double-ring infiltrometer tests were conducted in two 0.7 m deep test pits. The tests entailed driving the two rings into the in-situ material in the base of each test pit. Water was then added to the space between the inner and outer ring to a height of 150 mm above the testing surface and maintained there for the duration of the tests. The inner ring was filled with water to a height of 150 mm above the testing surface and the tests were commenced. The time taken for the water height in the inner ring to fall by 10 mm was measured, it was refilled to a height of 150 mm and then timed again until the difference between each measurement was less than 3 s. This was taken to be when steady state flow had been achieved and the test was then repeated a minimum of three more times to gain accurate data for the calculation of the hydraulic conductivity of the in-situ material. The obtained test data is given in Tables 7 and 8. The test pits were also investigated further using a hand auger and profiled by an engineering geologist according to the methods described by Brink and Bruin (2001), "Guidelines for soil and rock logging in South Africa" as summarised in Appendix C.

4.2 BASIC MODEL

The basic model used in the BMA was an elementary 0.0875 m^3 volume representing an ICP. It consisted of a homogeneous layer of sand, in place of the actual complex sub-surface layer works, beneath a concrete brick surface layer. This elementary volume would be subjected to inclined hydraulic testing within the BMA. Instead of testing the full elementary volume right away, it was decided to conduct the testing in two parts to assist in the design of the ITA and the testing procedures to be used within it. The first part looked at the effect of incline on the flow through the sub-surface layers. The second part of the testing process looked at the effect that the addition of a surface layer, as defined in the South African standards document TRH14 (1980), has on flow through a paving system.

When selecting materials for the elementary volume, products and methods for the construction of ICP were evaluated and due to the large variety of them, one product, from one manufacturer, was selected for study in the basic model. The product selected for the surface layer was a standard rectangular paver with a beveled edge manufactured by MVA Bricks (Pty) Ltd, as shown in Fig. 16(a). In addition to this, an arrangement or laying pattern had to be selected for testing in the model. It was decided to use the herringbone pattern as described in Cairns, (N.D.) which is shown in Fig. 16(b) due to its widespread application in industry. Further information provided on the durability and absorption of the selected product is included in Appendix D.



Fig. 16: (a) The selected brick paving unit, Product 55: Bevelled and (b) the selected arrangement of bricks for the surface layer. (Supplied by MVA Bricks Pta. West)

The sand selected for the sub-surface component of the elementary volume was a standard contractor's coarse building sand, hereafter referred to as a P-Type 4 and further detailed in Section 6.3.5. The P-Type 4 sand was selected for this part of the model due to its widespread use in industry as a bedding sand in conventional ICP and because its hydraulic performance closely mimics that of several subgrades found throughout South Africa.

4.2.1 Preliminary Testing

The first step was to clean and prepare the BMA (Fig. 17(a)) by placing 2.5 mm aperture stainless steel mesh over all exit points, as seen in Fig. 17(b). This was done to prevent excessive loss of material from the homogeneous sand layer during testing. The next step was to fill the BMA with 0.0575 m³ of P-Type 4 sand representing the subsurface layer works of an ICP as shown in Fig. 17(c). The sand was then dry-compacted to a final volume of 0.055 m³ by hand. Compaction of to the specifications outlined in SANS 1200-MJ (1984), was not possible due to the strength limitations of the BMA. The wetting system was then placed over the BMA and the sand was saturated with water as shown in Fig. 17(d). Saturation was deemed to be achieved when a constant stream of water exited all four points in the base of the BMA simultaneously. Once the sand was saturated, the BMA was placed in a perfectly horizontal orientation and 5 ℓ of water was released onto the surface of the sand layer. The time taken for the 5 ℓ of water released to exit the system completely was measured. The start time was taken to be when water droplets exited the BMA at a rate of more than 1 droplet per second. The end time was taken to be when droplets exited the BMA at a rate of less than 1 droplet per second. This procedure was repeated four times and the results were recorded and tabulated in Table 9. A surface layer was then added to the elementary volume and it was tested one more time as a verification step. The average of these measured times was used as the termination time for individual tests thereafter, 7.5 min (449.8 s).

4.2.2 Sub-surface Testing

The testing procedure used in the BMA to evaluate the effect of incline on the flow through sub-surface layers of ICP is shown step-by-step in Fig. 17. This part of the testing procedure followed directly after the preliminary portion with the surface layer once again removed. Firstly, 5 ℓ of water was released onto the surface of the elementary volume and the volumes of water exiting at the various exit points were captured in 2 ℓ containers as shown Fig. 17(e). This procedure was repeated with the BMA at inclines of 0°, 2°, 6° and 10° respectively. Water captured at the exit points in each case was measured when droplets exited the BMA at a rate of less than one droplet per second or when the termination time was achieved. This was done with a graduated plastic measuring cylinder as shown in Fig. 17(f) and special care was taken to note any differences in the colour of the water at the various exit points.

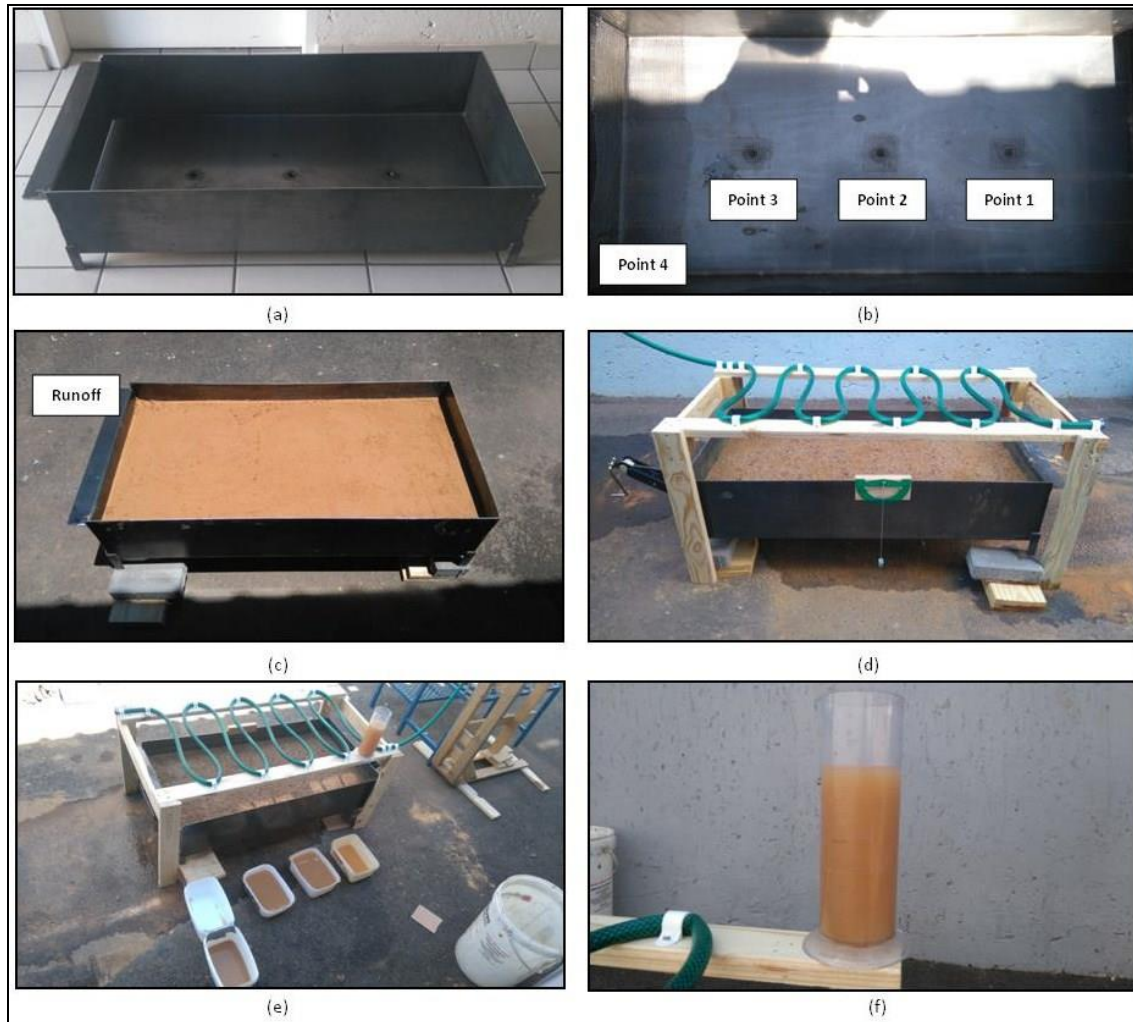


Fig. 17: A step-by-step illustration of the testing procedure used for the sub-surface layers of a concrete brick paving system.

4.2.3 Surface Testing

This part of the testing procedure is shown step-by-step in Fig. 18. The same configuration of the BMA was used in this portion of the testing procedure as before, however, a surface layer of concrete bricks was added to the elementary volume (Fig. 18(b)). The addition of the bricks would serve as the full elementary volume for the basic model and allow for the detection of the surface layer's influence on flow through an ICP. As before, after saturating the elementary volume, 5 ℓ of water was released into the BMA and the volume of water exiting at the various exit points was captured in 2 ℓ containers (Fig. 18(c)). This procedure also was repeated with the BMA at inclines of 0°, 2°, 6° and 10° respectively.

The water captured at the exit points was measured when droplets exited the BMA at a rate of less than one droplet per second or when the termination time was achieved, with a graduated measuring cylinder and the results were recorded and tabulated in Table 11. In addition, special care was taken to note any differences in the colour of the water at the various exit points.

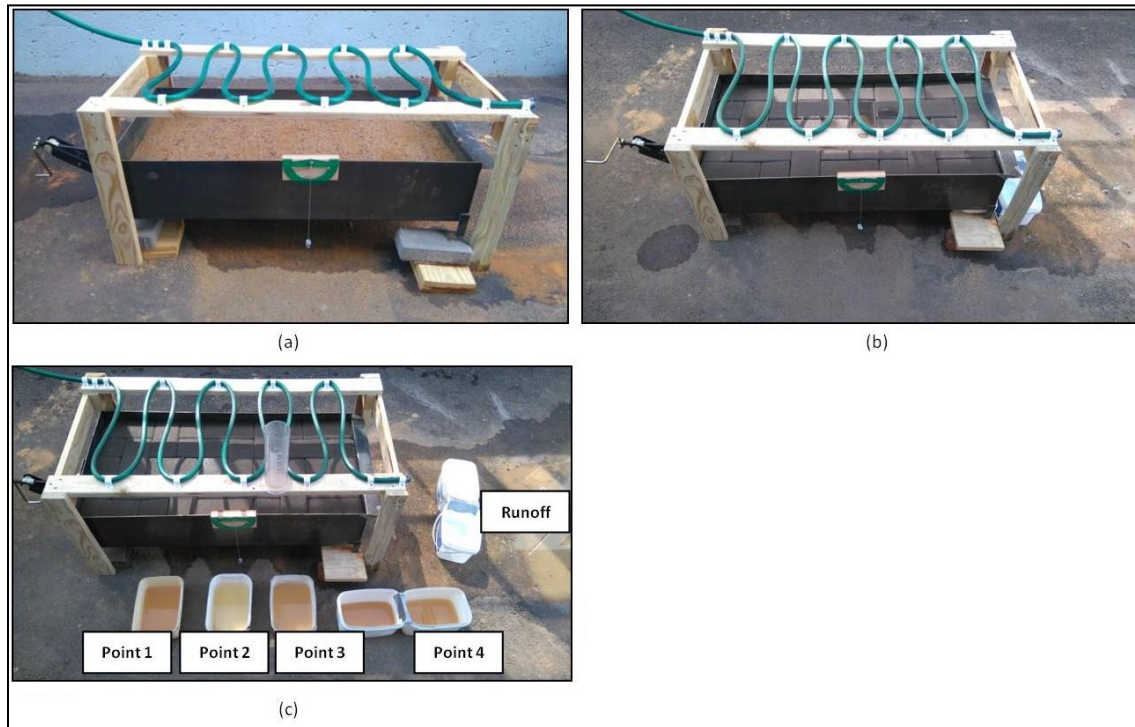


Fig. 18: A step-by-step illustration of the testing procedure used for the surface and sub-surface layers of a concrete brick paving system.

Following the testing process which entailed repeating the surface and sub-surface tests twice for each inclination, the recorded results were tabulated and statistically evaluated. The statistical evaluations are shown and discussed in Section 7.2 along with the implications they had on the Full-scale Model, the design of the ITA and the methods applied in it.

4.3 FULL-SCALE MODEL

The Full-scale Model was designed based on information obtained in the field and Basic Model testing. It consisted of a 3.36 m³ representative volume of Full Infiltration PICP which would be constructed exactly as in industry and subjected to hydraulic testing in the ITA. The model was designed to further inform on the overall hydraulic properties of PICP, the effect of different layer materials and incline on these properties. This resulted in a large number of variables for the study and so, before the design of this model was finalized, a number of preliminary tests were conducted to refine it and remove variables which had little to no effect on PICP hydraulic properties.

4.3.1 Model Design

Several practitioners and pieces of literature were consulted and a conceptual design for the Full-scale Model was tabled. It was based on the current industry requirements in South Africa, the experiences of these professionals and the questions they had pertaining to the performance of PICP. It took into consideration nearly every conceivable variable that could have an effect on PICP hydraulic properties which included, but was not limited to:

- 1) The effect of each separate layer;
- 2) The effect of the thickness of each layer;
- 3) The effect of the packing orientation (orientation of brick joints) in the surface layer;
- 4) The effect of different materials in each layer;
- 5) The effect of incline;
- 6) The effect of the volume of water influx;
- 7) The effect of different types of water influx (simulated rainfall vs. sheet flow).

This presented a unique challenge as the sheer quantity of different materials that had to be acquired would make the project unviable. It was then decided to select a generic layer works (GLW) and subject it to iterative testing to eliminate as many of the variables that had little to no effect on the model as possible. The first stage of the iterative testing looked at which layer had the largest effect on PICP hydraulic properties. This was done by constructing the full GLW, from top to bottom, one layer at a time and subjecting them to testing in the ITA each time a layer was added. All tests were done at maximum Q_{IN} , for approximately 10 minutes, at an incline of 2.5°.

The GLW consisted of five layers, explained in greater detail in Section 6.3.3, with the natural subgrade being removed from the model by the construction surface of the ITA, as follows:

- 1) Bosun Waterwise® bricks in a specific pattern for the surface layer (Fig. 19);
- 2) No fines sand (P-Type 1) for the jointing material/Other;
- 3) A 30mm thick layer of P-Type 1 sand for the bedding layer;
- 4) Bidum® A2 for the geotextile layer;
- 5) A 150 mm thick layer of 6 mm crushed quartzite for the upper sub-base layer;
- 6) A 150 mm thick layer of 20 mm crushed quartzite for the lower sub-base layer;

In the case of the surface layer, it was constructed above a 15 mm thick layer of 6 mm gravel, to eliminate interference from the 10 mm guide rods welded to the construction surface. It was also tested without the addition of jointing material, after which, different jointing and bedding courses were added and it was tested again. The volumes exiting through each outlet meter were recorded in each test and retained for comparison against the previous and next iteration.

Based on the information obtained in the first stage, the second was designed and commenced. It looked at the effect of packing orientation of the concrete bricks on PICP hydraulic properties. This was done by repacking the surface layer of the GLW with the bricks rotated horizontally by 45°, keeping the selected packing method or pattern constant. In the previous stage, the long joints of the bricks were parallel to the direction of flow, thus in the second, they were at 45° to the flow direction (Fig. 19). It was again subjected to testing in the ITA at maximum Q_{IN} , for approximately 10 minutes, at an incline of 2.5°. The results were recorded and retained for comparison as before.

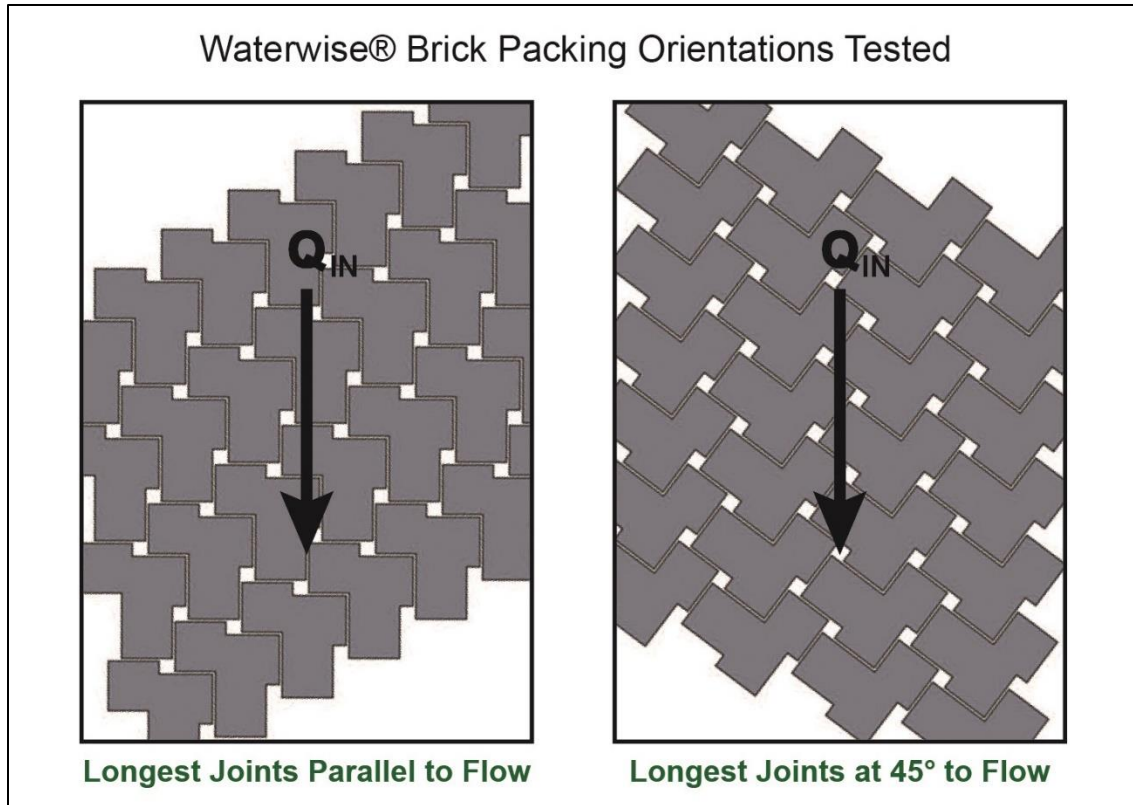


Fig. 19: A schematic diagram of the concrete brick orientations used in the surface of the Generic Layer Works during the Model Design Testing

Based on the results of the previous two stages, the third and final stage of preliminary testing was designed and commenced. This stage looked at the effect of incline on PICP hydraulic properties. The surface layer of the GLW was firstly returned to the orientation used in the first stage and then the GLW was subjected to testing in the ITA at maximum Q_{IN} , for approximately 10 minutes but this time, at inclines of 0°, 2.5° and 5° or 0%, 3.5% and 7.8% respectively. The results of each test were recorded for comparison and based on them and the results of the previous two stages, the final Full-scale Model was designed with special consideration to the effect of influx, the selected materials and incline.

4.3.2 Model Design: Influx

The ITA was originally designed to reproduce a wide variety of real-world situations for the purpose of this study. The first of these was a large water influx onto a pavement. The mechanism chosen to supply this influx was sheet flow as it most accurately represented what a section of PICP would experience below the downpipe of a large structure or if the PICP were in a low-lying position on site. Areas of PICP that are subjected to sheet flow commonly experience the highest influx of water and as such, are most likely to suffer damage. In the Pretoria area of South Africa, typical rainfall amounts can be as much as 54 mm during one 30 min storm (Fig. 20). As a result, PICP and their associated drainage systems, are commonly designed with the known values for the 1 in 20-year storm, in their installation region, in mind. Thus, the volume of influx that was selected for all tests in the Full-scale Model, was the maximum possible flow rate that the ITA could supply ($Q_{IN} = 0.027 \text{ m}^3/\text{min}$), far greater than typical rainfall quantities for this region.

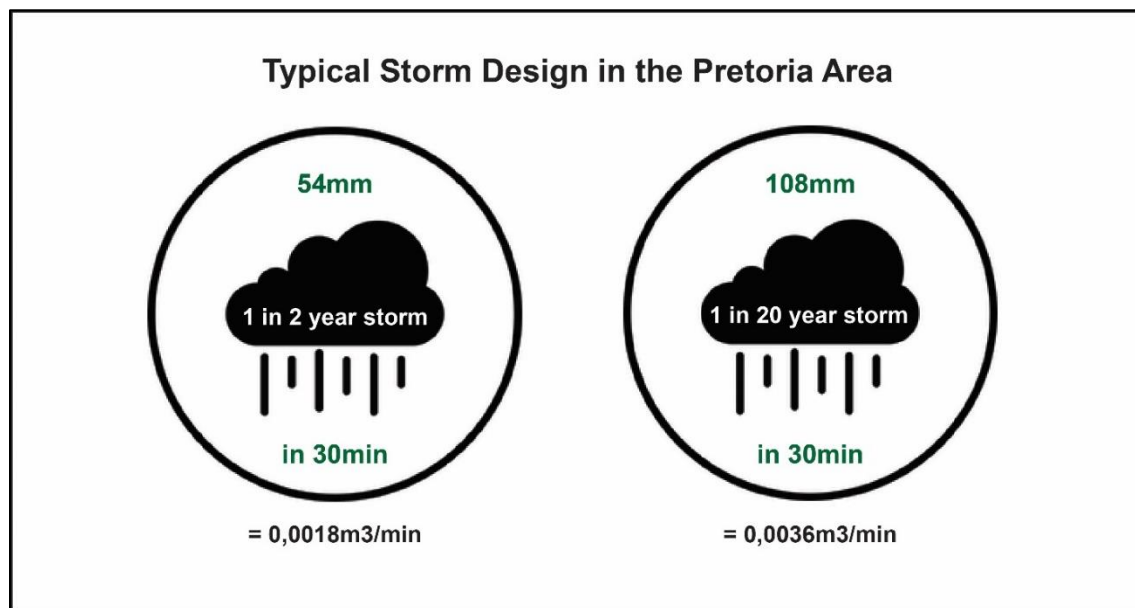


Fig. 20: Typical rainfall design parameters for the Pretoria area, South Africa – Courtesy of PVA Consulting Engineers cc.

4.3.3 Model Design: Layer Works

The layer works selected for the Full-scale Model was based on consultation with several practitioners, guidelines set out in Technicrete (2017) and TRH14 (1980) and the results of the preliminary testing. It aimed to encompass the most commonly applied materials and thicknesses used within the Pretoria region for a Type-A PICP. It consisted of the same five layers used in the GLW (Fig. 21), however, the surface, bedding and jointing materials were to be exchanged throughout testing to investigate their effect on the model performance as stated by Kumar et al.,

(2016) and Beeldens and Herrier, (2006). Starting at the top, the layer works for each test included; A surface layer consisting of one of two selected permeable pavement products, in combination with one of five selected bedding and jointing materials/sands, explained in greater detail in Section 6.3.5. For uniformity, the bedding sand and jointing sand consisted of the same material for each individual test and the bedding layer thickness was kept constant at 30mm.

Below that, a single geotextile layer of A2 Bidim® manufactured by Kaytech Pty Ltd. was placed. The geotextile was a nonwoven, needle-punched, continuous filament, polyester fabric with an average pore size of 170 µm and hydraulic conductivity of 4.2×10^{-3} m/s, similar to that of a uniform, coarse sand. This was followed by two 150 mm layers of 6 mm and 20 mm crushed quartzite gravel layers respectively to form the upper and lower sub-base layers. It was decided to exclude the effect of the subgrade in the model for two reasons. The first was that the variability of possible subgrades would be out of reach of this study in terms of its budget and time constraints. The second was that this study aimed at providing performance data for PICP without the influence of the subgrade, allowing for more effective pavement design over complex subgrades with known rates of influx from the planned pavement above.

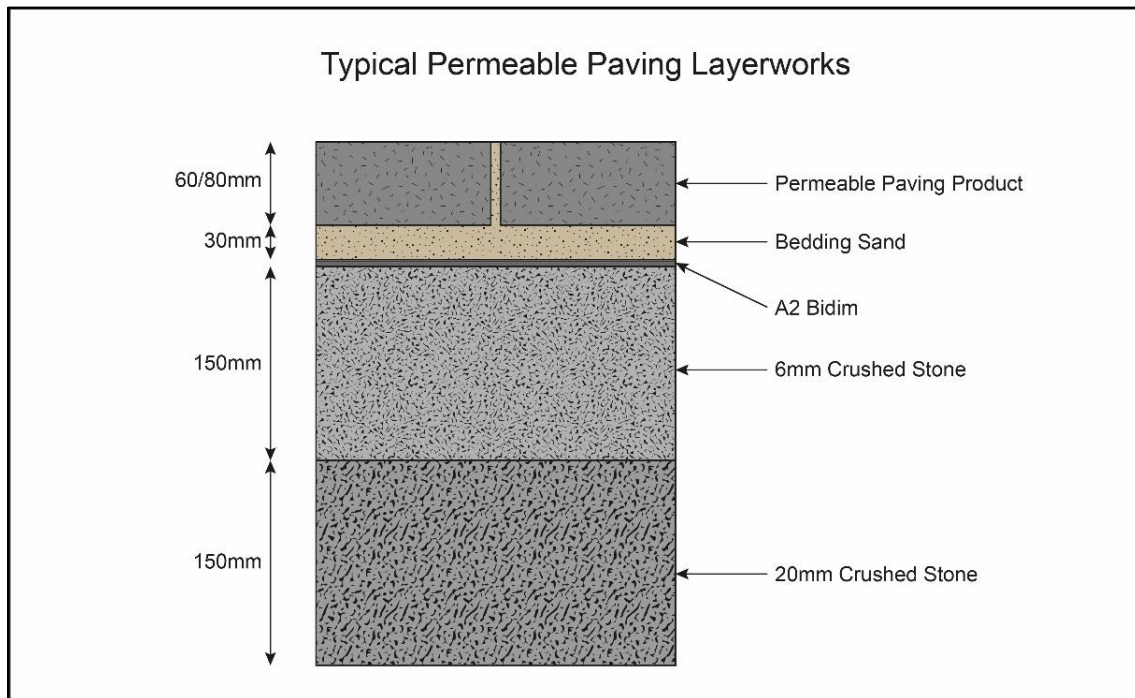


Fig. 21: A cross-section of the layer works used inside the Infiltration table apparatus for the study.

4.3.4 Model Design: Bricks

Following the design of the layer works of the Full-scale Model, several products and manufacturers were considered for use in the surface layer. Due to the large variety available, it was decided to use only two PICP capable products. These two products had to have similar dimensions to those most commonly applied in industry, but also had to differ from each other significantly enough to further inform on the effect of using different products as first highlighted by the preliminary tests. The two products chosen were the Waterwise® and Citylock®, manufactured by Bosun Brick (Pty) Ltd. These products had very similar dimensions to standard interlocking concrete bricks, both measuring 60 mm in height, were affordable enough for widespread application in industry and differed from one another in design (Fig. 22).



Fig. 22: Two of the permeable paving products available from Bosun.

In addition to their price and dimensions, the Waterwise® and Citylock® pavers had another attribute which made them attractive for application in the Full-scale Model; the ability to vary the permeability of the surface layer by using different packing methods. This provided flexibility for expansion of the testing procedure if required. Due to the findings in the preliminary testing and for the purposes of this study however, only one packing method was selected for each product (Fig. 23). The selected packing methods provided intermediate permeability, with the brick layer having approximately 20% of its surface area consisting of free space, to be filled by the jointing material. More information about the various packing methods can be obtained from Bosun Brick (Pty) Ltd.

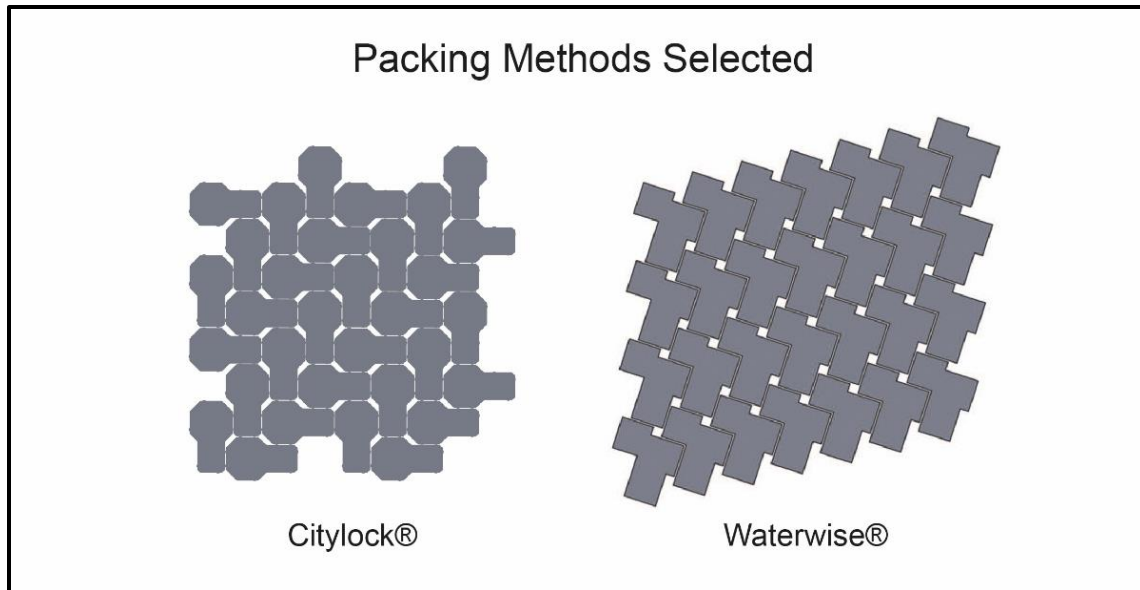


Fig. 23: The two packing methods selected for use in the Infiltration Table Apparatus.

4.3.5 Model Design: Bedding and Jointing Sand

Practitioners and literature recommend that the sand chosen for bedding and/or jointing material in PICP meet certain criteria. They should have no Plasticity Index (PI) and all particles should be at least 0.425 mm in diameter or larger. While a number of sands available throughout Southern Africa met these base criteria, the specific chemistry was not dealt with in great detail. Sands obtained in other regions or countries would most likely have different chemical compositions and thus a different long-term performance in PICP. To accommodate for this, it was decided to adopt a class system for the sands selected and used in this study, ensuring a degree of repeatability. Five classes were developed and one sand, meeting each class description was selected for use in the Full-scale Model.

No Fines Sand (P-Type 1):

This sand was a specially sourced, washed and sieved, silica rich, no-fines sand. This type of sand is commonly only available from specialist suppliers and is less affordable than most other sands on the market. This is due to the high degree to which its particle size is controlled. P-Type 1 sands are widely recommended by practitioners for use in PICP. Any chemically stable, adequately hard sand, with 80% of particles by weight falling between 1.0 – 5.0 mm in diameter, was classed a P-Type 1 sand (Fig. 24). A P-Type 1 sand was selected for use in the Full-scale model to inform on the hydraulic properties of an ideal PICP.

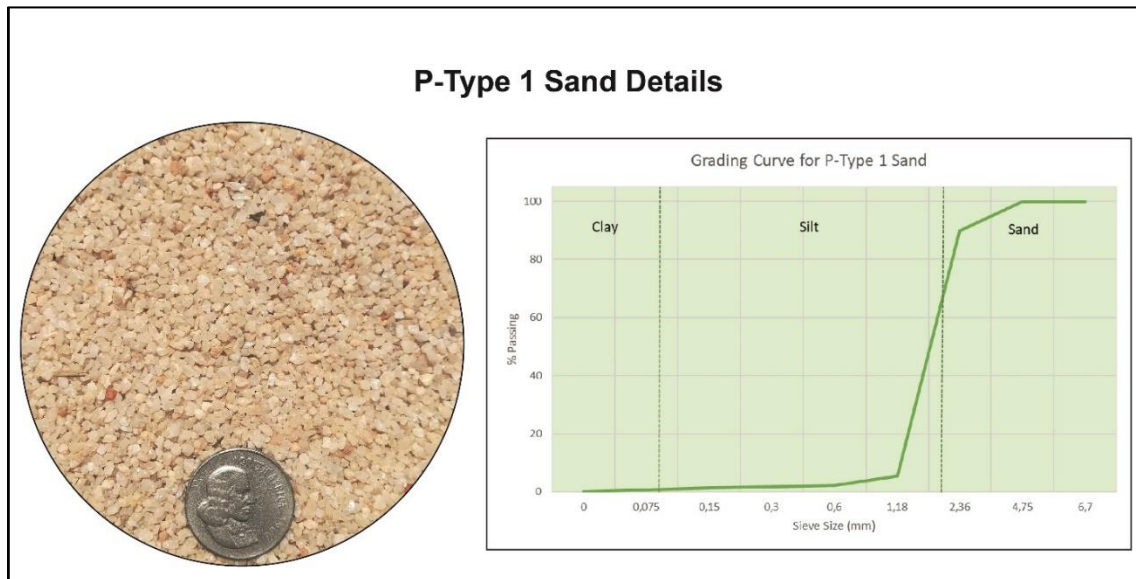


Fig. 24: The basic profile of what was termed a P-Type 1 sand for the purposes of this study.

No Fines Sand 2 (P-Type 2):

This sand was selected for use in the Full-scale Model as a verification of the P-Type 1 sand's effect on PICP hydraulic properties. It was also a specially selected, washed and sieved, silica rich, no-fines sand but from a different source to that of the P-Type 1. Its particle size was also highly controlled but not to the degree of the P-Type 1. The P-Type 2 sand was cheaper but could also only be sourced from a specialist supplier, making it less affordable than its more poorly sorted counterparts. Any chemically stable, adequately hard sand, with 80% of particles by weight falling between 0.85 – 5.0 mm in diameter, was classed a P-Type 2 sand (Fig. 25).

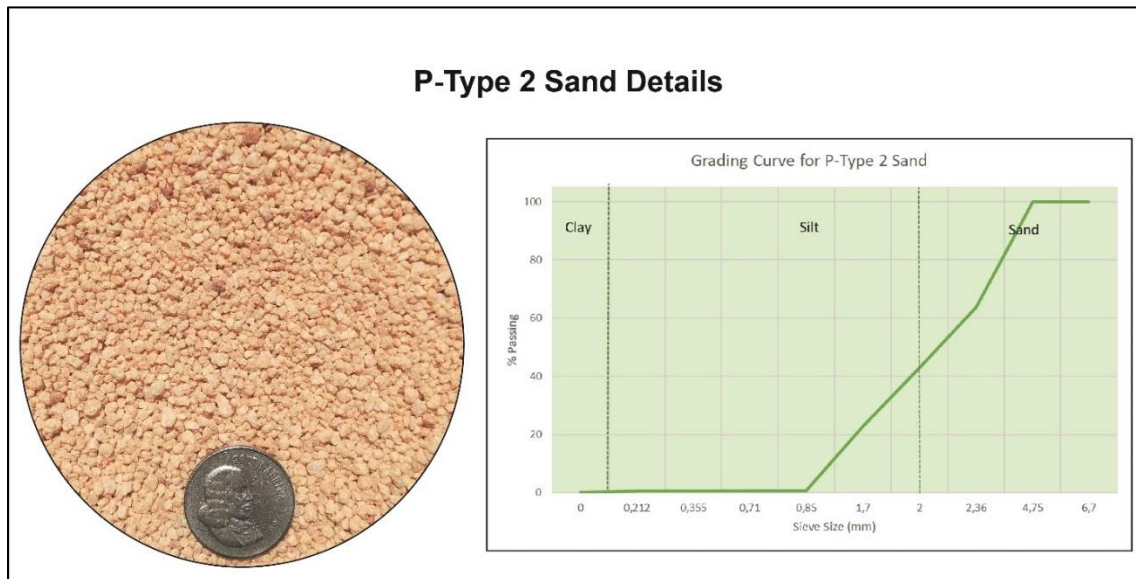


Fig. 25: The basic profile of what was termed a P-Type 2 sand for the purposes of this study.

Crushed Stone (P-Type 3):

This sand-like material was a finely crushed stone and is commonly available from quarries that are capable of providing a fair degree of particle size control. It was selected to investigate the effect of more affordable alternatives to P-Type 1 & 2 sands on PICP hydraulic properties. A sand-like material made from crushed rock, could have a lower chemical stability and durability than that of its counterparts if the parent material is of igneous origin such as a granite or is a chemical sedimentary rock such as dolomite. This is because these rock types rapidly weather, producing fine particles that may decrease the structural integrity and performance of PICP in the long term. For this reason, it was decided that a crushed stone rich in Quartz would be selected in this position in the Full-scale Model. Any quartz-rich, chemically stable, adequately hard crushed stone, with 80% of particles by weight falling between 0.4 – 2.0 mm in diameter, was classed a P-Type 3 sand (Fig. 26).

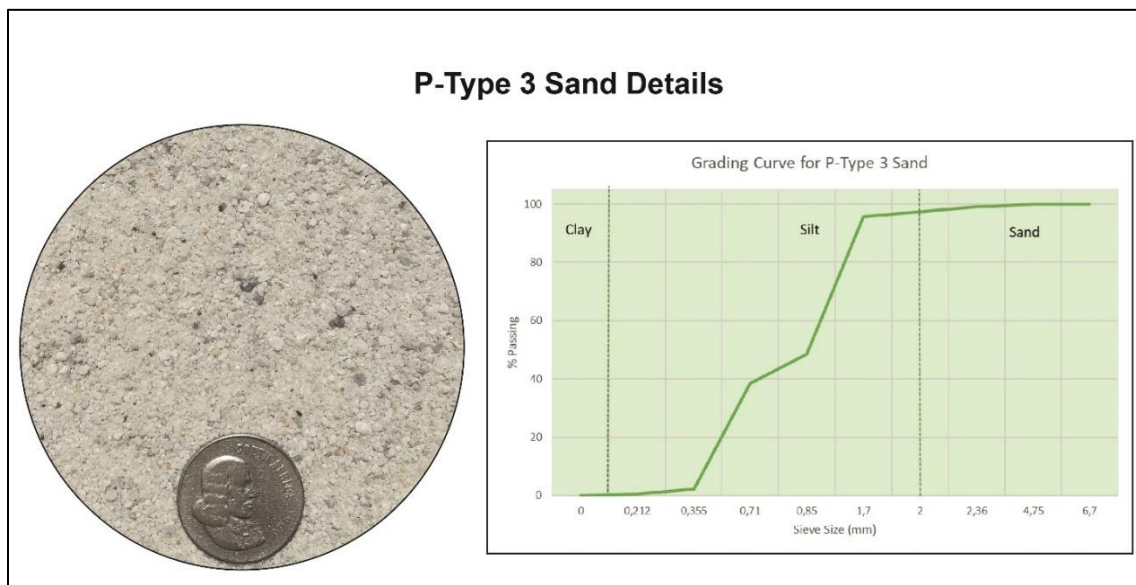


Fig. 26: The basic profile of what was termed a P-Type 3 sand for the purposes of this study.

Coarse Building Sand (P-Type 4):

The P-Type 4 sand was a silica rich, well-graded, general purpose building sand with a moderate number of particles below 0.425 mm in diameter and a low clay content. It was selected for use in the Full-scale Model to inform on the effect of using a highly affordable and available jointing and bedding sand on PICP hydraulic properties. This was done because many projects in industry do not require the full performance of PICP or simply do not have the budget. Any chemically stable, adequately hard sand, with 80% of particles by weight falling between 0.2 – 5.0 mm in diameter was classed a P-Type 4 sand (Fig. 27).

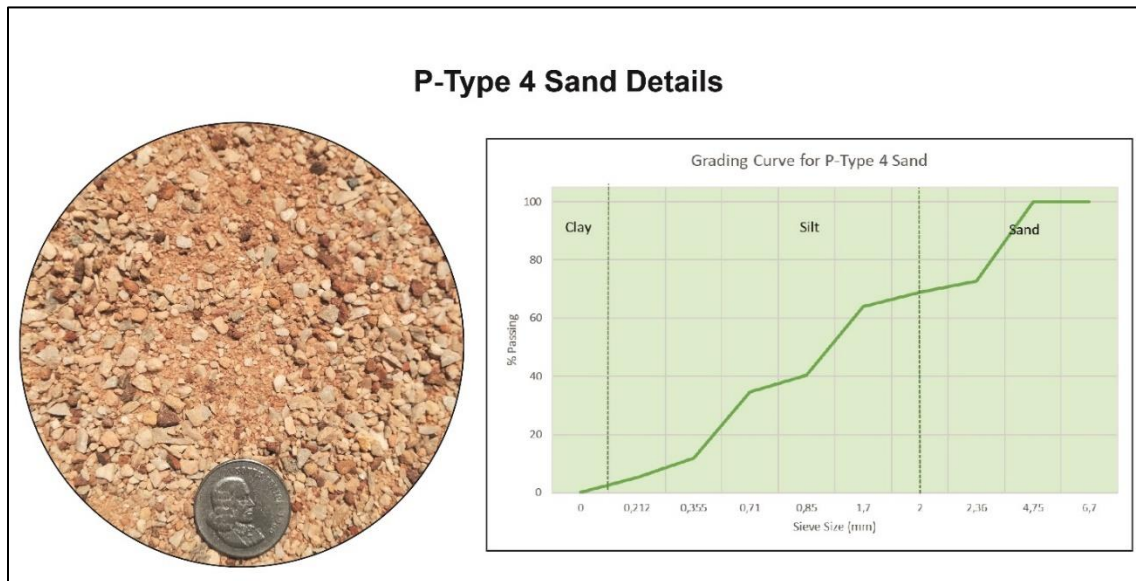


Fig. 27: The basic profile of what was termed a P-Type 4 sand for the purposes of this study.

Fine Building Sand (P-Type 5):

The sand selected for this class in the Full-scale Model was a poorly sorted, general purpose building sand, commonly used with a mixture of aggregate and cement to produce concrete. It consisted of a variety of minerals was highly affordable and readily available at even retail hardware outlets. This was done to represent the poorest possible construction of PICP and the effect of selecting such a sand on PICP hydraulic properties. Any sand with 80% of particles by weight falling between 0.2 – 2.36 mm in diameter was classed a P-Type 5 sand, regardless on chemical composition or hardness (Fig. 28).

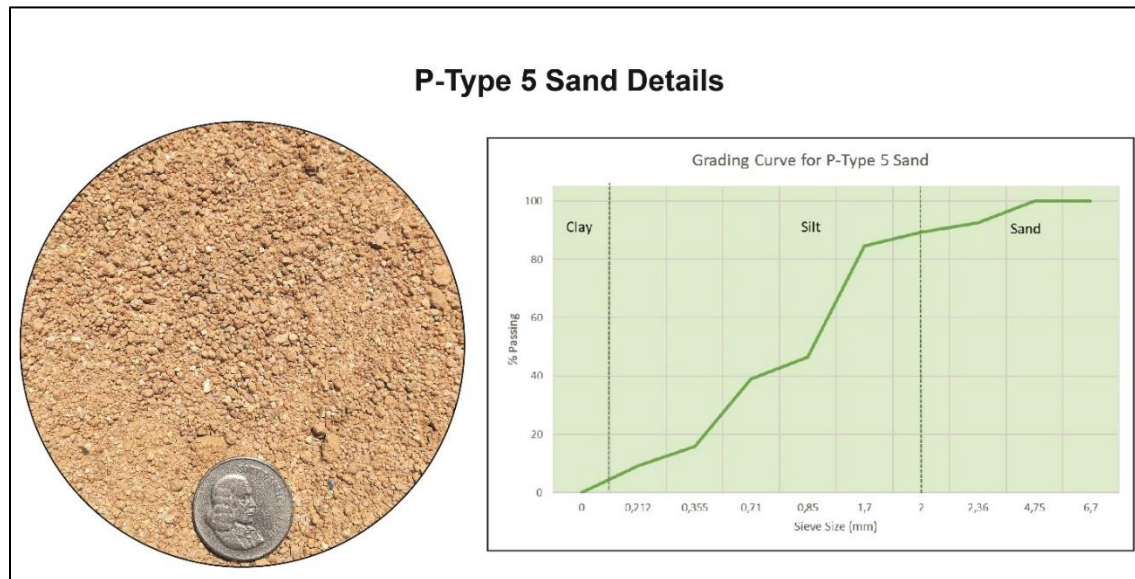


Fig. 28: The basic profile of what was termed a P-Type 5 sand for the purposes of this study.

4.3.6 Model Design: Incline

Information obtained from testing in the Basic Model, the preliminary tests and from consultation with practitioners showed that the effect of incline on the hydraulic properties of PICP could not be ignored. Inclines of as little as 2° or 3.5% that extend over a large area of any pavement can also have a profound impact on downslope drainage and many heavy vehicles have limits to the inclines they can traverse. For this reason, pavements are commonly designed to have the minimum possible incline but sometimes, the site topography, available space and project budget dictate otherwise. Thus, all Full-scale Model testing was conducted three inclines namely; 0°, 2.5° and 5° or 0%, 3.5% and 7.8% respectively.

4.3.7 Model Testing Procedure

Testing of the Full-scale Model was conducted in an iterative manner as well. The first step was to set the ITA to an incline of 0° and then construct the required layer works of the Full-scale Model for the current test. In all tests, the sub-base layers and the geotextile were kept constant, exchanging only the bedding sand, joint material and concrete brick combination to those required. Once the required layer works was in place, the valve of the supply tank was then opened followed by the ball cocks at the inlet meters. This was done to fill the ITA reservoir to the point where water just started flowing out of its slot and onto the layer works being tested. The ball-cocks at the inlet meters were then immediately closed and the readings on all three inlet meters were recorded. This was taken as the start volumes at the inlet meters. The taps after the outlet meters were then opened to drain any water that had flowed through the layer works and entered the drainage system during the filling process of the ITA reservoir. The readings on all five outlet meters were then recorded and this was taken as start volumes at the outlet meters.

Following this, all three ball cocks at the inlet meters were opened fully to provide the maximum possible Q_{IN} and a stop watch was started simultaneously. This was considered the start of that test. Outlet meter readings were recorded in high definition video for later analysis but manual readings were also taken at each meter, every 5 min, to determine the termination time for that test. The termination time of each test was taken to be when steady state flow through the layer works was achieved, which was when the readings on each outlet meter differed by approximately the same amount every 5 min, to two decimal places (Discharge, Q (m^3/min)). Once steady state flow was achieved, all ball cocks at the inlet meters were closed and the stop watch was stopped simultaneously. This was taken to be the termination time of the test and final readings on all the flow meters were recorded.

These readings were taken to be the end volume readings for that test and the difference between them and the start readings was taken to be the total volume of water that passed through the layer works for that test. The ITA was then allowed to drain completely and set to the next incline required before the entire process was repeated again. After a specific layer works was subjected to testing at inclines of 0°, 2.5° and 5° or 0%, 3.5% and 7.8% respectively, the ITA was reset to 0° and the next layer works required for testing was constructed. Testing was carried out in this manner on the following layer works constructions of the Full-scale Model, at all three inclines, for this investigation:

- 1) Waterwise® brick surface with P-Type 1 jointing and bedding course;
- 2) Waterwise® brick surface with P-Type 2 jointing and bedding course;
- 3) Waterwise® brick surface with P-Type 3 jointing and bedding course;
- 4) Waterwise® brick surface with P-Type 4 jointing and bedding course;
- 5) Waterwise® brick surface with P-Type 5 jointing and bedding course;
- 6) Citylock® brick surface with P-Type 1 jointing and bedding course;
- 7) Citylock® brick surface with P-Type 2 jointing and bedding course;
- 8) Citylock® brick surface with P-Type 3 jointing and bedding course;
- 9) Citylock® brick surface with P-Type 5 jointing and bedding course;

The results of each test were then compared to that of the field and Basic Model testing and analyzed as shown in Section 7.3.

4.3.8 Additional Model Testing

Lastly, double-ring infiltrometer tests were carried out with the smaller custom apparatus on the Full-scale Model. Tests were only conducted on Citylock® brick surface layer works combinations for comparison to the ITA data. The rings were secured to the surface with adhesive putty before testing after which, water was then added to the space between the inner and outer ring to a height of 110 mm above the testing surface and maintained there for the duration of the tests. The inner ring was filled with water to a height of 110 mm above the testing surface and the tests were commenced in the same procedure described in Section 6.1. The results of these tests are presented in Section 7.3.4.

5 RESULTS AND DISCUSSION

5.1 FIELD TESTING

The fifteen double ring infiltration tests conducted for this portion of the study took place on 20 September 2017 in the base of two separate test pits on the Brooks Street site in Pretoria. The two test pits were labeled HA01 and HA02 with nine infiltrometer tests being conducted in the former and six in the latter (Tables 7 and 8). Both test pits contained primarily a thin fill layer on surface, followed by a silty-clayey sand with abundant highly weathered quartzite gravel to the base and below. Typical permeabilities for such materials should be in the order of $0.1 - 10^{-3}$ cm/s (Powers, 1992) and their hydraulic conductivities will be similar, however, the material on this site displayed significantly higher values, behaving more like uniform or well graded gravel.

As stated before, this type of soil, once compacted, is commonly accepted as a fair subgrade in many pavements throughout South Africa, which had several implications for the design of the Full-scale Model and ITA. This meant that the construction surface of the ITA, despite having large slots in it, might still perform in a similar way and represent the presence of a subgrade which was unwanted in the Full-scale Model. Even if the layer works had a higher permeability, the results would be superseded by the lower permeability of the construction surface (deck) of the ITA. It was for this reason, that it was decided to allow the slots in the construction surface to be sufficiently big enough to model a far greater permeability than this material in the design phase, so as not to interfere with the Full-scale Model results. This meant that the flow meters at the outlets had to be large enough to accommodate the corresponding discharge of each of these slots as well.

Table 7: Infiltrometer results for HA01			
Test	Reading (s)	Infiltration Rate (cm/s)	Infiltration Rate (m³/s)
T1	25	0.4	6.16E-06
T2	24	0.416666667	6.41E-06
Steady State Flow			
T3	32	0.3125	4.81E-06
T4	32	0.3125	4.81E-06
T5	31	0.322580645	4.97E-06
T6	30	0.333333333	5.13E-06
Average	31.25	0.320228495	4.93E-06

Table 8: Infiltrometer results for HA02			
Test	Reading (s)	Infiltration Rate (cm/s)	Infiltration Rate (m³/s)
T1	21	0.476190476	7.33E-06
T2	39	0.256410256	3.95E-06
T3	25	0.4	6.16E-06
Steady State Flow			
T4	17	0.588235294	9.06E-06
T5	16	0.625	9.62E-06
T6	18	0.555555556	8.55E-06
T7	20	0.5	7.70E-06
T8	22	0.454545455	7.00E-06
T9	19	0.526315789	8.10E-06
Average	18.66666667	0.541608682	8.34E-06

In addition to considerations made for the construction surface of the ITA and the outlet meters, these results implied that testing of the Full-scale Model had to occur at water influx rates greater than these values as well. If a silty-sand could have such a high permeability in the field, it was suspected that PICP would have permeabilities at least one order greater. Thus, in an attempt to discern when the Full-scale Model would reach saturation and to model an event larger than a 1 in 20-year storm, the Q_{IN} value of 0.027 m³/min was selected in the design process. Unfortunately, field testing data of PICP installed on site could not be obtained for comparison to the data from the Brooks Street site, due to sealing issues experienced while using the custom single-ring and double-ring infiltrometer apparatuses, explained in greater detail in Section 7.3.4.

5.2 BASIC MODEL

5.2.1 Preliminary Testing

The first portion of the testing procedure conducted on the Basic Model yielded the time taken for 5ℓ of water to flow through the elementary volume. This was done for the elementary volume representing the sub-surface layer works only at first and then the full Basic Model as a verification step (Table: 9). As stated before, this data was then used to determine two parameters namely; the termination time that would be applied to each test and the discharge for the elementary volume (Eq. 2). Firstly, using this termination time ensured that sufficient time was given for the full 5ℓ to flow through the Basic Model and that volume measurements were taken soon enough to omit any water used to saturate the model before the test, from the results. Secondly, the discharge (Q_{OUT}) calculated from this time yielded an indication of the model's hydraulic conductivity or permeability (K) and would be used to verify the results obtained in further testing (Eq. 3).

Table 9: The times taken for 5ℓ of water to migrate through the Basic Model.				
Test	Condition	Volume (ℓ)	Incline (°)	Time (s)
1	No Bricks	5	0	578
2	No Bricks	5	0	402
3	No Bricks	5	0	369
4	No Bricks	5	0	355
5	Bricks	5	0	545
Average				449.8

$$\begin{aligned}
 Q_{OUT} &= \frac{\text{Volume passing through the model}}{\text{Average time}} & (2) \\
 &= \frac{5 \ell}{449.8 \text{ s}} \\
 &= 1.11 \times 10^{-5} \text{ m}^3/\text{s}
 \end{aligned}$$

$$\begin{aligned}
 K(\text{Permeability}) &= \frac{Q_{OUT}}{\text{Surface Area of BMA}} \times 100 \text{ cm/m} & (3) \\
 &= \frac{1.11 \times 10^{-5} \text{ m}^3/\text{s}}{0.5 \text{ m}^2} \times 100 \text{ cm/m} \\
 &= 2.22 \times 10^{-3} \text{ cm/s}
 \end{aligned}$$

In addition, it was expected that poor performance PICP layer works in the Full-scale Model would have a similar permeability and discharge to ICP. Thus, the calculated discharge and permeability of the Basic Model were used in the design process of the Full-scale Model to indicate the minimum detection range of the outlet meters. Most flow meters have a minimum and maximum discharge or flow rate that they can detect and accommodate without retarding the flow respectively. While an attempt was made to select flow meters with the highest sensitivity, the maximum possible discharge at each point had to also be accounted for and thus the Madalena DS TRP meters were selected for the Full-scale Model.

The results obtained during further testing of the Basic Model are summarized in Tables 10 and 11. All exit points of the BMA were at the same elevation during the horizontal tests but during all further inclined tests, measurements at Point 1 were at the highest elevation and Points 2 to 4 decreased in elevation systematically. The volumes exiting each point were converted to percentages of the total volume that exited the BMA in each test as opposed to percentages of the 5ℓ that entered the model. This was done to emphasize any effects incline might have on the flow through the model and thus, further assist in the design of the Full-scale Model.

5.2.2 Sub-surface Testing

Looking at the test data for the elementary volume representing sub-surface layer works, a clear correlation could be seen between incline and the volumes of water captured at each exit point of the BMA. Average percentages of water exiting at each point for this portion of the testing procedure are shown in Table 10 and are represented graphically in Fig. 29. It can be clearly seen that as the incline is increased, a much greater percentage of the volume entering the model, flowed to points of lower elevation before exiting. This implied that the horizontal component of flow in a pavement, may increase with incline while the vertical flow component decreases. This suggested that the effect of incline had to be further investigated in the Full-Scale Model, provided that the addition of a surface layer did not prove otherwise.

Table 10: Average percentages of water volumes captured at each exit point for the elementary volume representing a sub-surface layer works only.

Incline	0°	2°	6°	10°
Point 1	29.445	23.51	13.74	7.97
Point 2	34.275	29.455	22.24	12.25
Point 3	26.17	26.825	21.32	14.64
Point 4	10.105	20.205	42.705	65.145
Runoff	0	0	0	0
Total	99.995	99.995	100.005	100.005

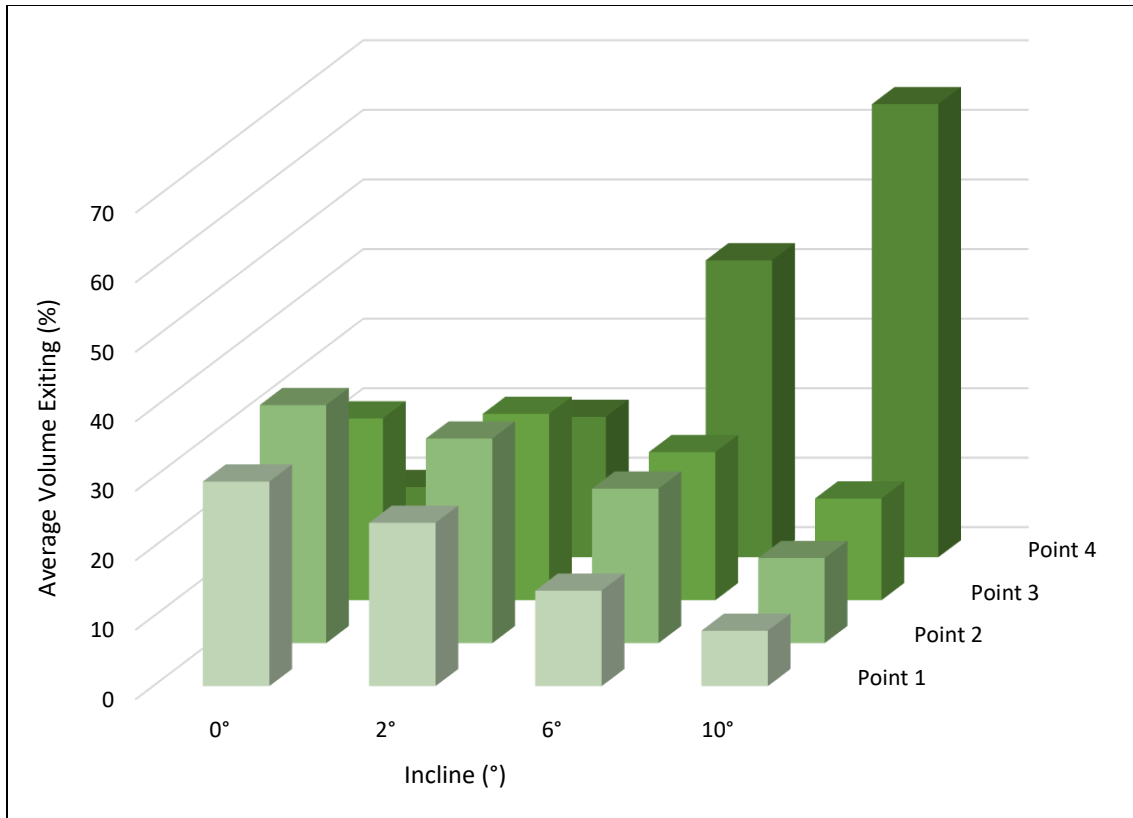


Fig. 29: A column graph showing the comparison of water volume percentages captured at each point for tests using a sub-surface layer works only, at various inclines.

5.2.3 Surface Testing

The average volume percentages exiting the BMA containing the full Basic Model, are shown in Appendix E, summarised in Table 11 and graphically represented in Fig. 30. It is evident that the same trend is present in the model in this case, as is in the elementary volume that represented the sub-surface layer works only. It seems that the addition of the surface layer had little to no effect on the volume percentages captured at the lowest exit point, as incline was increased. What was noted however, were smaller differences between the volumes captured at points 1 to 3 for all inclines compared to that occurring during the sub-surface layer works elementary volume testing. The exit volumes of the full Basic Model measured in tests at 0° incline for example, differed by less than 6% with the presence of the surface layer. In contrast, the volumes measured at these points in tests using no surface layer, differed by more than 20%.

This implied that the presence of a surface layer in ICP, results in a more lateral distribution of water ingress into the layer works due in part, to the geometry of the bricks themselves. The bricks are essentially impervious, causing water falling on their surfaces to move laterally to one of the joints between them, before migrating downward into the remainder of the layer works. The effect may also be aggravated by a low performance jointing material. This further motivated the need to include the effect of incline and the effect of each separate layer of PICP in the Full-scale Model.

Table 11: Average percentages of water volumes captured at each exit point for an elementary volume consisting of a surface and sub-surface layer works.

Incline	0°	2°	6°	10°
Point 1	26.75	19.945	13.12	8.575
Point 2	28.035	22.705	17.62	14.58
Point 3	22.025	18.975	16.545	14.685
Point 4	23.19	38.375	52.715	62.165
Runoff	0	0	0	0
Total	100	100	100	100.005

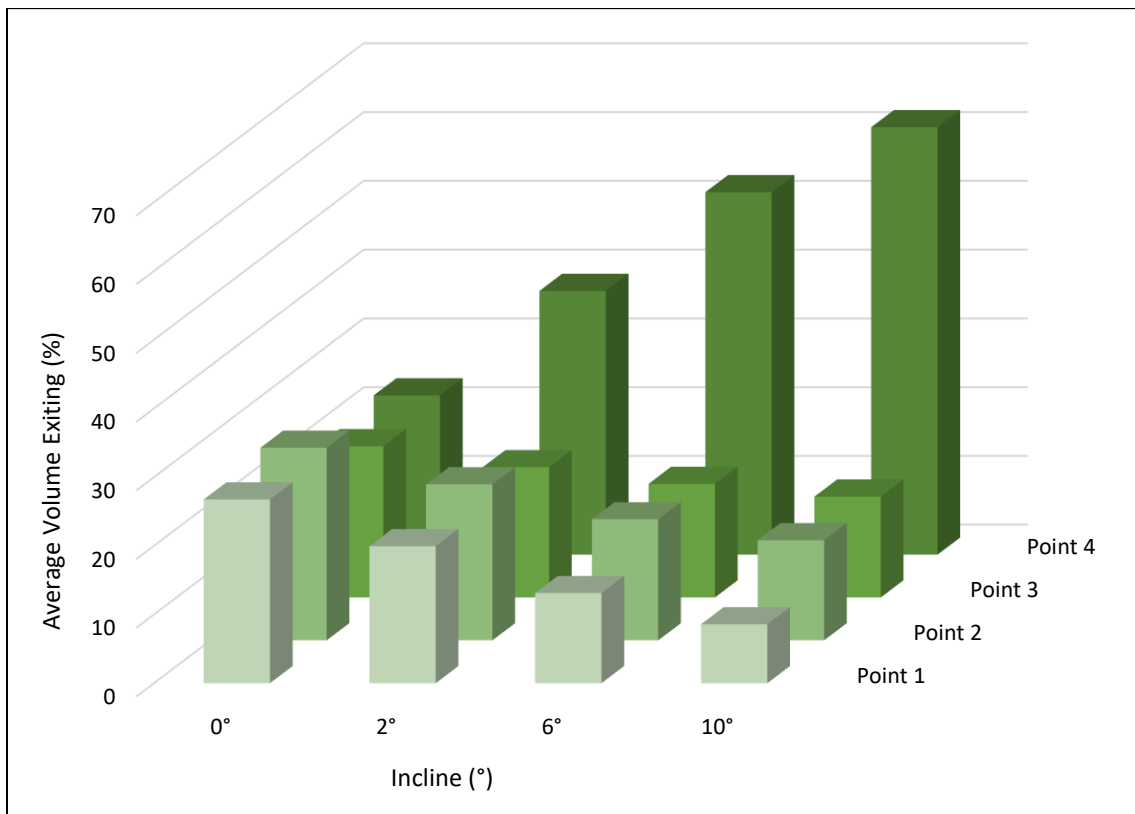


Fig. 30: A column graph showing the comparison of water volume percentages captured at each point for tests using a surface and sub-surface layer, at various inclines.

5.2.4 Additional Observations

Furthermore, looking at observations made during inclined testing, it was noted that incline affected the quantity of fines present in the captured water volumes. The difference was observed during testing of the elementary volume representing a sub-surface layer works and during testing of the full Basic Model. It was a distinct change in the colour of the water volumes captured at points 2 and 3 for inclines of 0° (Fig. 31(a)) and 6° (Fig. 31(b)). In general, far less fines were present in water captured at these points as the incline of the model was increased, resulting in clear water exiting these points at 6° . The washing out of fines can have serious implications in any pavement. One result of the removal of fines, is the creation of inter-granular voids, into which, consolidation can occur. Consolidation of a pavement can cause potholes, subsidence and unwanted depressions which decrease its overall performance. Another issue that could be caused is that the removed fines could be emplaced in another area of the pavement resulting in a local variation of a pavement's hydraulic properties leading to ponding, blistering and clogging.

Fines can only be removed when the flow through the medium achieves a certain minimum velocity. These observations imply that this minimum velocity was achieved in the lateral flow component and not in the vertical, making lateral flow the dominant regime once a certain incline or greater was reached. The earliest sharp volumetric difference between the volumes exiting points 1 and 4 existed between 2° and 6° , implying that a critical angle may exist between them which results in lateral flow becoming dominant. This angle was suspected to be around 5° . The same situation would most likely exist in PICP. If constructed on a great enough incline, it is possible that a PICP may no longer be as effective at retarding lateral flow and result in piping or erosion at its downslope boundaries. This further motivated the inclusion of the effect of incline in the Full-scale Model.

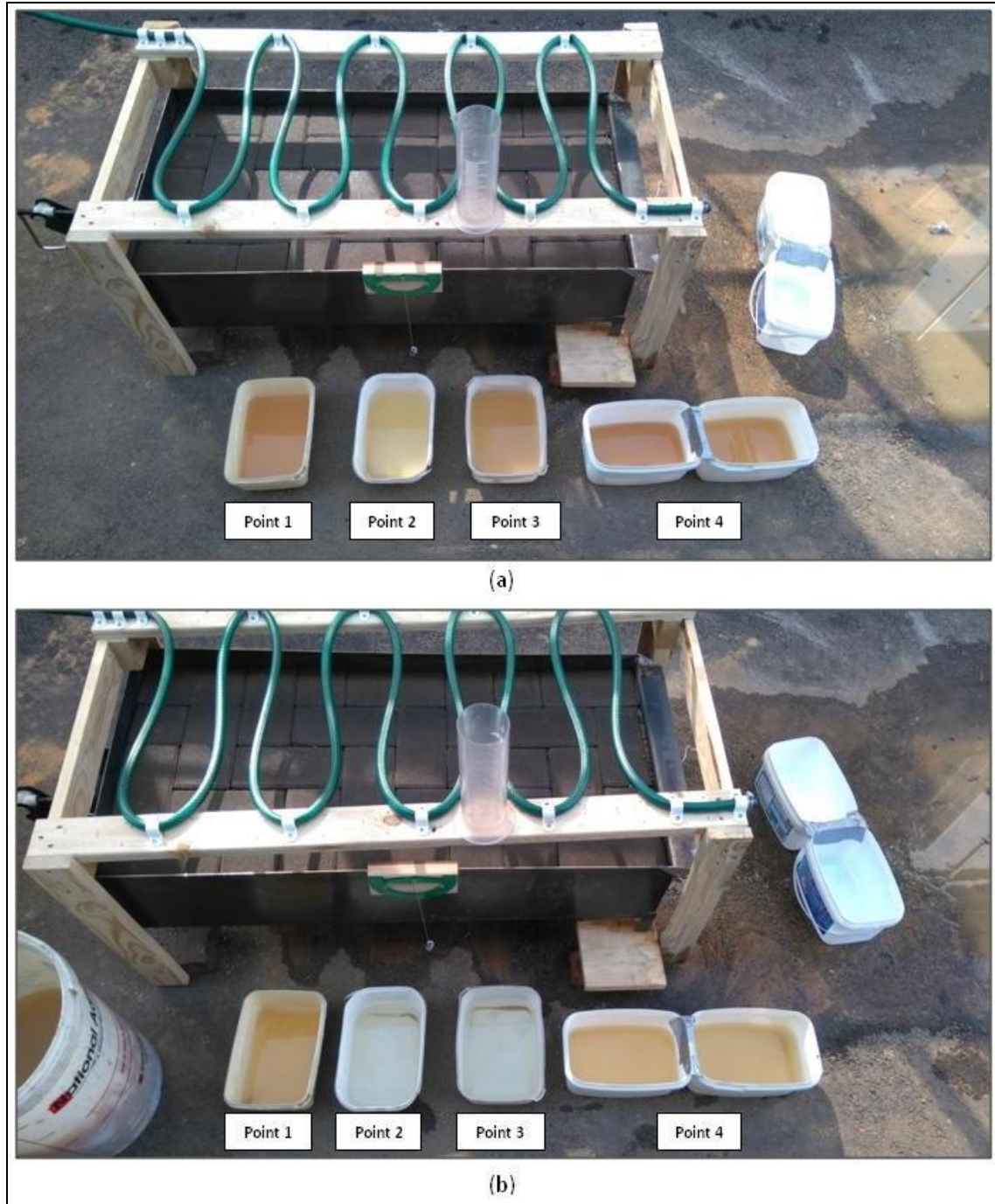


Fig. 31: A comparison of the color of water captured from different exit points at (a) an incline of 0° and (b) an incline of 6° .

5.3 FULL-SCALE MODEL

5.3.1 Model Design

The results for the iterative tests conducted for the Full-scale Model design portion of this study are summarized in Fig. 32 and tabulated in Appendix F. During the first iterations of these tests, where the ITA contained only a surface layer of Waterwise® bricks alone, followed by the bricks with P-Type 1 jointing material, all water ingress took place within the first linear meter of pavement. In both cases, only the outlet meter connected to Q_1 displayed a reading, accounting for 100% of the volume that passed through the selected layer works. The next tests with the addition of the bedding sand, Bidim® and upper sub-base, displayed very similar behavior.

The first change was noted with the addition of the Lower Sub-base which caused a slight increase in the volume measured at Q_2 . This was most likely due to the increased vertical distance that water now had to travel through the selected layer works. The increased vertical distance allowed for the development of the lateral flow component which arises as incline increases, first noticed in the Basic Model. The increase at Q_2 was however, an order of magnitude smaller than that of Q_1 for this test and the discharge remained very similar to the previous iterations. In addition, in all of these tests, no runoff (Q_5) was measured. This implied that the addition of any specific layer, in a recommended PICP layer works, does not drastically affect its hydraulic properties but rather performs a structural function such as preventing smaller layer particles from migrating downward, adding bearing capacity to the pavement and increasing its water storage capacity. Understandably, a drastic change in selection of materials and thicknesses, for any layer, is widely ill-advised by practitioners and literature however, slight variations in the particle diameters and layer thicknesses are permissible without negative impact on the overall performance.

What does occur in industry however, is a variation in the selection of the bedding and jointing sand. This can be for several reasons such as material availability, a lack of experience or an attempt to reduce costs and can often lead to failure of the PICP (Technicrete, 2017). To complicate this, the bedding and jointing sand is the pavement material type with the largest geological and thus commercial variety. Literature shows that such a change could have a drastic effect on the permeability of PICP. If the surface of a PICP layer works has a low permeability, despite all other layers having the recommended properties, the entire pavement would be limited to that of the surface. To verify this, one of the iterative tests was conducted using a P-Type 5 sand as bedding and jointing material.

The change in volumes measured from points Q₂-Q₄ for this test were dramatically higher, while a decrease was observed at Q₁. Most notably however, was the occurrence and the magnitude of runoff, displayed by the volume measured at Q₅ (Fig.32). This implied that the combination of materials chosen for the surface i.e. the concrete brick, jointing and bedding sand combination, had a profound impact on the hydraulic properties of the model and thus PICP. For this reason, it was decided to deeply investigate the effect of material selections in the bedding and surface layers of the Full-scale Model.

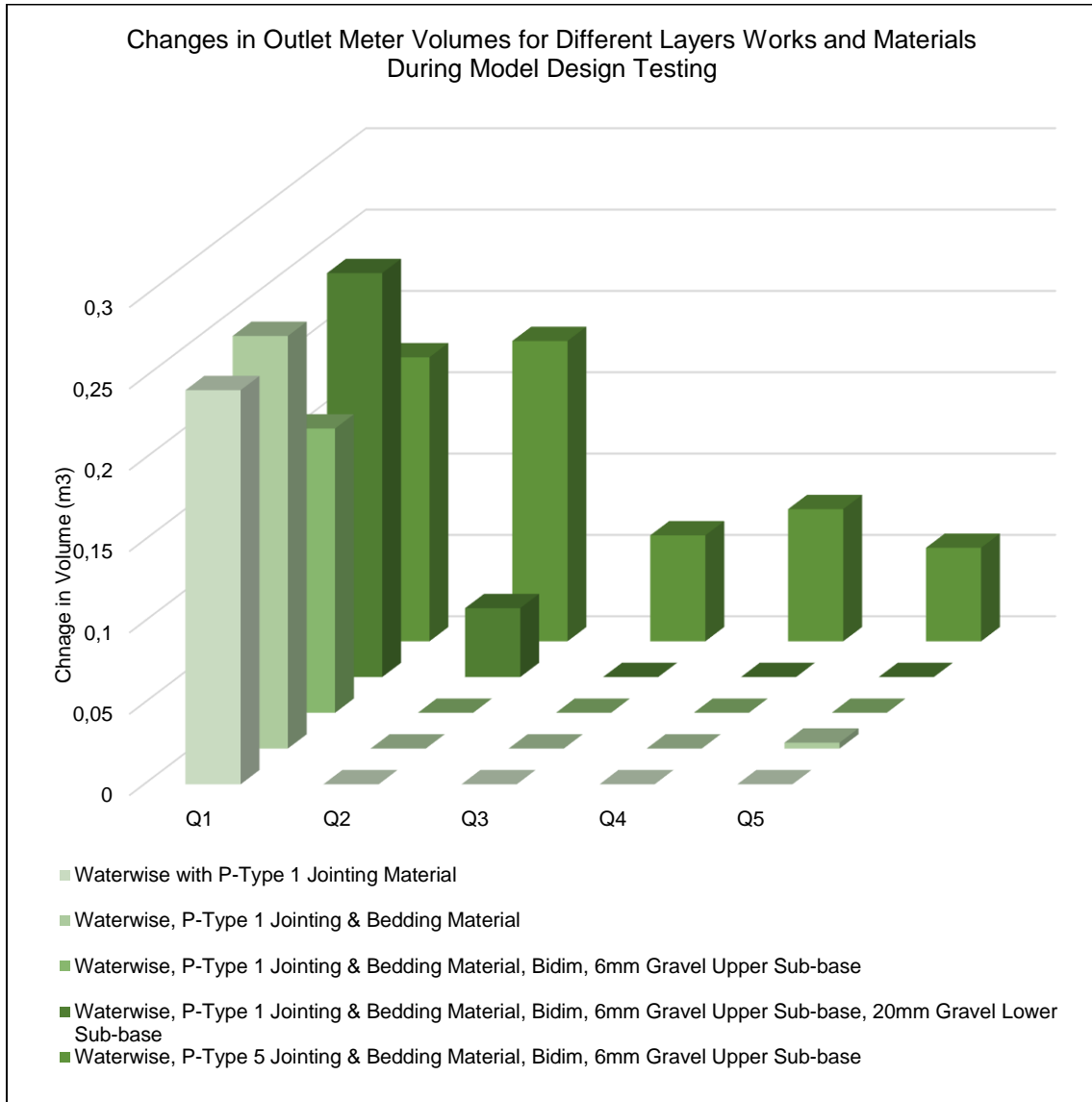


Fig. 32: A column graph showing the comparison of water volume changes at each point for model design tests using different layers of the GLW.

There was another structural property of a layer however, that was suspected to have an effect on the hydraulic properties of PICP namely; the orientation of the bricks in the surface layer. Considering PICP constructed on an incline, it was suspected that if the joints of the concrete bricks were either aligned or at an angle to the direction of flow, there would be a slight change in the discharge. This was based on the results of the Basic Model testing that evaluated the effect of the surface layer. The suspicion was that joints aligned with the direction of flow (downslope) would provide preferential flow paths, transmitting water further downslope before it could infiltrate the remainder of the layer works, while joints at an angle to the direction of flow would present longer flow paths and allow more time for water to infiltrate. To evaluate this, testing was done as described in Section 6.3.1 but no change in discharge was observed. Thus, the orientation of concrete bricks in the surface layer were not investigated in the Full-scale Model.

Based on findings from testing in the Basic Model, it was expected that a change in incline would affect the hydraulic properties of PICP. The full GLW was again subjected to inclined testing in the ITA and the results of those tests are given in Appendix F and represented graphically in Fig. 33. As before, the GLW attenuated almost all of the water entering the system within the first linear meter of pavement. There was however, a notable decrease in the volumes and thus discharges, of water exiting points Q_1 and Q_2 as incline was increased. In general, more of the incoming volume of water was moving to downslope exit points but the sharpest increase of these exit volumes occurred at an incline of 5° . This supported the findings of the Basic Model namely; that a lateral flow component develops strongest or reaches a high velocity within pavements at inclines equal to or greater than, 5° . This cemented the need to evaluate incline in the Full-Scale Model.

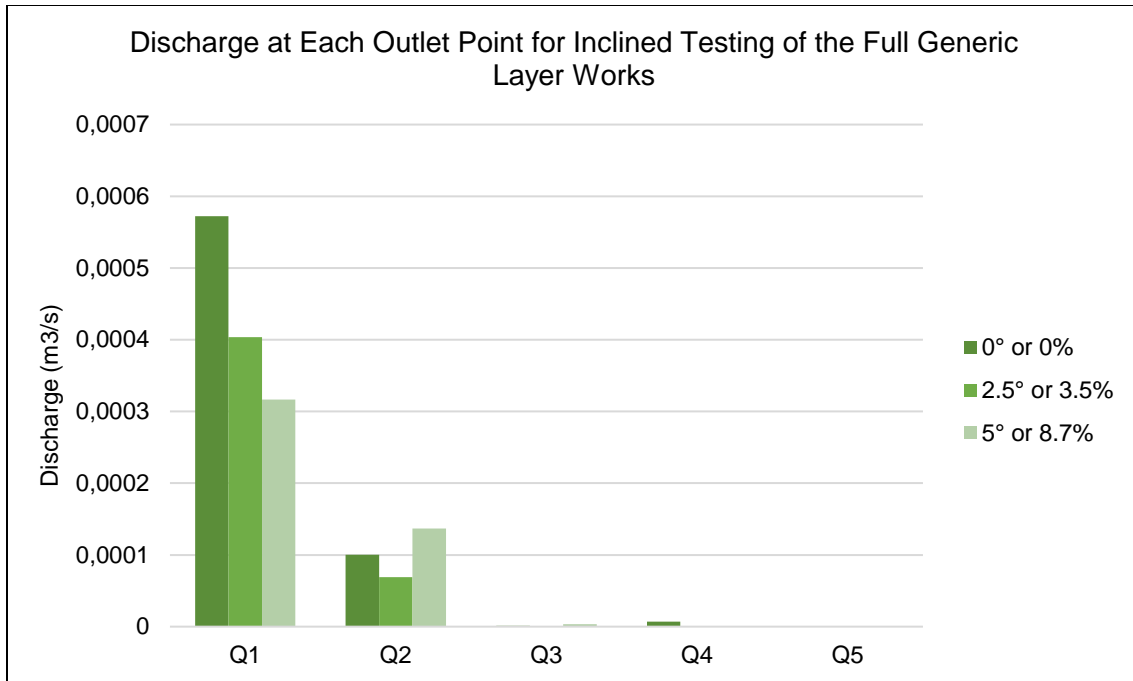


Fig. 33: A column graph showing discharges at different exit points of the Infiltration Table Apparatus as incline increased.

The Full-scale Model was then designed based on the findings of the Model Design tests and those before them. It was then subjected to inclined testing in the ITA, using different combinations of materials in the surface and bedding of the layer works and at different inclines. The results for these tests are given in Appendix G, yielding two primary findings described in further detail in Sections 7.3.1 and 7.3.2. Before discussing these results however, it is pertinent to describe their presentation. The times and their corresponding readings for each test are presented in five-minute intervals, starting at 10min. This was done because, in most of the tests of the Full-scale Model, steady state flow was achieved within approximately ten minutes of testing or less. An example of this is displayed in Table 12 which shows the results of a test conducted on the Full-scale Model with a P-Type 1 sand and Waterwise® combination layer works, at an incline of 2.5° and in one-minute intervals. It can be seen from these results that the model achieved steady state flow between 2 and 3min of testing (Fig. 34). Thus, each test conducted on the model containing a Waterwise and P-Type 1 combination layer works, is presented as tested, in five-minute intervals, while all other combinations were allowed more time respectively to ensure that steady state flow would be achieved. Furthermore, the mean discharge (Q_{Mean}) at any one exit point was calculated based only on the data of the steady state flow portion of that test. This ensured that discharges occurring after the ballcocks at the inlet meters had been closed or while the test was reaching steady state flow, were not included.

Table 12: Short interval test results for a Waterwise® and P-Type 1 combination layer works of the Full-scale Model													
06-09-2018													
Incline 2.5° or 3.5%													
Time (min):	Inlet Meters (m³)			Outlet Meters (m³)									
	1	2	3	Q ₁	Discharge Q ₁ (m³/min)	Q2	Discharge Q2 (m³/min)	Q3	Discharge Q3 (m³/min)	Q4	Discharge Q4 (m³/min)	Q5	Discharge Q5 Runoff (m³/min)
0	3.30763	4.3863	2.77682	0.63688	0	0.31758	0	0.2441	0	0.46075	0	1.07115	0
1	-	-	-	0.6405	0.00362	0.31758	0	0.2441	0	0.46075	0	1.07115	0
2	-	-	-	0.66223	0.02173	0.32114	0.00356	0.2441	0	0.46075	0	1.07115	0
3	-	-	-	0.68618	0.02395	0.3256	0.00446	0.2441	0	0.46075	0	1.07115	0
4	-	-	-	0.70922	0.02304	0.32948	0.00388	0.2441	0	0.46075	0	1.07115	0
5	-	-	-	0.73215	0.02293	0.33315	0.00367	0.2441	0	0.46075	0	1.07115	0
6	-	-	-	0.75377	0.02162	0.33681	0.00366	0.2441	0	0.46075	0	1.07115	0
7	-	-	-	0.77548	0.02171	0.34043	0.00362	0.2441	0	0.46075	0	1.07115	0
8	-	-	-	0.79821	0.02273	0.34428	0.00385	0.2441	0	0.46075	0	1.07115	0
9	3.4205	4.52323	2.84195	0.82011	0.0219	0.34829	0.00401	0.2441	0	0.46075	0	1.07115	0
End				0.88521	0.0651	0.35992	0.01163	0.2441	0	0.46075	0	1.07115	0
(Q_{Mean}) (m³/min)	0.011287	0.013693	0.06513		0.020358889		0.0034122		0		0		0

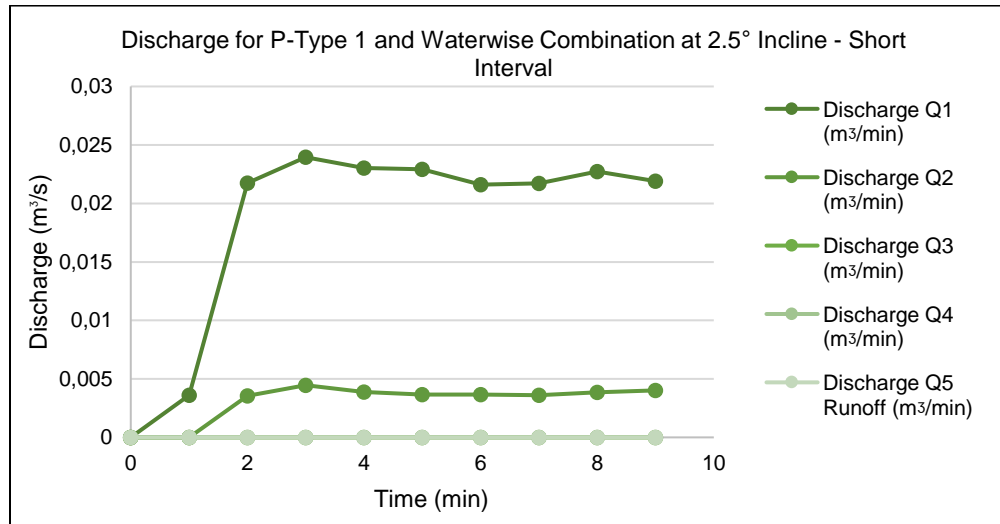


Fig. 34: A graph of the short interval discharges at different points of Full-scale Model with a Waterwise and P-Type 1 combination layer works.

5.3.2 The Effect of Surface Materials

For this portion of the investigation, only results of the Full-scale Model testing at a 2.5° incline were considered. This was done to make the surface material choices in the layer works, the only variable in this instance. This incline was also chosen as it was great enough to give rise to a lateral flow component, as identified in the Basic Model and Model Design phase, without that component being dominant over the vertical. This would further emphasize any differences in flow caused by the choice of materials, over the length of the model. The results considered can be seen in Appendix G and from them, several deductions can be made.

Firstly, it was found that the surface material selections and combinations dictate the permeability of PICP, provided the subsurface layers have higher permeabilities. In addition, changing one component of the surface material combination, can also affect this permeability. Looking at a change in the choice of concrete bricks in the surface combination only, it can be seen that using the Citylock® product resulted in permeabilities ($K_{p/m}$) that were between 5% and 48% higher than that of an identical layer works containing Waterwise bricks instead (Table 13). These permeabilities were calculated according to the same method applied in the Basic Model (Eq. 4). Unfortunately, the model containing a layer works with a Citylock® and P-Type 4 surface combination, could not be tested due to the time constraints of the project. The maximum permeability per liner meter of this combination however, can be estimated to be very similar (within 5%) to that of a Waterwise® and P-Type 4 combination, by considering the data of the other layer works.

$$K_{p/m} = \frac{Q_{Mean}(m^3/s)}{\text{Surface Area of 1 linear m of pavement } (m^2)} \times 100 \text{ cm/m} \quad (4)$$

Where:

$K_{p/m}$ = Permeability of linear meter of pavement 1, 2, 3 or 4 (Runoff is not considered)

Q_{Mean} = The mean discharge of the linear meter of pavement in question

Table 13: Maximum discharge and permeability values per linear meter of pavement for different surface material combinations at 2.5° incline

Product	Sand Type	Maximum Q_{Mean} (m ³ /min)	Maximum $K_{p/m}$ (cm/s)	Percentage Decrease vs. P-Type 1	Percentage Improvement vs. Waterwise
Citylock	P-Type 1	0.028702	2.39E-02	-	48.0%
	P-Type 2	0.020015	1.67E-02	30.27%	2.0%
	P-Type 3	0.020185	1.68E-02	-0.85%	4.1%
	P-Type 4	Not Tested	±8.00E-03 Expected	52.44%	NA
	P-Type 5	0.0018075	1.51E-03	81.17%	5.2%
Waterwise	P-Type 1	0.0193876	1.62E-02	-	-
	P-Type 2	0.019626	1.64E-02	-1.23%	-
	P-Type 3	0.019395	1.62E-02	1.18%	-
	P-Type 4	0.009344333	7.79E-03	51.82%	-
	P-Type 5	0.001718	1.43E-03	81.61%	-

Furthermore, a change in the type of sand used for the jointing material and bedding layer had a more drastic effect on the permeability of the model (Fig 35). Sands that met the criteria for P-Type 1, 2 and 3 classifications performed best, attenuating between 60% and 70% of water flowing into the model, within the first linear meter of pavement (Q_1) with no runoff whatsoever. Comparing the maximum permeability per linear meter of the model ($K_{p/m}$) resulting from the use of these sands in Table 13, to known material permeabilities, it can be seen that they cause the entire PICP to perform like well graded or uniform sands (Powers, 1992). This verifies what is said in literature by Technicrete, (2017), Kumar et al., (2016) and Beeldens and Herrier, (2006) and would make material selections such as these, prime candidates for use in PICP.

The surface combination of Waterwise® bricks and P-Type 4 sand however, had a detrimental effect on the performance and thus the permeability of the model (Fig 35). For this combination there was a 50% decrease in the water volume attenuated in the first linear meter of pavement (Q_1) and a sharp increase of between 8% and 10% in the volumes measured at Q_2 , Q_3 and Q_4 when compared to P-Type 1, 2 and 3 combinations. This material selection caused the model to perform like a silty sand despite being comprised of multiple high permeability gravel layers as well (Powers, 1992). In addition, 7% of the influx volume was not attenuated by the layer works at all and exited the model as runoff. This implies that selecting a P-Type 4 sand for the surface combination of PICP results in a large lateral dispersion of water before any infiltration can take place and most notably, in runoff occurring. When runoff occurs in PICP, it denotes a critical failure in its ability to attenuate water and should only ever occur at extreme influx rates such as 1 in 100year storms. It is therefore recommended that P-Type 4 sands not be selected for use in PICP in industry.

Surface combinations using P-Type 5 sands in the model performed even worse than those using P-Type 4. Between 60% and 80% of the volume influx exited the model as runoff with the remainder infiltrating through the model at Q₁, Q₂, Q₃ and Q₄ in quantities between 0% and 7% (Fig 35). This resulted in extremely low permeabilities per linear meter of pavement compared to that of other combinations and thus, in the model performing similarly to a silty sand (Powers, 1992). It is therefore recommended that P-Type 5 sands also not be selected for use in PICP in industry. In addition, these results support the reasoning that the material selection of the surface combination will limit the permeability of a PICP if it has the lowest permeability in the layer works, regardless of the properties of the subsurface layers. Thus, it can be seen that the hydraulic properties of PICP rely on the intrinsic properties of the materials in the layer works, rather than its structure i.e. the effect of the number of layers and their thicknesses on the permeability of PICP will be superseded by that of their material properties like void content, porosity, density and permeability.

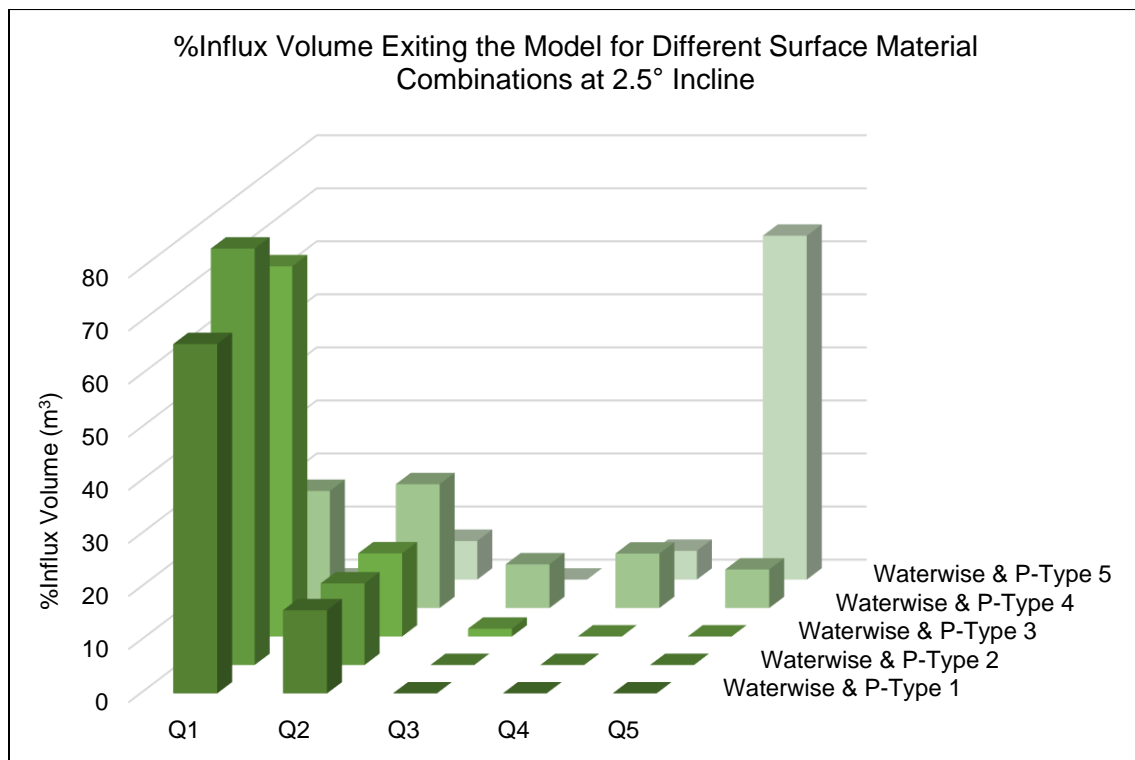


Fig. 35: A column graph comparing the percentages of the influx volume exiting each point for different surface material combinations in the Full-Scale Model at a 2.5° incline.

5.3.3 The Effect of Incline

As demonstrated by Castro et al., (2007), Kamali et al., (2016), the Basic Model and Model Design tests, the testing of the Full-scale Model further illustrated that incline has a remarkable effect on the hydraulic properties of PICP, most notably, their permeability (K). Considering the results in Appendix G once again, it can be seen that in general, an increase in incline will decrease the permeability per linear meter ($K_{p/m}$) of PICP. Summaries of these results for the Full-scale Model with a layer works containing Waterwise® and Citylock® surface material combinations are given in Tables 14 and 15, with their maximum discharge per linear meter ($\text{Max } Q_{\text{Mean}}$) represented graphically in Fig. 36 and 37. Looking at the results for Waterwise containing surface combination layer works, it can be seen that regardless of the choice of bedding and jointing material, an increase in inline resulted in a decrease in the discharge through the pavement. More of the influx volume was thus exiting the model as runoff. This is especially apparent with a low permeability surface material choice like that of P-Type 5 sands, where the difference in permeability per linear meter of pavement decreased by two orders of magnitude from 0° to 5° incline. In simpler terms, this changed the behavior of the model from a silty sand to a low-plasticity silt, severely limiting its performance (Powers, 1992). The same general trend was observed in the Full-scale Model for surface material combinations containing Citylock® bricks. Once again, the layer works containing P-Type 5 sand experienced the most dramatic change in maximum permeability per linear meter, differing by an order of magnitude from 0° to 5° incline and changing in behavior from a silty sand to a clayey sand (Powers, 1992). In both cases, the behavior of the model during an increase of incline, suggests that it discharges far less water from its base, despite the material remaining the same. This gives further evidence that a lateral component of flow develops in PICP and becomes more dominant as incline increases.

Table 14: A data comparison of Full-scale Model layer works with surface combinations containing Waterwise® bricks at different inclines

Incline	Parameter	Waterwise & P-Type 1	Waterwise & P-Type 2	Waterwise & P-Type 3	Waterwise & P-Type 4	Waterwise & P-Type 5
0°	Max Q_{Mean} (m ³ /min)	0.0346	0.0309	0.0232	0.0169	0.0055
	Max $K_{p/m}$ (cm/s)	2.89E-02	2.58E-02	1.93E-02	1.40E-02	4.60E-03
2.5°	Max Q_{Mean} (m ³ /min)	0.0194	0.0196	0.0194	0.0093	0.0017
	Max $K_{p/m}$ (cm/s)	1.62E-02	1.64E-02	1.62E-02	7.79E-03	1.43E-03
5°	Max Q_{Mean} (m ³ /min)	0.0188	0.0146	0.0124	0.0066	0.0001
	Max $K_{p/m}$ (cm/s)	1.57E-02	1.22E-02	1.03E-02	5.49E-03	9.55E-05

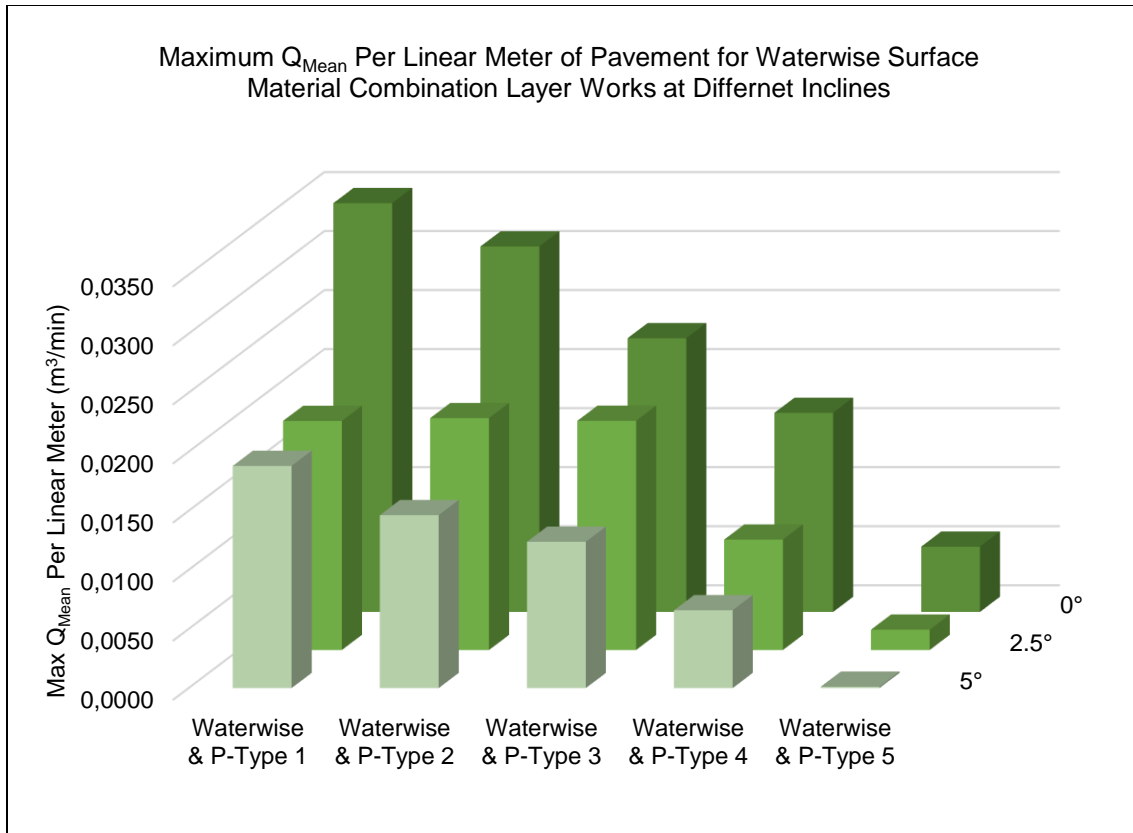


Fig. 36: A column graph showing the maximum mean discharge per linear meter of pavement for waterwise containing surface material combination layer works in the Full-scale Model at different inclines.

Table 15: A data comparison of Full-scale Model layer works with surface combinations containing Citylock® bricks at different inclines

Incline	Parameter	Citylock & P-Type 1	Citylock & P-Type 2	Citylock & P-Type 3	Citylock & P-Type 5
0°	Max Q_{Mean} (m^3/min)	0.0407	0.0175	0.0218	0.0060
	Max $K_{p/m}$ (cm/s)	3.39E-02	1.46E-02	1.82E-02	5.04E-03
2.5°	Max Q_{Mean} (m^3/min)	0.0287	0.0200	0.0202	0.0018
	Max $K_{p/m}$ (cm/s)	2.39E-02	1.67E-02	1.68E-02	1.51E-03
5°	Max Q_{Mean} (m^3/min)	0.0286	0.0214	0.0106	0.0003
	Max $K_{p/m}$ (cm/s)	2.38E-02	1.78E-02	8.82E-03	2.25E-04

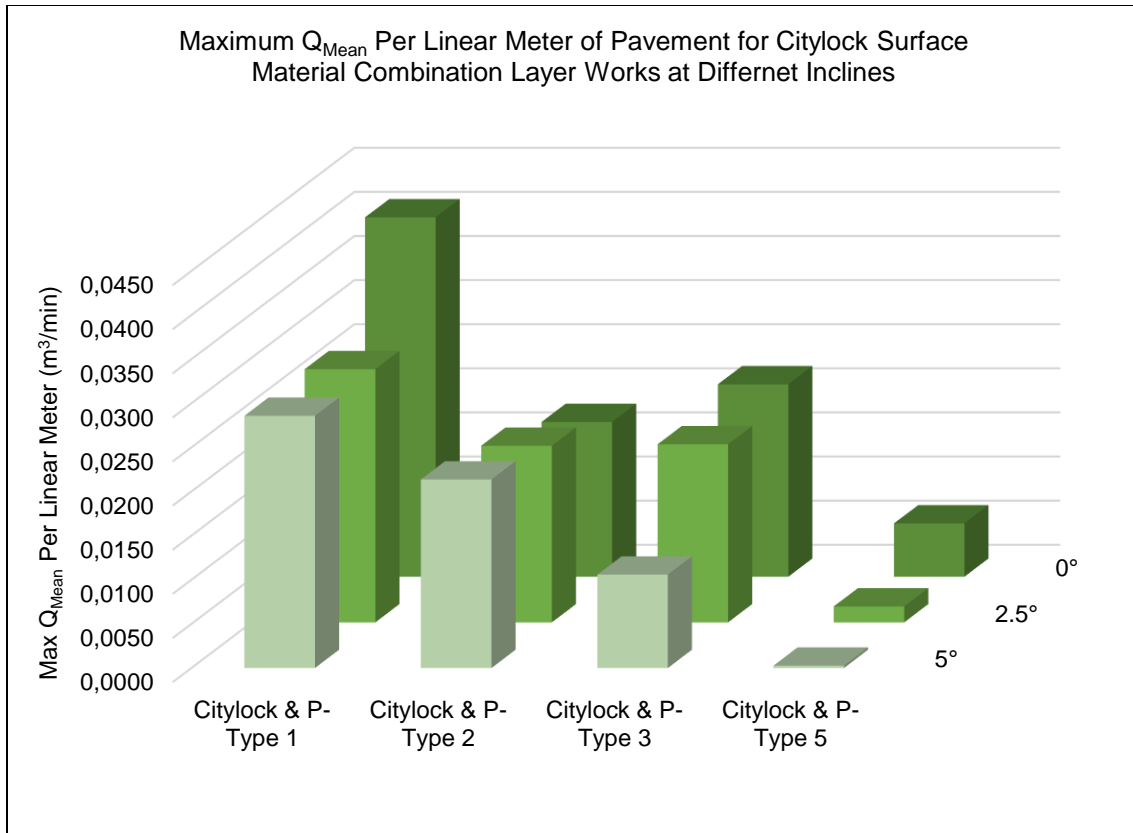


Fig. 37: A column graph showing the maximum mean discharge per linear meter of pavement for waterwise containing surface material combination layer works in the Full-scale Model at different inclines

From these results and findings by Castro et al., (2007), and Kamali et al., (2016), it can be deduced that two components of unsaturated flow develop within pavements namely; a vertical (FV_{Vert}) and lateral (FV_{Lat}) component, with a resultant (FV_{Res}) in the direction of gravitational acceleration (Fig. 38). Taking into account the findings of the Basic Model described in Section 7.3.1, it can also be deduced these components denote the velocity at which flow is occurring within the pavement, in different directions. At low inclines, FV_{Lat} is extremely small and thus the majority of flow is directed downward by gravity, making FV_{Vert} the dominant component. When incline is increased however, such as when PICP are constructed on a footslope, FV_{Res} begins to favor FV_{Lat} and FV_{Vert} decreases in response. Understandably, a critical angle must exist where FV_{Lat} becomes dominant over FV_{Vert} . Data obtained from the Basic Model suggested that this angle lies between 2° and 6° while data from the Full-scale Model indicates that it is between 2.5° and 5° (Appendix E). This is due to the fact that the outlet volumes measured from Q2 to Q5 of almost all the tests conducted on the Full-scale Model, show the sharpest increases between inclines of 2.5° and 5°.

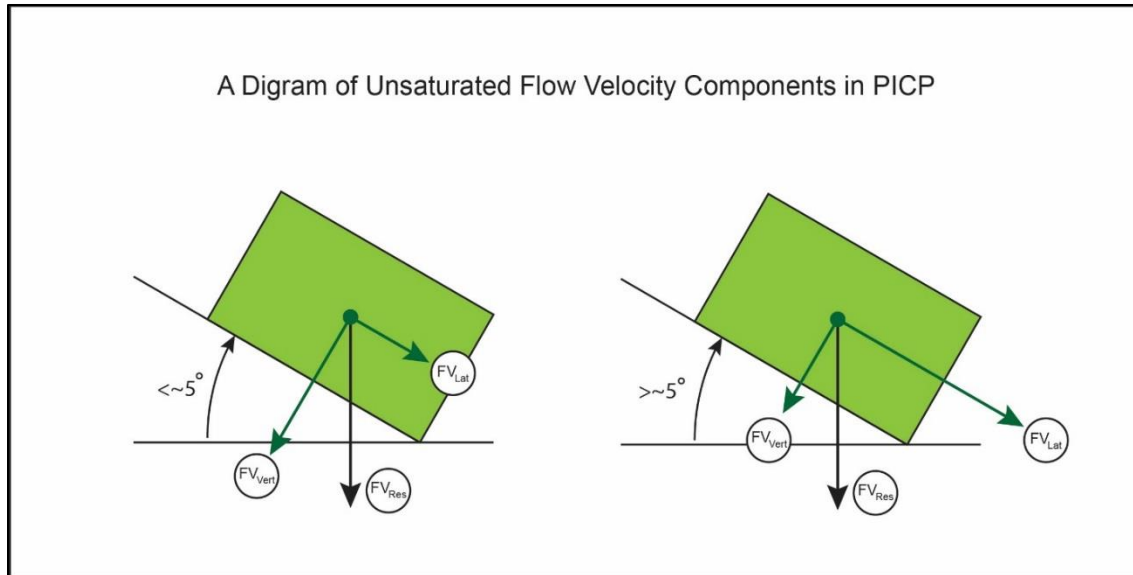


Fig. 38: A schematic diagram of the observed unsaturated flow velocity components in Permeable Interlocking Concrete Pavements at different inclines.

The reason for this behavior in pavements may be that an unsaturated flow mechanism such as capillary barriered perching is occurring in the surface materials at low inclines (Dippenaar and van Rooy, 2018). The surface material combination usually has a lower permeability than that of the upper and lower sub-base layers and as a result, the boundary between them may behave similarly to the bottom of a horizontal fracture or the soil rock interface. Water is then expected to build up on this “horizontal boundary”, due to the longer pathway and higher energy requirement that lateral movement presents (Jones et al., 2018). It is then thought that enough water would build up on this boundary in close proximity to the source, to overcome the strong adhesion and suction pressures within the surface layers and migrate downward, before large amounts of lateral flow can occur. At increased inclines however, it is suspected that another type of unsaturated flow mechanism is occurring. Water may be preferring to migrate downslope within the pavement by percolation in this orientation, along the boundary between the surface combination and base layers instead. This is because more energy would be required in this orientation to break the strong adhesion and suction pressures in the surface materials, than for downslope migration to an area of lower saturation by cohesion and gravity (Dippenaar and van Rooy, 2018).

5.3.4 Additional Observations

In addition to the quantitative results obtained during the Full-scale Model testing, interesting qualitative observations were made that illuminate the unsaturated flow mechanisms occurring in PICP. Firstly, looking at a test conducted on a layer works containing a Citylock® and P-Type 3 surface material combination, it was noted that tendrils of water developed in the sub-base layers above Q_1 , despite the surface material combination in this area being nearly saturated (Fig 39). The test was conducted at 0° incline and its results can be seen in Table G-22 in Appendix G. Similar observations were made for other tests where the model contained P-Type 1 and 2 sands as well as Waterwise bricks, at inclines of up to 2.5° . The appearance of these tendrils may imply that the flow occurring in the sub-base layers of the model resemble unsaturated fracture flow, where only 30% of fracture volume is actually used for flow (Brouwers and Dippenaar, 2018). It is thought that these tendrils were formed where water built up and broke through the adhesion and suction pressures in the surface material combination, crossing the boundary between it and the sub-base layers. This in turn would decrease invasion pressures at those points and create preferential pathways for further flow resulting in persisting and non-migrating tendrils or rivulets (Fig. 40). This would further support the concept of capillary barred perching being the dominant unsaturated flow mechanism in the surface layers of PICP at low inclines.



Fig. 39: Tendrils formed in the sub-base layers for Full-scale Model testing of a layer works containing a Citylock® and P-Type 3 sand surface combination at an incline of 2.5°

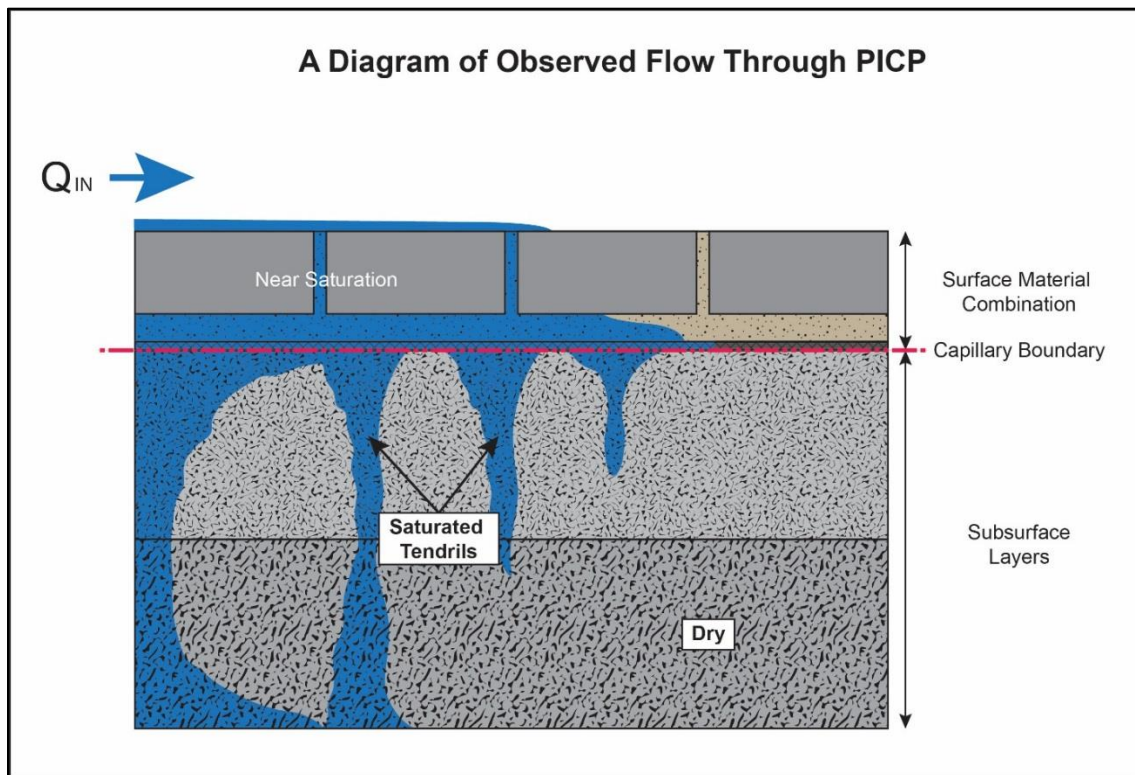


Fig. 40: A schematic representation of the flow mechanisms observed during testing of the Full-scale Model.

Another observation made during testing of the Full-Scale model highlighted a flaw in the Interaction between single-ring and double-ring infiltrometer tests and PICP. In order to verify the results obtained from the model in the ITA, double-ring infiltrometer tests were attempted inside it for layer works with Citylock® bricks and P-Type 1 and 5 surface material combinations at inclines of 0°. In each case, the infiltrometer tests produced overestimated and unexpected permeabilities in the order of 0.14cm/s which were similar to that of a well graded gravel, even on P-Type 5 combinations. The primary reason for this was the development of leakages between the rings and pavement within the joints between the bricks, despite the use of sealant as described by Bean et al., (2007) (Fig. 41).



Fig. 41: The erosion of jointing material beneath the sealant of the inner ring of the double-ring infiltrometer constructed for this study

The leakages were not due to failure of the sealant used but rather as a result of the nature of the jointing materials themselves. Compared to ICP, the jointing material in PICP rest in larger spaces between the bricks and are specifically selected to be non-cohesive. As such, the particles under those that had adhered to the sealant in the joints, were washed away by piping, allowing water to escape the rings laterally and not vertically through the pavement (Fig. 42). This does not occur in ICP because the jointing material used in them has a much flatter grain size distribution and a larger proportion of clay sized particles. This results in it being more cohesive, making it less likely to erode under the rings of infiltrometer tests.

In addition, there was considerable difficulty involved in supplying enough water to the inner and outer ring to maintain the required hydraulic head within them for the duration of the tests. This was due in part to the leaks developed at the joints but more so to the rapid infiltration rate of the pavement (Bean et al., 2004). For this reason, single and double ring infiltrometers are not ideal for accurately evaluating the hydraulic properties of PICP and as the ASTM C1701 and NCAT permeameter methods return slightly conservative values due to the small area on which permeameter tests are conducted on, there is a need for better field testing procedures for use on PICP (Li et al., 2013).

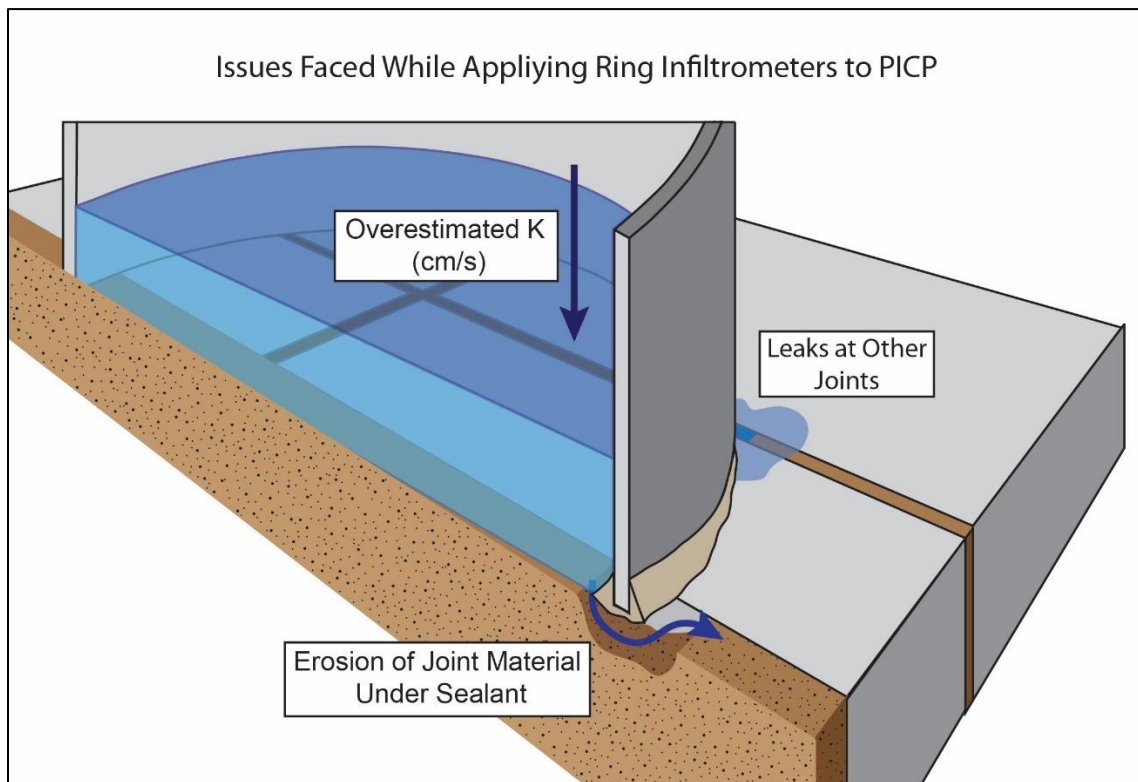


Fig. 42: A schematic diagram of the reason for the failure of ring infiltrometer tests in Permeable Interlocking Concrete Pavements

6 CONCLUSION

Based on the multiple stages of verification and testing conducted for this study, an overarching concept becomes clear; that the current design approaches and layer works of PICP being applied in industry are highly effective at managing peak flow and achieving large-volume water attenuation, regardless of the specific purpose of that pavement and, that the benefits to the application of PICP in industry are numerous. It was found that they can be applied in situations where flow occurs instantaneously or over a long period of time, that a small area of PICP is capable of absorbing large volumes of water and that they can retard flow within their layer works to prevent overload of drainage systems, all while maintaining structural integrity. However, PICP will only perform as intended if they are designed and constructed in a responsible and consistent manner.

6.1 KEY FINDINGS

- 1) The hydraulic properties of any PICP depend primarily on the intrinsic properties of the materials used within them and the subgrade on which they are constructed. While the number of layers and their respective thicknesses play a vital role in the performance and structural integrity of PICP, or any pavement for that matter, the permeability of the pavement as a system, will rather be determined by characteristics such as the porosity, permeability of the construction materials and that of the subgrade in Type-A and B PICP.
- 2) The choice of surface materials such as the bedding course and joint fill is of critical importance to the permeability of PICP and are able to limit the performance of the entire pavement, regardless of the material selection below them. The use of a single low permeability material in the layer works can limit the system permeability by as much as 80% in some cases;
- 3) The orientation of the joints between bricks in the surface layer does not affect the permeability of the pavement;
- 4) The incline on which a PICP is constructed and thus the topography of its subgrade affects its permeability. More interflow is induced at steeper inclines while more percolation occurs at flat to shallow inclines, despite no runoff being present. The incline will thus also control the migration of pollutants and particles through PICP;
- 5) There exists a critical incline angle, beyond 5°, where even the most permeable layer works will no longer have acceptable permeability (or performance) and will not retard sub-surface flow within it;

- 6) A typical Type-A PICP will subject its subgrade a maximum mean infiltration rate 0.0407 m³/min or 3.39E-02 cm/s which can decrease to around 0.0286 m³/min or 2.38E-02 cm/s with an increase in construction incline or slope of 5° or 7.8%;
- 7) Lastly, the current hydraulic field investigation techniques available for pavements are invaluable to the longevity of PICP as part of a required maintenance routine but require substantial improvement and innovation before they can confidently be applied to PICP.

6.2 LIMITATIONS AND ASSUMPTIONS

While every effort was made to ensure that testing conducted in this study was representative and accurate, there were a few unavoidable limitations to the models that necessitated the making of some assumptions. For the Basic Model, assumptions made were firstly; that all the concrete bricks used in the surface layer were identical in every way. Secondly, it was assumed that fluctuations in humidity, temperature, atmospheric pressure etc. did not contribute to the behavior of the model and lastly, that the model was an effective representation of real-world application of ICP. This implied that the moisture content of the concrete bricks was representative, that the compaction of the subsurface layer was adequate and that its dry density resembled that of the full sub-surface layer works of a common ICP. A limitation of the Basic Model was that the exit points of the BMA were only 15 mm in diameter and as such may have limited the outflow at the base. Ideally a mesh or highly perforated base would have been more representative.

The Full-scale Model was based on similar assumptions to those made in the Basic Model. Firstly, it was assumed that all the Waterwise® and Citylock® Bricks were also identical to their counterparts respectively. Next, it was assumed again that environmental effects such as humidity, atmospheric pressure and so on, do not contribute to the behavior of the model. Lastly, it was assumed that the layer works selected were representative of a PICP commonly constructed in industry in Southern Africa and that the construction surface on which it was built, did not contribute to the behavior of the model as a subgrade. Understandably, this model also had some limitations; firstly, in that it only modeled sheet flow. A wetting system that simulated rainfall would have added to this study considerably but was out of reach in terms of the time constraints and costing of the project. Secondly, the model does not investigate the principle of clogging which is known to be the primary failure mechanism of PICP. Clogging falls outside of the project scope and is best described by dedicated investigation on its own. Thirdly, this study did not consider the effects of frost heave on PICP. Lastly, there are concerns highlighted by this

study in terms of the erodibility of the jointing material in PICP, however, these issues can easily be managed with the use of chemical binders or gravels which require more energy to mobilize.

6.3 WAY FORWARD

Permeable Interlocking Concrete Pavements are an extremely effective and environmentally friendly alternative to standard interlocking paving, especially with regard to the pressing issue of water management in Southern Africa. This study provides guideline permeability data, for a variety of conditions, which should aid practitioners in the design & construction of permeable pavements. A great deal of value would be added to our understanding of the hydraulic properties of PICP by performing similar studies with different conditions and investigating some of the principles that limited it, such as the effect of different wetting systems, clogging and the erodibility of the jointing material. The hope is that, at some stage, enough data will be available from studies on this topic to produce an internationally accepted and comprehensive set of standards for the manufacture, design, construction and field testing of PICP.

REFERENCES

- Addis, B. (2001), Chapter 1, Cementious Material. In: Addis, B. and Owens, G. Fulton's concrete technology 8th Ed. Cement and concrete institute, Midrand.
- Addis, B. (2001), Chapter 7, Strength of hardened concrete. In: Addis, B. and Owens, G. Fulton's concrete technology 8th Ed. Cement and concrete institute, Midrand.
- Addis, B. (2001), Chapter 11, Concrete Mix Design. In: Addis, B. and Owens, G. Fulton's concrete technology 8th Ed. Cement and concrete institute, Midrand.
- Alexander, M. (2001), Chapter 8, Deformation and volume change of hardened concrete. In: Addis, B. and Owens, G. Fulton's concrete technology 8th Ed. Cement and concrete institute, Midrand.
- ASTM C29 (2009), Standard Test Method for Bulk Density and Voids In Aggregate.
- ASTM C1688 (2013), Standard Test Method for Density and Void Content of Freshly Mixed, Pervious Concrete.
- ASTM C1701/C1701M-09 (2009), Standard Test Method for Infiltration Rate of In Place 1 Pervious Concrete, ASTM International, West Conshohocken, PA, 2009.
- ASTM C1754 (2012), Standard Test Method for Density and Void Content of Hardened, Pervious Concrete.
- ASTM C1781 (2013), Standard Test Method for Surface Infiltration Rate of Permeable Unit Pavement Systems.
- ASTM D2434 (2006), Standard Test Method for the Permeability of Granular Soils (Constant Head).
- ASTM D3385 (2009), Test Method for Infiltration Rate of Soils In Field Using Double-Ring Infiltrimeters.
- ASTM D5084 (2010), Standard Test Methods for Measurement of Hydraulic Conductivity of Saturated Porous Materials Using a Flexible Wall Permeameter.
- Ballim, Y. and Basson, J. (2001), Chapter 9 Durability of concrete. In: Addis, B. and Owens, G. Fulton's concrete technology 8th Ed. Cement and concrete institute, Midrand, pp. 135 – 161.
- Bean, E. Z., Hunt, W. F., & Bidelspach, D. A. (2007). Field Survey of Permeable Pavement Surface Infiltration Rates. *Journal of Irrigation and Drainage Engineering*, 2007 pp. 249-255.
- Bean, E. Z., Hunt, W. F., & Bidelspach, D. A. (2007). Evaluation of four permeable pavement sites in eastern North Carolina for runoff reduction and water quality impacts. *Journal of Irrigation and Drainage Engineering*, 133, pp. 583–592.
- Beeldens, A., and Herrier, G., (2006), Water pervious pavement blocks: The Belgian experience, 8th International Conference on Concrete Block Paving, November 6-8, 2006 San Francisco, California USA.
- Bosman, R. (2017), Critical water shortages disaster plan - Public Summary, Safety and Security Department, City of Cape Town, www.capetown.gov.za/thinkwater .
- Bosun Brick (Pty) Ltd., (2017-2019), No. 9 Cresset Rd, Choolorkop, Edenvale, 1624.
- Boyd, K. (No Date), Crushing Plant Design and Layout Considerations, Material Handling, AMEC Mining & Metals, Vancouver.

- Brouwers, L. B. and Dippenaar, M. A., (2018), Partially saturated flow from sand into a discrete smooth open vertical fracture at the soil–rock interface: experimental studies, Bulletin of Engineering Geology and the Environment, Springer-Verlag GmbH Germany.
- Cairns, J. C. (N.D.), A Step-by-step Guide to Perfect Paving, Concrete Manufacturers Association NPC, Isikhova Publishing & Communications, Johannesburg.
- Cairns, J. C. (2009), Chapter 22, Precast Concrete Products. In: In: Addis, B. and Owens, G. Fulton's concrete technology 8th Ed. Cement and concrete institute, Midrand.
- Castro, D., Gonzalez-Angullo, N., Rodríguez, J. and Calzada, M., (2007), The influence of paving-block shape on the infiltration capacity of permeable paving. Land Contamination and Reclamation 15 Vol. 3, pp. 335-344.
- Concrete. (2011). Encyclopædia Britannica. Encyclopædia Britannica Ultimate Reference Suite. Chicago: Encyclopædia Britannica.
- Department for Environment, Food and Rural Affairs (DEFRA), (2011), National Standards for sustainable drainage systems, Designing, constructing, operating and maintaining drainage for surface runoff, DEFRA, Area 2A, Ergon House, London.
- Dippenaar, M. A., and van Rooy, L. J., (2018), Vadose Zone Characterisation for Hydrogeological and Geotechnical Applications, IAEG/AEG Annual Meeting Proceedings, San Francisco, California, 2018, Vol. 2.
- Domone, P. and Illston, J., (2010), Construction Materials: Their nature and behaviour, 4th Ed., Spon Press, London.
- Dreelin, E. A., Fowler, L., and Ronald Carroll, C. (2006), A test of porous pavement effectiveness on clay soils during natural storm events. Water Resources, 40, Vol. 4, pp. 799–805.
- EN 1097-3 (1998), Tests for mechanical and physical properties of aggregates, Determination of loose bulk density and voids.
- Fassman, E. A., and Blackbourn, S., (2010), Urban Runoff Mitigation by a Permeable Pavement System over Impermeable Soils, Journal of Hydrologic Engineering, ASCE, 2010, pp. 475-485.
- Ferguson, B. K., (2006), Porous pavements: The making of progress in technology and design, 8th International Conference on Concrete Block Paving, November 6-8, 2006 San Francisco, California USA.
- Gonzalez de Vallejo, L. I. and Ferrer, M. (2011), Geological Engineering, CRC Press, Netherlands.
- Grieve, G. (2001), Chapter 3, Aggregates for concrete. In: Addis, B. and Owens, G. Fulton's concrete technology 8th Ed. Cement and concrete institute, Midrand.
- Henning, B. J., (2015), A specialist report on the soils, agricultural potential and land capability for the Doornhoek fluorspar mining right application in the Ngaka Modiri Molema district, North west province, prepared on behalf of SA Fluorite (Pty) Ltd. By Exigo Sustainability, 54 Impy Road, Lynnwood Glen, Pretoria, 0081.
- Interpave, (2005), Permeable pavements – guide to the design, construction and maintenance of concrete block, permeable pavements. 3rd Ed.

- Jones, B. R., van Rooy, L. J., and Dippenaar M. A., (2018), On the Differing Role of Contact Obstacles on Variably Saturated Flow in Vertical and Horizontal Fractures, IAEG/AEG Annual Meeting Proceedings, San Francisco, California, 2018, Vol. 4.
- Kamali, M., Delkash, M., Tajrishy, M., (2017), Evaluation of permeable pavement responses to urban surface runoff, *Journal of Environmental Management*, 187, pp. 43-53.
- Kelly A., Collins, E. I., William F., Hunt, P.E., Jon M., Hathaway, E. I., (2007), Hydrologic and water quality comparison of four types of permeable pavement and standard asphalt in eastern North Carolina, Interlocking Concrete Pavement Institute, 1444 I Street, NW - Suite 700, Washington, DC.
- Kumar, K., Kozak, J., Hundal, L., Cox, A., Zhang, H. and Granato, T., (2015), In-situ infiltration performance of different permeable pavements in a employee used parking lot - A four-year study, *Journal of Environmental Management*, 167, pp. 8-14.
- Kuosa, H., Niemelainen, E. and Korkealaakso, J., (2014), Previous pavement testing methods – State-of-the-art and laboratory and field guideline for performance assessment, Research report VTT-R-08225-13, VTT, Finland.
- Lane, J. (2001), Chapter 20, Concrete masonry units and paving blocks. In: Addis, B. and Owens, G. Fulton's concrete technology 8th Ed. Cement and concrete institute, Midrand.
- Li, H., Kayhanian, M., and Harvey, J. T., (2013), Comparative field permeability measurement of permeable pavements using ASTM C1701 and NCAT permeameter methods. *Journal of Environmental Management*, 118, pp. 144–152.
- Lian, C. and Zhuge, C. (2010), Optimum mix design of enhanced permeable concrete: an experimental investigation, In: *Construction and Building Materials*, Vol. 24. pp. 2664-2671.
- Lucke, T., Boogaard, F. and van de Ven, F., (2014), Evaluation of a new experimental test procedure to more accurately determine the surface infiltration rate of permeable pavement systems, *Urban Planning and Transport Research*, Vol. 2, No. 1, pp. 22-35.
- Lucke, T., White, R., Nichols, P. and Borgwardt, S., (2015), A Simple Field Test to Evaluate the Maintenance Requirements of Permeable Interlocking Concrete Pavements, *Water 2015 – Open Access Journal*, Vol. 7, pp. 2542-2554.
- Morquecho, R.E., Pitt, R. and Clark, S., (2005), Pollutant associations with particulates in stormwater. *Impacts Global Climate Change* 173, Vol. 216, pp. 1-12.
- Oberholster, B. (2001), Chapter 10, Alkali-silica reaction. In: Addis, B. and Owens, G. Fulton's concrete technology 8th Ed. Cement and concrete institute, Midrand.
- Pavey, M. J. (2019), *New South Wales Government Gazette*, No. 55 of 31, May 2019.
- Pezzaniti, D., Beecham, S., and Kandasamy, J. (2009), "Influence of clogging on the effective life of permeable pavements." *Water Management*, No. 162, Vol. 3, pp. 211–220.
- Powers, J. P., (1992), *Construction Dewatering: New methods and applications*, 2nd Ed., John Wiley and Sons, New York.

- Salberg, D. B. (1997), Surface water drainage: revised designs and maintenance standards, IMIESA, The official journal of the Institution of Municipal Engineering of South Africa, Vol. 22, No. 11, pp. 25-30.
- SANS 927 (2007), Precast concrete kerbs, edging and channels.
- SANS 1058 (2012), Concrete Block Paving, Standard specification for concrete masonry units.
- SANS 1200-MJ (1984), Standardised specification for civil engineering construction – Laying of paving.
- South African Pavement Engineering Manual (SAPEM), (2013), Chapter 8: Material Sources, South African National Roads Agency.
- Stewart, D. A., (1951), The design and placing of high quality concrete, London: Spon.
- Technicrete, (2017), Permeable Paving: Aqua Trojan Slab®, Square® and Aqua Zig-zag®, Technicrete House, Cnr. Main Reef Road and Houtkapper Street, Roodepoort, 1725.
- Taylor, P. (2001), Chapter 5, Chemical Admixtures. In: Addis, B. and Owens, G. Fulton's concrete technology 8th Ed. Cement and concrete institute, Midrand.
- Torncoro (N.D.), Technical Guide 2: The use and design of concrete bricks and brickwork, Lithotone, Durban.
- TRH 14, (1985), Guidelines for road construction materials, Committee of State Road Authorities, Pretoria.
- TRH 20, (1990), The structural design, construction and maintenance of unpaved roads, Committee of State Road Authorities, Pretoria.
- United States Department of Agriculture (USDA), (2012), Chapter 3: Engineering Classification of Earth Materials, Part 631: National Engineering Handbook, Amendment 55, January 2012.
- Weinert, H. H., (1980) The natural road construction materials of Southern Africa, National Institute for Transport and Road Research, Pretoria.
- Woods-Ballard, B., Kellagher, R., Martin, P., Jefferies, C., Bray, R., Shaffer, P., (2007), The SuDS manual, CIRIA C698, Construction industry research and information association (CIRIA), Classic House, 174–180 Old Street, London.
- Yin, S. Yang, Y. Zhang, T. Guo, G. Yu, F. (2015), Effect of carbonic acid water on the degradation of Portland cement paste: Corrosion process and kinetics, Construction and Building Materials, School of Materials Science and Engineering, South China University of Technology, Guangzhou.

APPENDIX A

Technical and design drawings of the Basic Model Apparatus (BMA) and Infiltration Table Apparatus (ITA)

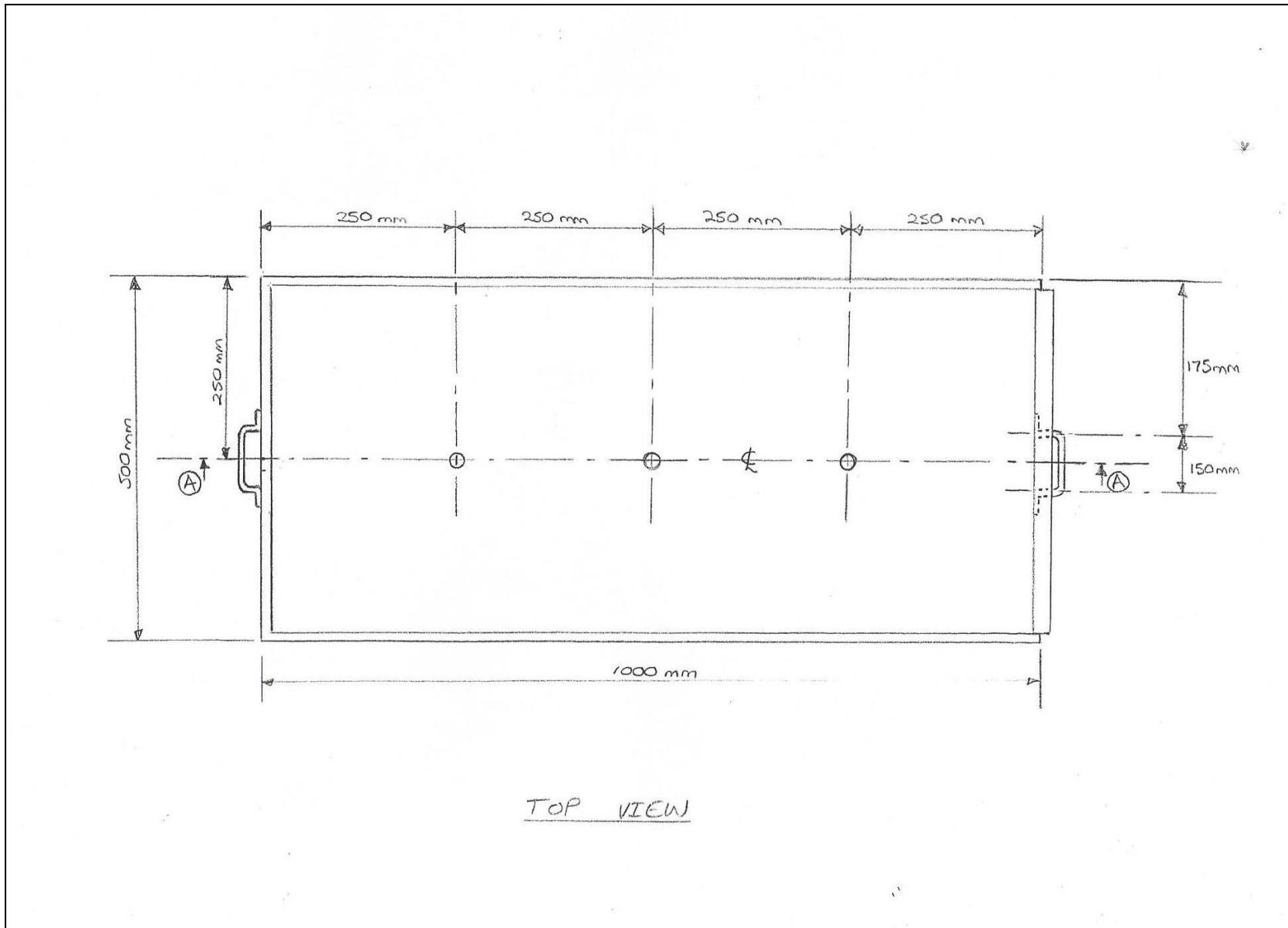


Fig. A-1: The top view of the Basic Model Apparatus design drawing.

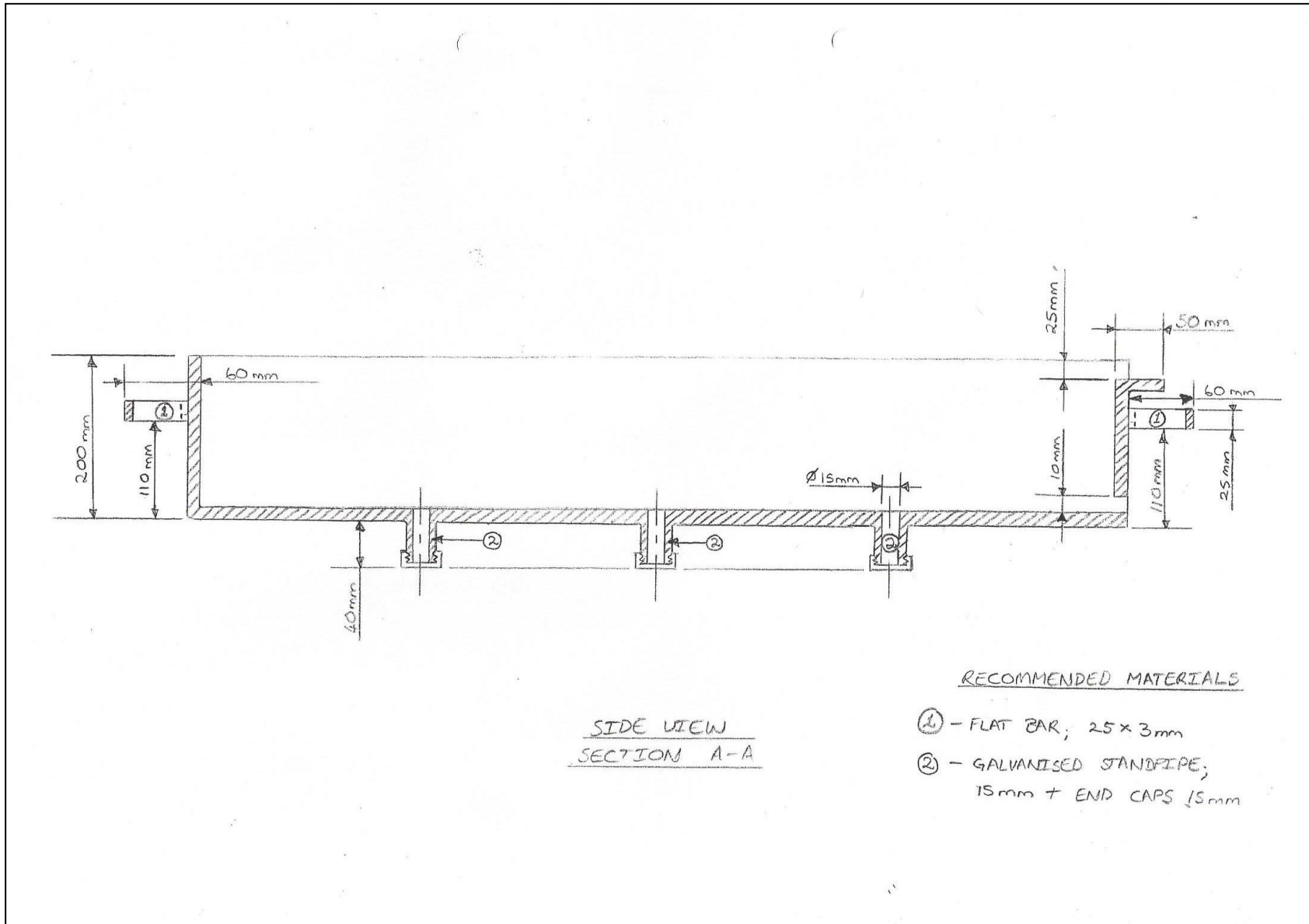


Fig. A-2: A section of the side view of the Basic Model Apparatus design drawing.

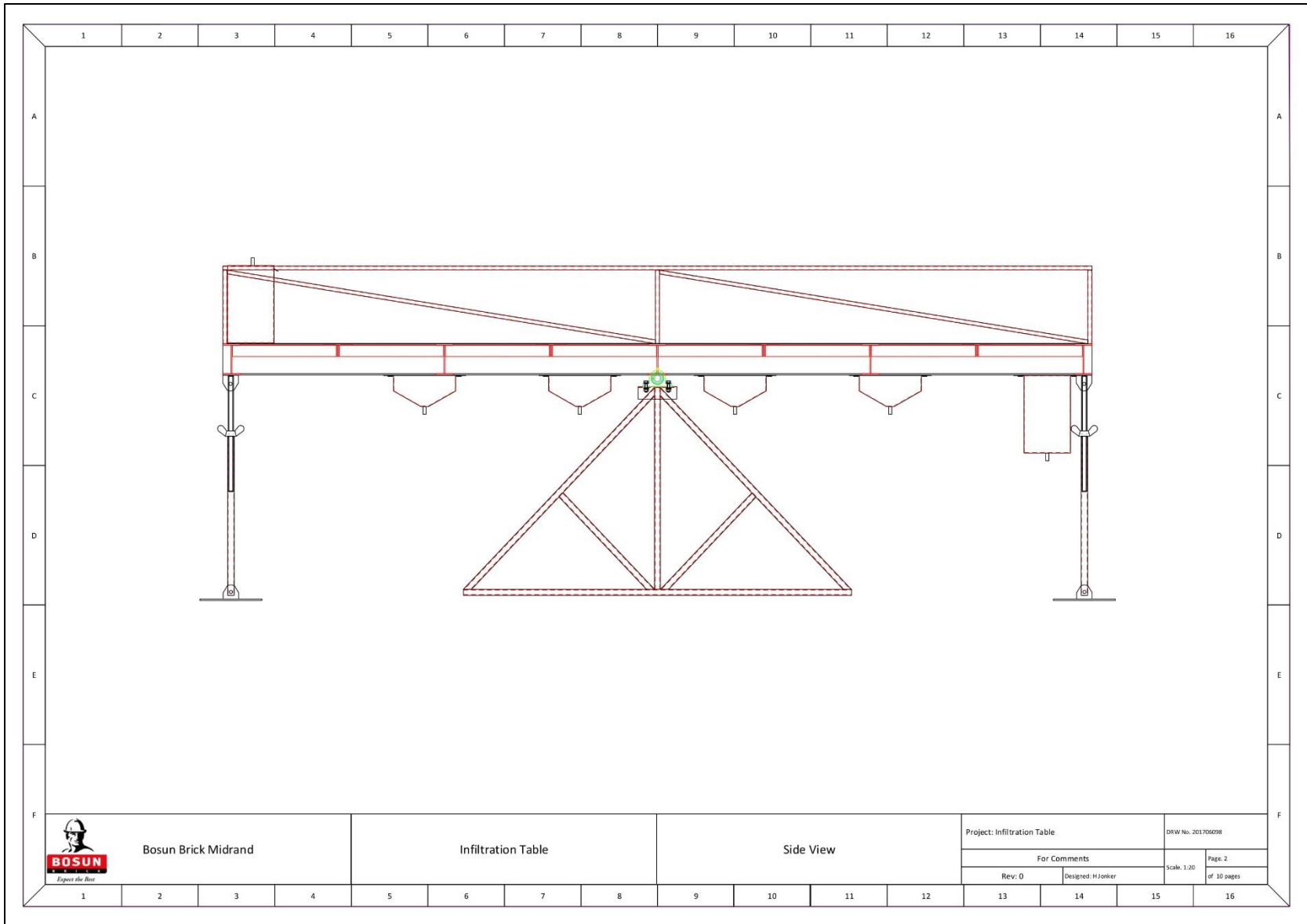


Fig. A-3: The side view of the Infiltration Table Apparatus design drawing. (Bosun Midrand, 2017)

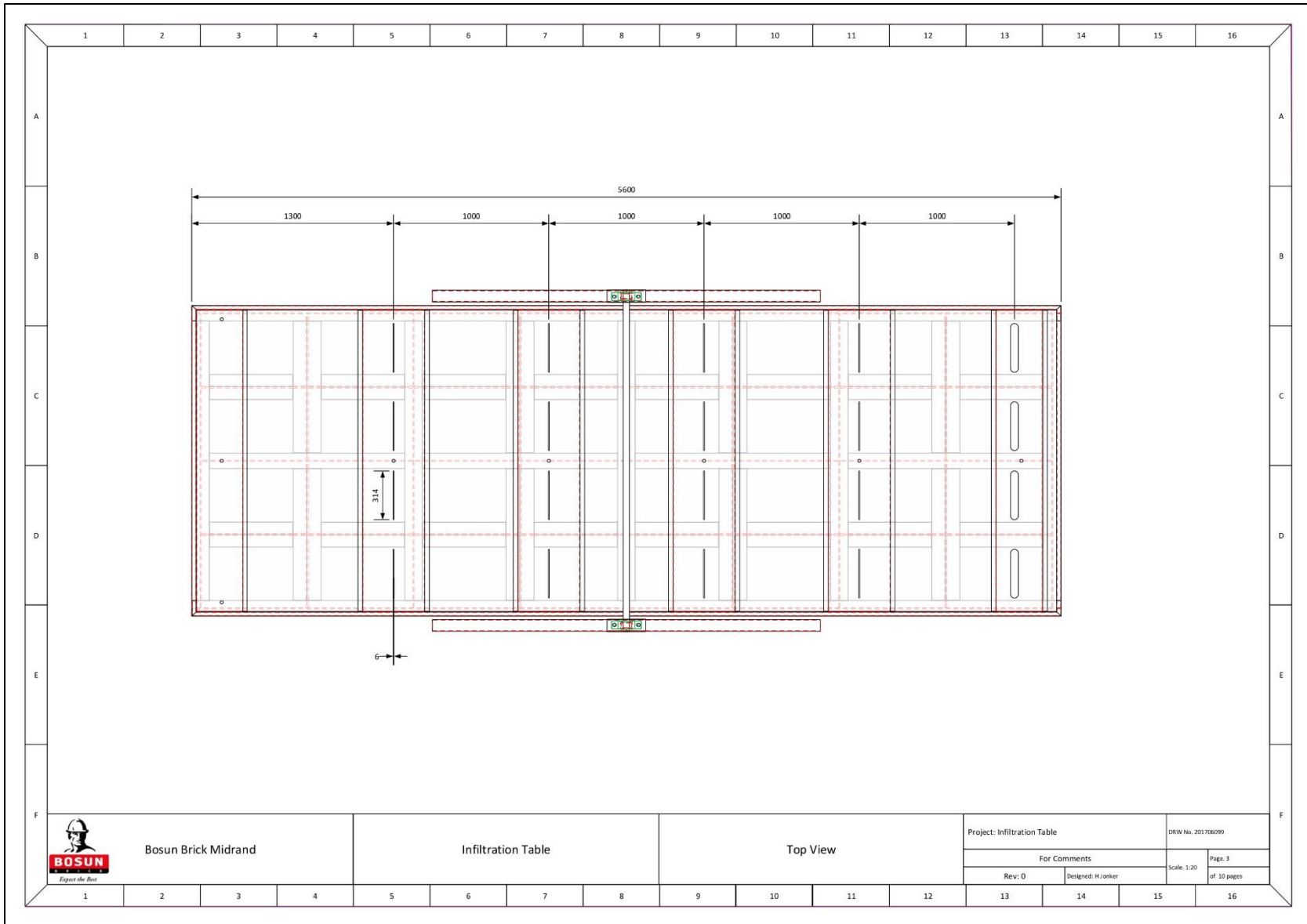


Fig. A-4: The top view of the Infiltration Table Apparatus design drawing. (Bosun Midrand, 2017)

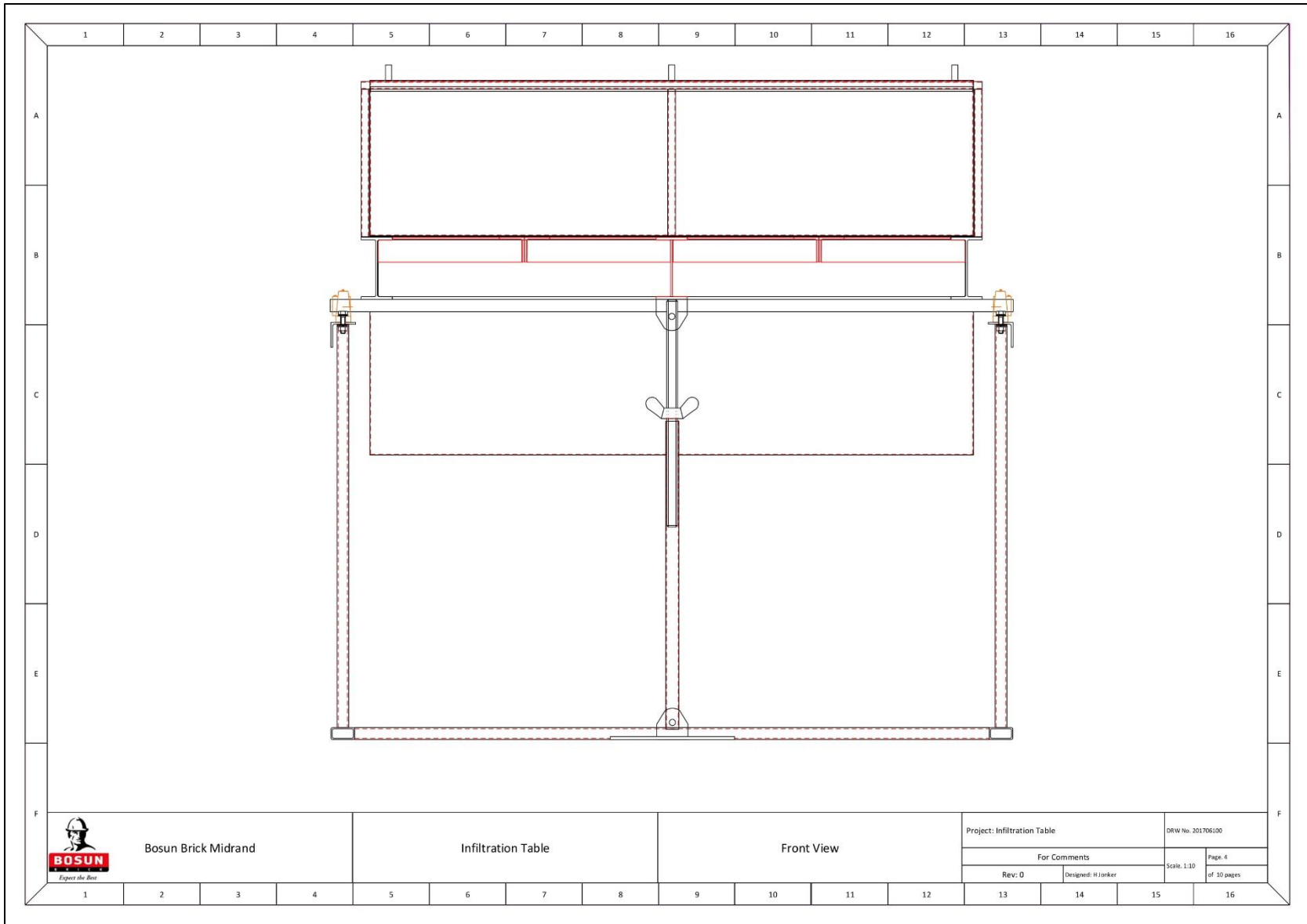


Fig. A-5: The front view of the Infiltration Table Apparatus design drawing. (Bosun Midrand, 2017)

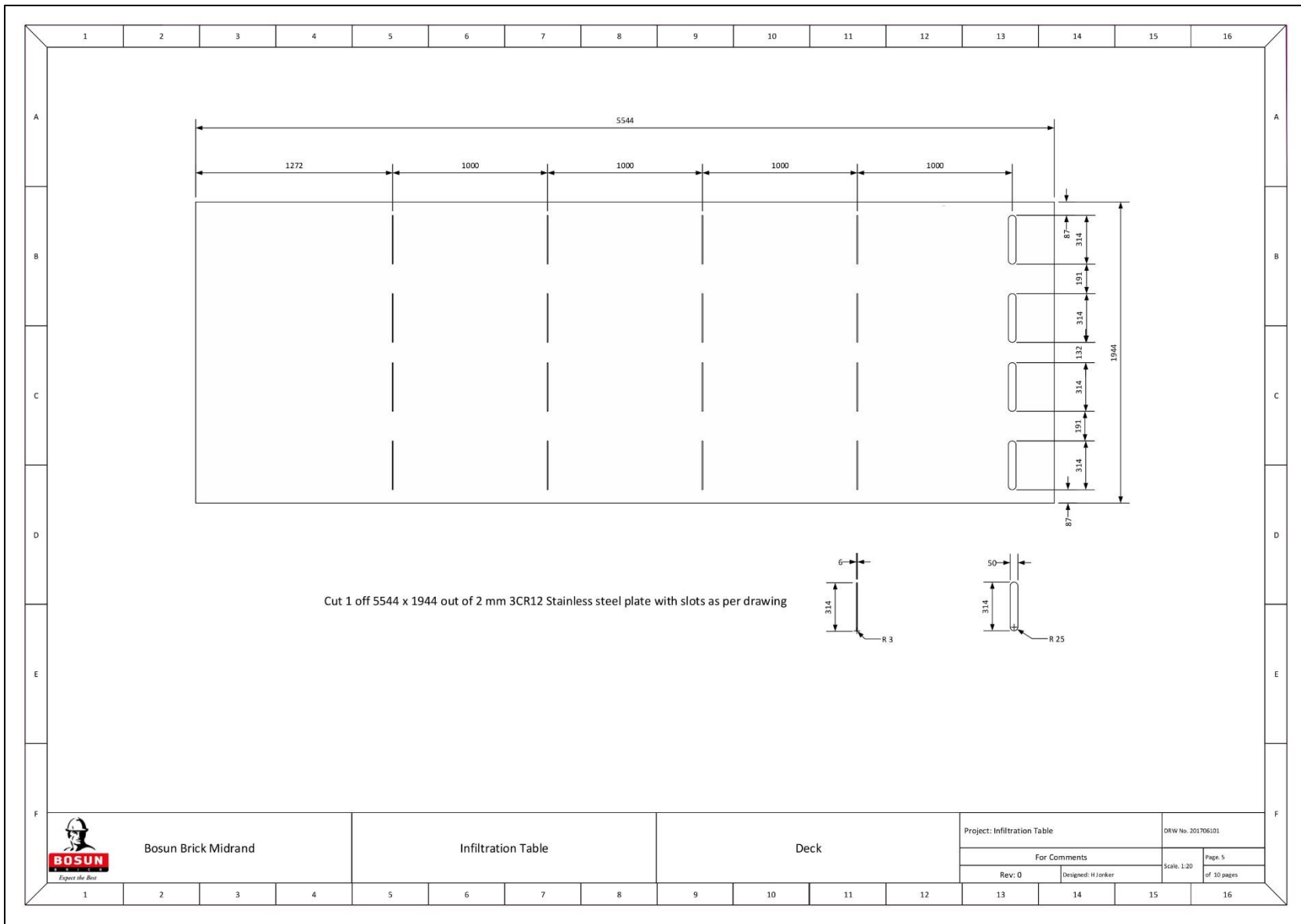


Fig. A-6: The design drawing of the construction surface (deck) of the Infiltration Table Apparatus. (Bosun Midrand, 2017)

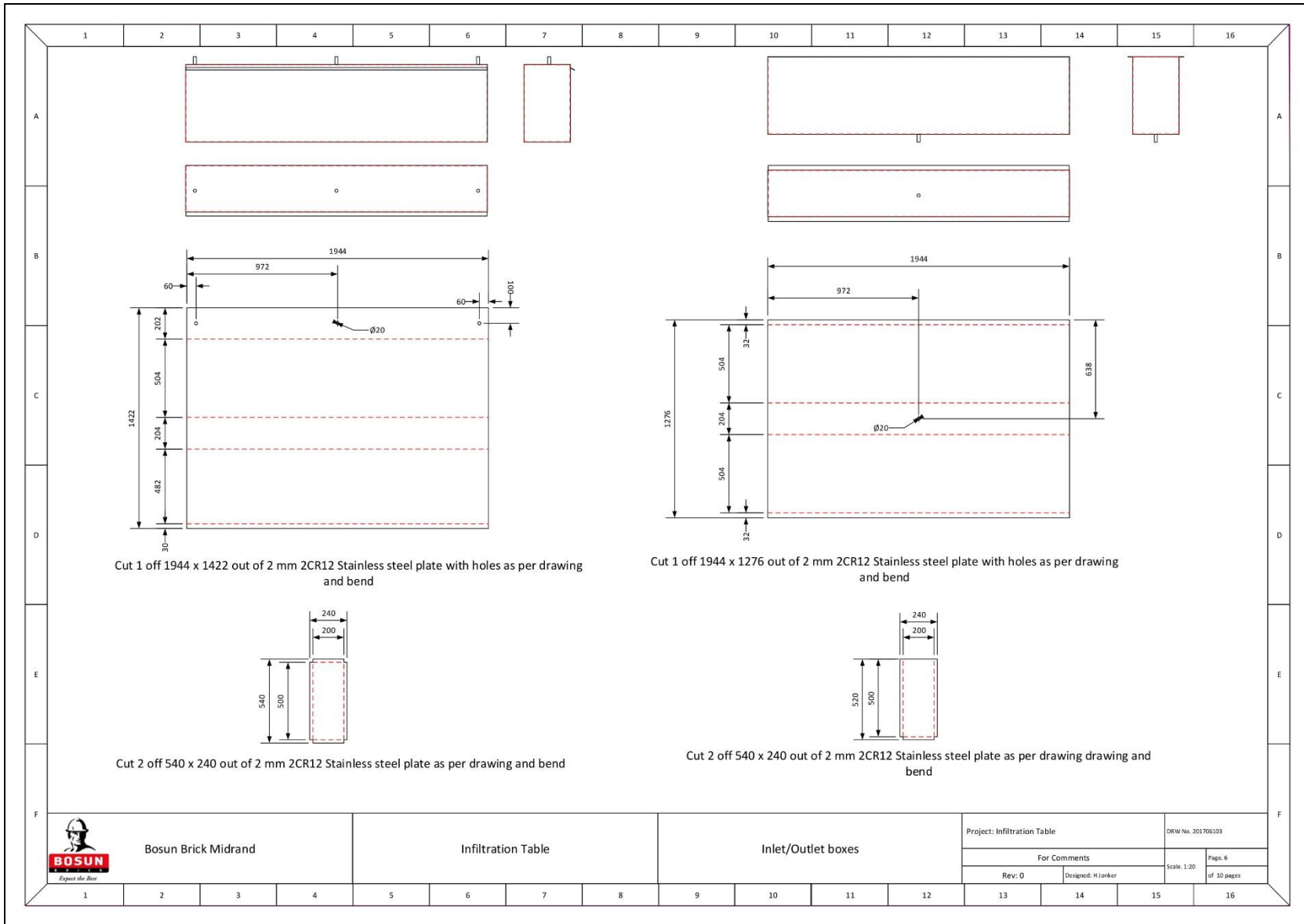


Fig. A-7: The design drawing of the ITA reservoir (Inlet Boxes). (Bosun Midrand, 2017)

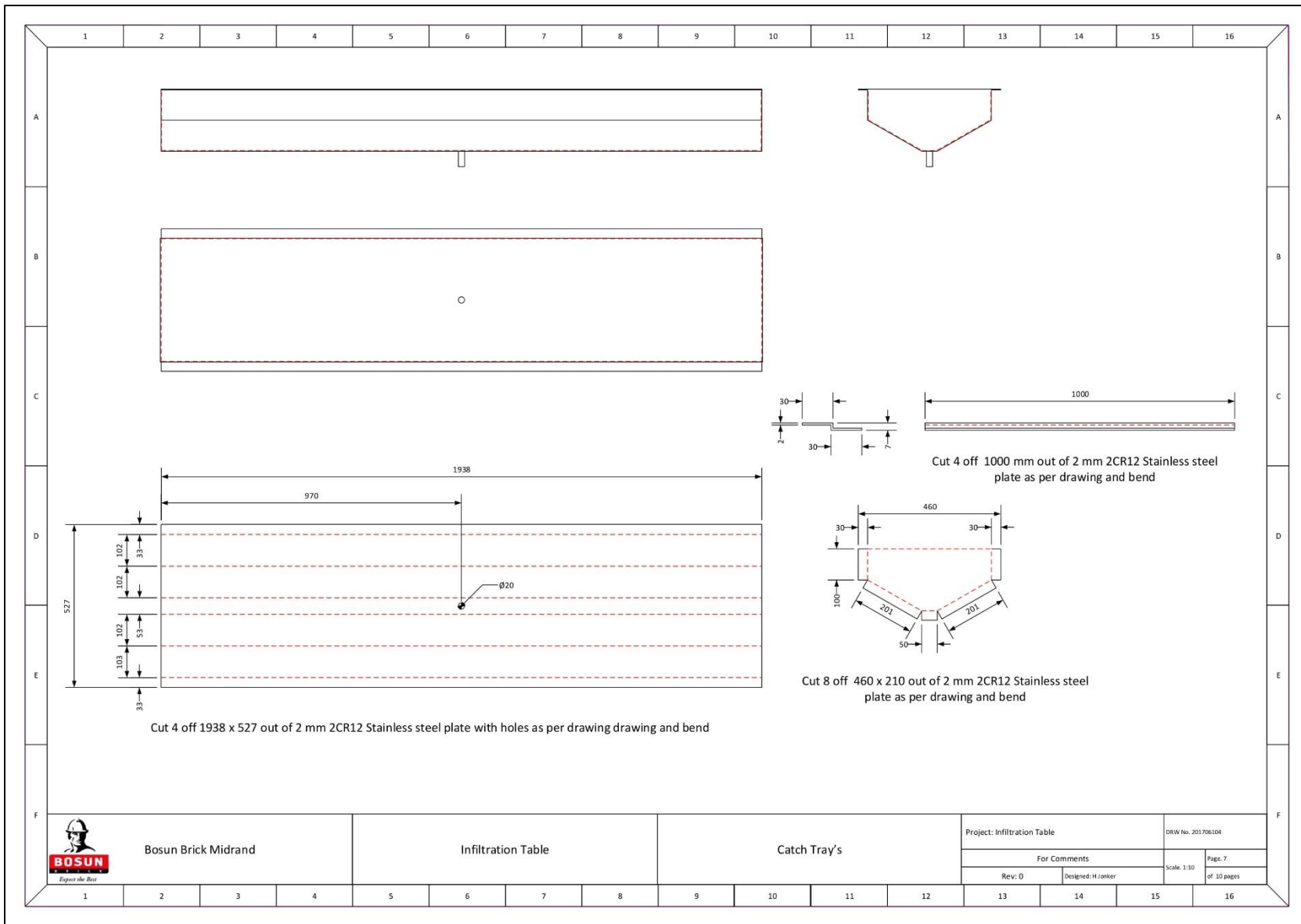


Fig. A-8: The design drawing of the collection bins (catch tray(s)) of the Infiltration Table Apparatus. (Bosun Midrand, 2017)

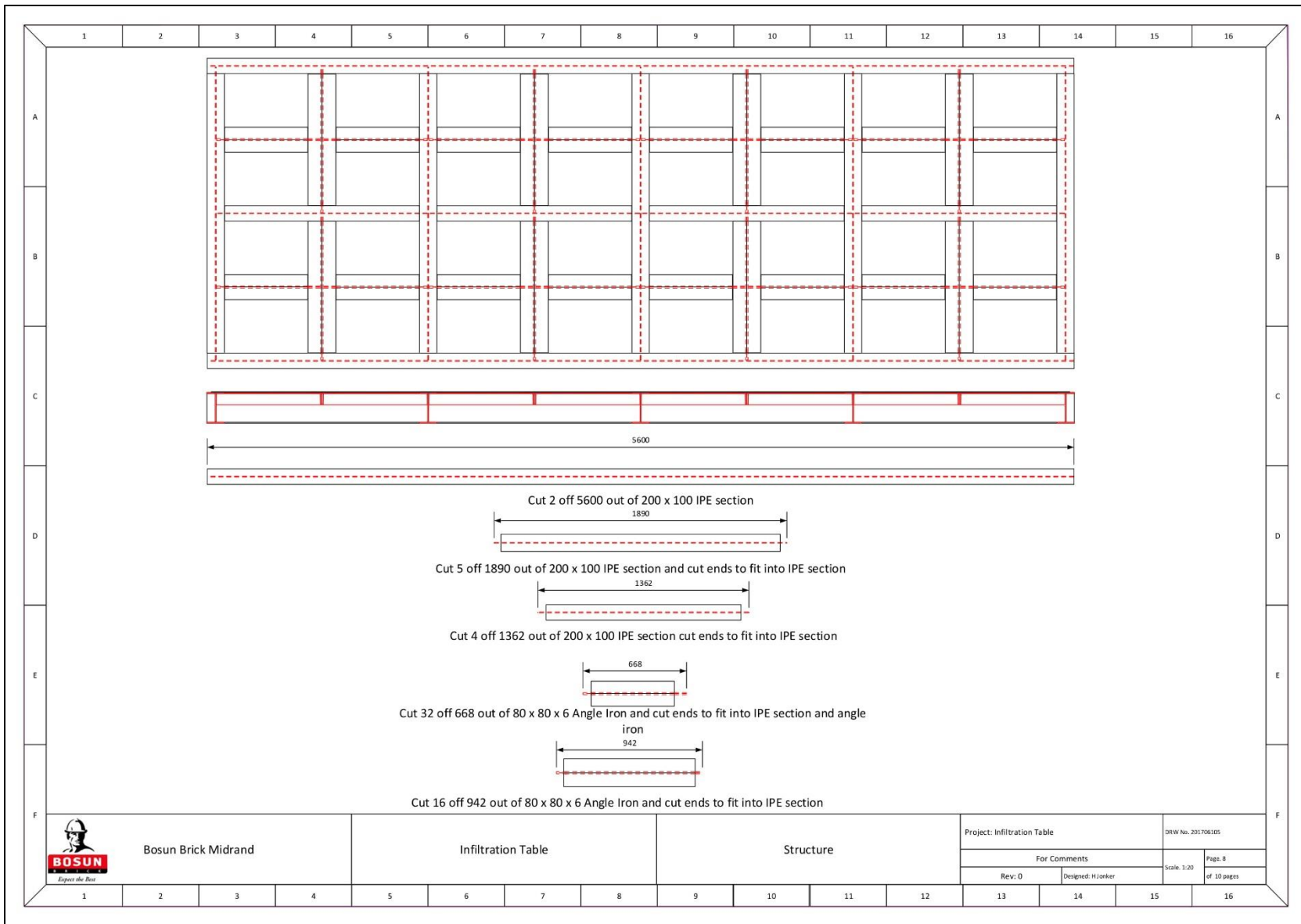


Fig. A-9: The design drawing of the supports under the construction surface of the Infiltration Table Apparatus. (Bosun Midrand, 2017)

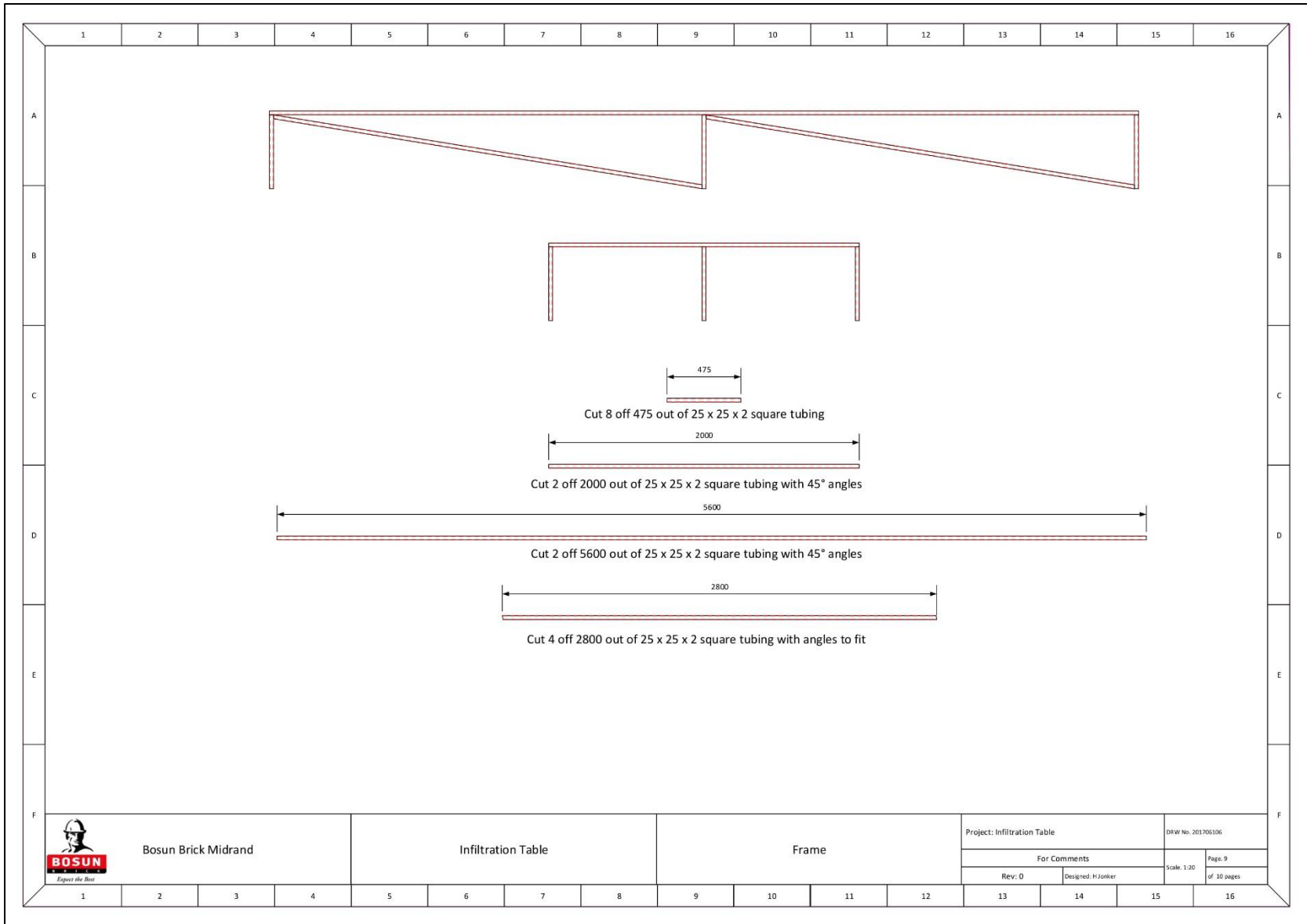


Fig. A-10: The design drawing of additional components that retained the glass sides of the Infiltration Table Apparatus. (Bosun Midrand, 2017)

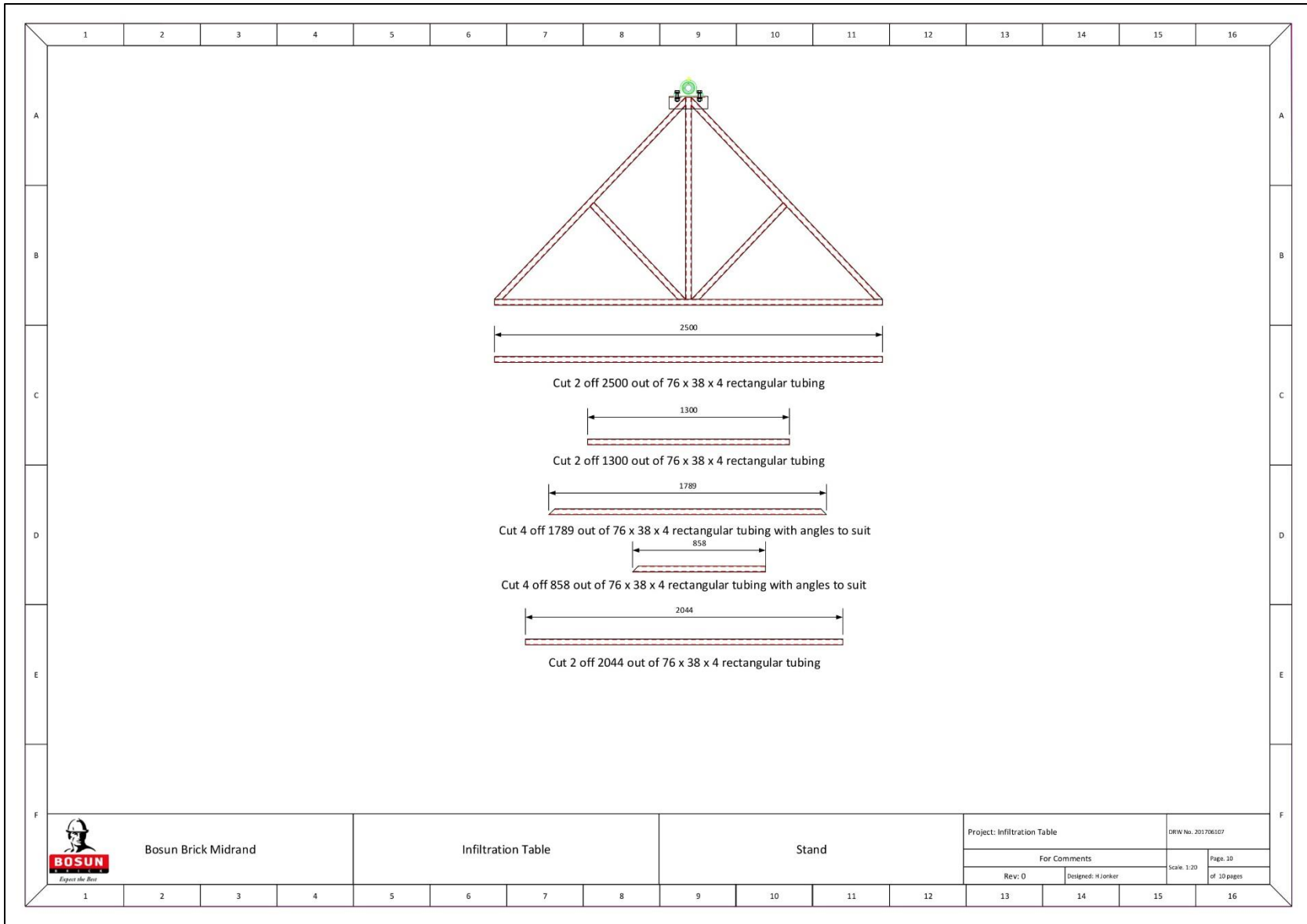


Fig. A-11: The design drawing of additional components that allowed for the tilting of the Infiltration Table Apparatus. (Bosun Midrand, 2017)

APPENDIX B

Additional photography of the Infiltration Table Apparatus (ITA)



Fig. B-1: An image of the Infiltration Table Apparatus showing the guide rods welded to the construction surface (deck).



Fig. B-2: An image of the bibum being cut to size for use in the Full-scale Model Testing.



Fig. B-3: An image of the way the Waterwise® concrete bricks were laid during construction of the Full-scale Model layer works.

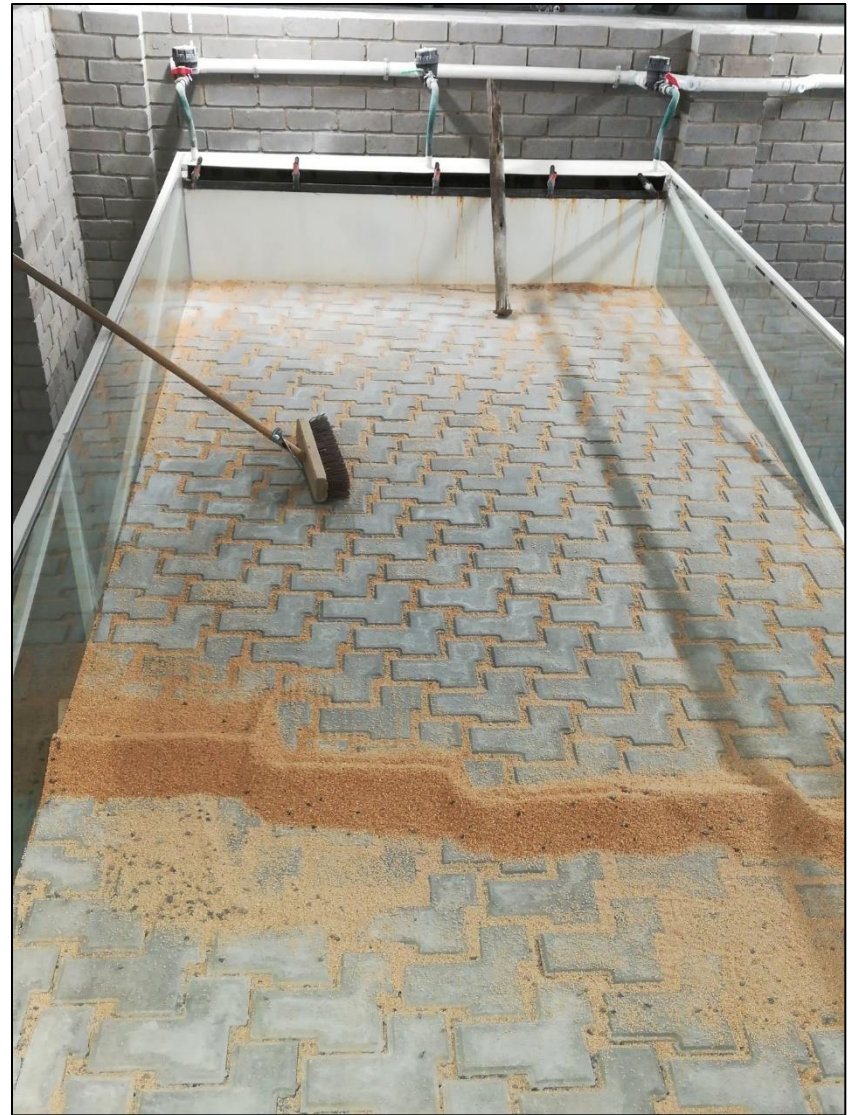


Fig. B-4: An image of P-Type 1 jointing material being added to a Waterwise®-containing layer works in the Model Design Testing



Fig. B-5: An image showing the completed construction of a Citylock® and P-Type 1 sand containing layer works in the Full-scale Model shortly before testing.



Fig. B-6: An image showing the side view of a completed construction of a Citylock® and P-Type 1 sand containing layer works in the Full-scale Model shortly before testing. Here, the filter media can be seen in the collection bins below the ITA and the block and tackle used to change the incline above.



Fig. B-7: An image showing the testing of a Waterwise® and P-Type 5 sand containing layer works during the Model Design testing. Here, the wetting front can be seen traversing the full length of the pavement.

APPENDIX C

Geotechnical logs of the test pits at the Brooks Street Site

Table C-1: The geotechnical log of test pit HA01

Trench/Pit	HA01
Date Profiled:	29 - 09 - 2017
GPS Coords:	27 Y-086051; X2897446 1328m AMSL
Profiled by:	J.H. van Vuuren
Machine Type:	Hand Auger
<i>Feature and bedding orientations are reported in dip and azimuth. " ~ " Refers to approximately. Notes are enclosed in the following brackets: {}.</i>	
Section:	0-0.7m
0-0.2m	Fill comprised of building rubble, assorted cobbles and roots in a matrix of brown silty SAND.
0.2-0.4m	Slightly moist, reddish-brown, medium dense, granular, silty-clayey fine SAND with abundant highly weathered, fine gravel and pebbles. {Abundant roots.}
0.4-0.5m	Slightly moist to dry, reddish-brown silty-clayey SAND with abundant greyish-yellow and greyish-pink, stained brow, highly weathered, mudstone/igneous gravel. {Minor amounts of black stained brow, highly weathered ferruginous concretions.}
0.5-0.7m	Reddish-brown stained yellow-brown, Highly weathered residual IGNEOUS with abundant clayey-silty sand. {Minor to trace amounts of reddish-brown stained black, ferruginous concretions and light grey stained red-brown highly weathered vein quartz.}
EOH	
* Refusal on cobble/boulder. No seepage.	

Table C-2: The geotechnical log of test pit HA02	
Trench/Pit	HA02
Date Profiled:	29 - 09 - 2017
GPS Coords:	29 Y0075847 X2850508 1354m AMSL
Profiled by:	J.H. van Vuuren
Machine Type:	Hand Auger
<i>Feature and bedding orientations are reported in dip and azimuth. " ~ " Refers to approximately. Notes are enclosed in the following brackets: {}.</i>	
Section:	0-0.7m
0-0.5m	Slightly moist, reddish-brown, medium dense, granular, silty-clayey fine SAND with abundant highly weathered, fine gravel and pebbles. {Abundant roots.}
0.5-0.7m	Slightly moist to dry, reddish-brown silty-clayey SAND with abundant greyish-yellow and greyish-pink, stained brow, highly weathered, mudstone/igneous gravel. {Minor amounts of black stained brow, highly weathered ferruginous concretions.}
EOH	
* Refusal on cobble/boulder. No seepage.	

APPENDIX D

Absorption data of interlocking concrete brick products

MVA BRICKS

TITLE:	MEASUREMENT, ANALYSIS AND IMPROVEMENT		
SUBTITLE:	WATER ABSORPTION TESTING TO SANS 1058:2012 / ABRASION RESISTANCE TESTING TO SANS 1058:2012		Swart
Document No.:	W.I. 8.2.4 (p)	Effective Date: 18 March 2015	Page 38 (b) of 65
Compiler:	FRANS BENEKE	Signature:	Copy No.
Approving Officer:	SAREL MAREE	Signature:	Rev (Amdt) No. 2

WATER ABSORPTION TESTING TO SANS 1058:2012

PLANT: A MANUFACTURE DATE: 7-9-16 TEST DATE: 14-9-16

Product

50	<input checked="" type="checkbox"/>	55	<input type="checkbox"/>	60	<input type="checkbox"/>	80	<input type="checkbox"/>	ILC	<input type="checkbox"/>	BEV	<input checked="" type="checkbox"/>	Twin Cobble	<input type="checkbox"/>	Other
----	-------------------------------------	----	--------------------------	----	--------------------------	----	--------------------------	-----	--------------------------	-----	-------------------------------------	-------------	--------------------------	-------

Time in Oven: 7:00 Time Out: 7:00
Time in Water: 7:00 Time Out: 7:00

TIME IN: 7:00 TIME OUT: 7:00

	DRY MASS	MASS AFTER TEST	RESULT	INDIV/ABSORP
1	2032	2113	90	4.4
2	2124	2214	90	4.2
3	1922	2010	88	4.5
4	1912	2000	88	4.6
5	1813	1904	91	5.
6	1926	2011	85	4.4
TOTAL				
AVERAGE:	1953.33			88.66
ABSORPTION:				45%

SIGNATURE: Alebau DATE: 14-9-16

ABRASION RESISTANCE TESTING TO SANS 1058:2012

PLANT: A MANUFACTURE DATE: 7-9-16 TEST DATE: 14-9-16

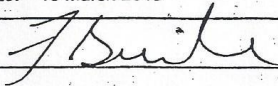

Time in Oven: 7:00 Time Out: 7:00
Time in Tumbler: 10:30 Time Out: 11:30

VW	DRY MASS	MASS AFTER TEST	RESULT	FAILED
1	2030	2015	15	
2	1954	1941	13	
3	1923	1910	13	
4	1979	1970	9	
5	1963	1955	8	
6	1929	1924	5	
7	1928	1924	4	
8	1915	1900	15	
AVERAGE:	1952.62		10.2	

SIGNATURE: Alebau DATE: 14-9-16

Fig. D-1: Absorption test results for MVA bricks product 50 with black colouring. (MVA Bricks, 2016)

MVA BRICKS

TITLE:	MEASUREMENT, ANALYSIS AND IMPROVEMENT		Rooi
SUBTITLE:	WATER ABSORPTION TESTING TO SANS 1058:2012 / ABRASION RESISTANCE TESTING TO SANS 1058:2012		
Document No.:	W.I. 8.2.4 (p)	Effective Date: 18 March 2015	Page 38 (b) of 65
Compiler:	FRANS BENEKE	Signature: 	Copy No.
Approving Officer:	SAREL MAREE	Signature: 	Rev (Amdt) No. 2

WATER ABSORPTION TESTING TO SANS 1058:2012

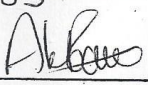
PLANT: A MANUFACTURE DATE: 6-9-16 TEST DATE: 13-9-16

Product

50 <input checked="" type="checkbox"/>	55	60	80	ILC	BEV <input checked="" type="checkbox"/>	Twin Cobble	Other
--	----	----	----	-----	---	-------------	-------

Time in Oven: 7:00 Time Out: 7:00
 Time in Water: 7:00 Time Out: 7:00

	DRY MASS	TIME IN: <u>7:00</u>	MASS AFTER TEST	TIME OUT: <u>7:00</u>	RESULT	INDIV/ABSORP
1	1924		2016		92	4.7
2	2064		2109		45	2.1
3	1841		1910		69	3.7
4	1882		1942		60	3.2
5	1863		1923		60	3.2
6	2023		2111		88	4.3
TOTAL						
AVERAGE:	1932.83					69.00
ABSORPTION:						3.5%

SIGNATURE:  DATE: 13-9-16

ABRASION RESISTANCE TESTING TO SANS 1058:2012

PLANT: A MANUFACTURE DATE: 6-9-16 TEST DATE: 13-9-16

Time in Oven: 7:00 Time Out: 7:00
 Time in Tumbler: 14:45 Time Out: 15:45

VW	DRY MASS	MASS AFTER TEST	RESULT	FAILED
1	1931	1920	11	
2	2012	2009	3	
3	2134	2132	2	
4	1953	1950	3	
5	2086	2083	3	
6	2013	2008	5	
7	2077	2076	1	
8	1891	1883	8	

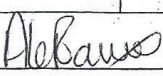
SIGNATURE:  DATE: 13-9-16

Fig. D-2: Absorption test results for MVA bricks product 50 with red colouring. (MVA Bricks, 2016)

MVA BRICKS

TITLE:	MEASUREMENT, ANALYSIS AND IMPROVEMENT		Clay
SUBTITLE:	WATER ABSORPTION TESTING TO SANS 1058:2012 / ABRASION RESISTANCE TESTING TO SANS 1058:2012		
Document No.:	W.I. 8.2.4 (p)	Effective Date: 18 March 2015	Page 38 (b) of 65
Compiler:	FRANS BENEKE	Signature:	Copy No.
Approving Officer:	SAREL MAREE	Signature:	Rev (Amdt) No. 2

WATER ABSORPTION TESTING TO SANS 1058:2012

PLANT: A MANUFACTURE DATE: 7-9-16 TEST DATE: 14-9-16

Product

50 <input checked="" type="checkbox"/>	55 <input type="checkbox"/>	60 <input type="checkbox"/>	80 <input type="checkbox"/>	ILC <input type="checkbox"/>	BEV <input checked="" type="checkbox"/>	Twin Cobble <input type="checkbox"/>	Other <input type="checkbox"/>
--	-----------------------------	-----------------------------	-----------------------------	------------------------------	---	--------------------------------------	--------------------------------

Time in Oven: 7:00 Time Out: 7:00
 Time in Water: 7:00 Time Out: 7:00

TIME IN: 7:00 TIME OUT: 7:00

	DRY MASS	MASS AFTER TEST	RESULT	INDIV/ABSORP
1	1939	2016	77	3.9
2	1837	1920	83	4.5
3	2047	2122	75	3.6
4	2041	2124	83	4.1
5	2032	2111	79	3.8
6	1826	1909	83	4.5
TOTAL				
AVERAGE:	<u>1953.66</u>			<u>80</u>
ABSORPTION:				<u>4.1%</u>

SIGNATURE: [Signature] DATE: 14-9-16

ABRASION RESISTANCE TESTING TO SANS 1058:2012

PLANT: A MANUFACTURE DATE: 7-9-16 TEST DATE: 14-9-16

Time in Oven: 7:00 Time Out: 7:00
 Time in Tumbler: 11:45 Time Out: 12:45

VW	DRY MASS	MASS AFTER TEST	RESULT	FAILED
1	2006	1994	12	
2	1912	1897	15	
3	1905	1900	5	
4	2079	2069	10	
5	1999	1987	12	
6	1917	1934	13	
7	1908	1900	8	
8	2001	1995	6	

SIGNATURE: [Signature] DATE: 14-9-16

Fig. D-3: Absorption test results for MVA bricks product 50 with clay (terracotta) colouring. (MVA Bricks, 2016)

MVA BRICKS

TITLE:	MEASUREMENT, ANALYSIS AND IMPROVEMENT		Clay
SUBTITLE:	WATER ABSORPTION TESTING TO SANS 1058:2012 / ABRASION RESISTANCE TESTING TO SANS 1058:2012		
Document No.:	W.I. 8.2.4 (p)	Effective Date: 18 March 2015	Page 38 (b) of 65
Compiler:	FRANS BENEKE	Signature:	Copy No.
Approving Officer:	SAREL MAREE	Signature:	Rev (Amdt) No. 2

WATER ABSORPTION TESTING TO SANS 1058:2012

PLANT: A MANUFACTURE DATE: 14-10-16 TEST DATE: 21-10-16

Product	50 <input checked="" type="checkbox"/>	55	60	80	ILC	BEV <input checked="" type="checkbox"/>	Twin Cobble	Other
---------	--	----	----	----	-----	---	-------------	-------

Time in Oven: 7:00 Time Out: 7:00
 Time in Water: 7:00 Time Out: 7:00

	TIME IN: <u>7:00</u>	TIME OUT: <u>7:00</u>		
	DRY MASS	MASS AFTER TEST	RESULT	INDIV/ABSORP
1	2087	2167	80	3.8
2	1959	2040	81	4.1
3	1842	1912	70	3.8
4	1987	2020	83	4.2
5	2023	2100	77	3.8
6	2016	200	84	4.1
TOTAL				79.16
AVERAGE:	1977.33			39.90
ABSORPTION:				

SIGNATURE: Atekwu DATE: 21-10-16

ABRASION RESISTANCE TESTING TO SANS 1058:2012

PLANT: A MANUFACTURE DATE: 14-10-16 TEST DATE: 21-10-16

Time in Oven: 7:00 Time Out: 7:00
 Time in Tumbler: 15:35 Time Out: 16:35

VW	DRY MASS	MASS AFTER TEST	RESULT	FAILED
1	2038	2030	8	
2	2032	2020	12	
3	1954	1951	3	
4	1826	1810	16	
5	1963	1960	3	
6	1841	1840	1	
7	2032	2020	12	
8	1826	1810	16	

SIGNATURE: 1939 Atekwu DATE: 21-10-16

Fig. D-4: Absorption test results for MVA bricks product 50 with clay (terracotta) colouring. (MVA Bricks, 2016)

MVA BRICKS

TITLE:	MEASUREMENT, ANALYSIS AND IMPROVEMENT		
SUBTITLE:	WATER ABSORPTION TESTING TO SANS 1058:2012 / ABRASION RESISTANCE TESTING TO SANS 1058:2012		Plum
Document No.:	W.I. 8.2.4 (p)	Effective Date: 18 March 2015	Page 38 (b) of 65
Compiler:	FRANS BENEKE	Signature:	Copy No.
Approving Officer:	SAREL MAREE	Signature:	Rev (Amdt) No. 2

WATER ABSORPTION TESTING TO SANS 1058:2012

PLANT: A MANUFACTURE DATE: 18-10-16 TEST DATE: 25-10-16

Product cottage

50	55	60	80	ILC	BEV	Twin Cobble	Other
----	----	----	----	-----	-----	-------------	-------

Time in Oven: 7:00 Time Out: 7:00
 Time in Water: 7:00 Time Out: 7:00

	DRY MASS	TIME IN: <u>7:00</u> MASS AFTER TEST	TIME OUT: <u>7:00</u> RESULT	INDIV/ABSORP
1	3038	3116	78	2.5
2	2967	3021	54	1.8
3	2831	2909	78	2.7
4	2842	2911	69	2.4
5	2938	3024	86	2.9
6	3029	3116	87	2.8
TOTAL				
AVERAGE:	2940.83			75.35
ABSORPTION:				2.5%

SIGNATURE: Aleba DATE: 25-10-16

ABRASION RESISTANCE TESTING TO SANS 1058:2012

PLANT: A MANUFACTURE DATE: 18-10-16 TEST DATE: 25-10-16

Time in Oven: 7:00 Time Out: 7:00
 Time in Tumbler: 11:25 Time Out: 12:25

VW	DRY MASS	MASS AFTER TEST	RESULT	FAILED
1	2975	2968	7	
2	3186	3179	7	
3	2924	2917	7	
4	2891	2884	7	
5	3130	3125	5	
6	2991	2984	7	
7	3073	3068	5	
8	2994	2989	5	

SIGNATURE: 3020.5 Aleba DATE: 25-10-16

Fig. D-5: Absorption test results for MVA bricks product 50 with plum colouring. (MVA Bricks, 2016)

APPENDIX E

Data obtained from the Basic Model

Table E-1: Volumes of water exiting the Basic Model representing a sub-surface layer works only.

Test	0°				2°				6°				10°			
	Test 1		Test 2		Test 1		Test 2		Test 1		Test 2		Test 1		Test 2	
	Volume (ml)	%	Volume (ml)	%	Volume (ml)	%	Volume (ml)	%	Volume (ml)	%	Volume (ml)	%	Volume (ml)	%	Volume (ml)	%
Point 1	1320	30.41	1390	28.48	1090	22.95	1040	24.07	620	13.84	420	13.64	500	9.69	180	6.25
Point 2	1490	34.33	1670	34.22	1380	29.05	1290	29.86	960	21.43	710	23.05	780	15.12	270	9.38
Point 3	1080	24.88	1340	27.46	1350	28.42	1090	25.23	950	21.21	660	21.43	830	16.09	380	13.19
Point 4	450	10.37	480	9.84	930	19.58	900	20.83	1950	43.53	1290	41.88	3050	59.11	2050	71.18
Runoff	0	0	0	0	0	0	0	0	0	0	0	0	0	0	0	0
Total	4340	99.99	4880	100	4750	100	4320	99.99	4480	100.01	3080	100	5160	100.01	2880	100

Table E-2: Volumes of water exiting the full Basic Model layer works

Test	0°				2°				6°				10°			
	Test 1		Test 2		Test 1		Test 2		Test 1		Test 2		Test 1		Test 2	
	Volume (ml)	%	Volume (ml)	%	Volume (ml)	%	Volume (ml)	%	Volume (ml)	%	Volume (ml)	%	Volume (ml)	%	Volume (ml)	%
Point 1	930	27.68	940	25.82	810	20.61	860	19.28	580	13.12	500	13.12	330	9.24	310	7.91
Point 2	970	28.87	990	27.2	930	23.66	970	21.75	780	17.65	670	17.59	540	15.13	550	14.03
Point 3	760	22.62	780	21.43	760	19.34	830	18.61	720	16.29	640	16.8	520	14.57	580	14.8
Point 4	700	20.83	930	25.55	1430	36.39	1800	40.36	2340	52.94	2000	52.49	2180	61.06	2480	63.27
Runoff	0	0	0	0	0	0	0	0	0	0	0	0	0	0	0	0
Total	3360	100	3640	100	3930	100	4460	100	4420	100	3810	100	3570	100	3920	100.01

APPENDIX F

Data obtained from Model Design testing on the Generic Layer Works

Table 16: Model Design testing volumes and discharges for different layers of the Generic Layer Works at 2.5°

Test date	Layers	Inlet Meters (m ³)			Outlet Meters (m ³)					Time	Discharge (m ³ /s)
		$\Delta 1$	$\Delta 2$	$\Delta 3$	ΔQ_1	ΔQ_2	ΔQ_3	ΔQ_4	ΔQ_5		
19/04/2018	Waterwise with P-Type 1 Jointing Material	0.09767	0.11496	0.1161	0.24226	0	0	0	0	7min 15sec	5.57E-04
26/04/2018	Waterwise, P-Type 1 Jointing & Bedding course	0.1152	0.12909	0.12052	0.25361	0	1E-05	0	0.00364	8min 45sec	4.83E-04
04/06/2018	Waterwise, P-Type 1 Jointing & Bedding course, Bidim, 6mm Gravel Upper Sub-base	0.0831	0.09058	0.086	0.17474	0	0	0	0	4min 45sec	6.13E-04
19/07/2018	Waterwise, P-Type 5 Jointing & Bedding course, Bidim, 6mm Gravel Upper Sub-base	0.250964	0.29055	0.24981	0.17457	0.18459	0.06512	0.08122	0.05748	20min	4.21E-04
06/09/2018	Waterwise, P-Type 1 Jointing & Bedding course, Bidim, 6mm Gravel Upper Sub-base, 20mm Gravel Lower Sub-base	0.11287	0.13693	0.06513	0.24833	0.04234	0	0	0	10min 15sec	4.73E-04
										Average	5.09E-04

* Discharge is calculated with outlet volumes from Q₁ to Q₄ only. Q₅ is considered runoff and is not included.

Table 17: Model design testing volumes and discharges of the full Generic Layer Works at different inclines

No Gravel at the base for levelling											
2018/09/06											
Incline:	Value	Inlet Meters (m ³)			Outlet Meters (m ³)					Time	Remarks:
		1	2	3	Q ₁	Q ₂	Q ₃	Q ₄	Q ₅		
0° or 0%	Start	3.19581	4.25544	2.68613	0.35635	0.26484	0.24247	0.45834	1.07115	8min	Wetting Front = 300mm
	End	3.30763	4.3863	2.77682	0.6311	0.31285	0.2431	0.46174	1.07115		
	Δ Volume	0.11182	0.13086	0.09069	0.27475	0.04801	0.00063	0.0034	0		
	Discharge (m³/s)	NA	NA	NA	0.000572	0.0001	1.31E-06	7.08E-06	0		
2.5° or 3.5%	Start	3.30763	4.3863	2.77682	0.63688	0.31758	0.2441	0.46075	1.07115	10min 15sec	Wetting Front = 400mm
	End	3.4205	4.52323	2.84195	0.88521	0.35992	0.2441	0.46075	1.07115		
	Δ Volume	0.11287	0.13693	0.06513	0.24833	0.04234	0	0	0		
	Discharge (m³/s)	NA	NA	NA	0.000404	6.88E-05	0	0	0		
5° or 8.7%	Start	3.4205	4.52323	2.84195	0.88521	0.35992	0.2441	0.46075	1.07115	10min 10sec	Wetting Front = 1m; More fines movement in 1
	End	3.52165	4.64677	2.90092	1.07828	0.44342	0.24609	0.46075	1.07115		
	Δ Volume	0.10115	0.12354	0.05897	0.19307	0.0835	0.00199	0	0		
	Discharge (m³/s)	NA	NA	NA	0.000317	0.000137	3.26E-06	0	0		

APPENDIX G

Data obtained from the Full-scale Model

Table G-1: Full-scale Model test data for a Waterwise® and P-Type 1 combination layer works at 0° incline													
06-09-2018													
Incline 0° or 0%													
Time (min):	Inlet Meters (m ³)			Outlet Meters (m ³)									
	1	2	3	Q1	Discharge at Q ₁ (m ³ /min)	Q2	Discharge at Q ₂ (m ³ /min)	Q3	Discharge at Q ₃ (m ³ /min)	Q4	Discharge at Q ₄ (m ³ /min)	Q5	Discharge at Q ₅ (m ³ /min)
0	3.19581	4.25544	2.68613	0.35635	0	0.26484	0	0.24247	0	0.45834	0	1.07115	0
5	-	-	-	0.52392	0.033514	0.29501	0.006034	0.24281	6.8E-05	0.46088	0.000508	1.07115	0
8	3.30763	4.3863	2.77682	0.6311	0.035727	0.31285	0.005947	0.2431	9.667E-05	0.46174	0.000287	1.07115	0
ΔV Total (m ³)	0.11182	0.13086	0.09069	0.27475		0.04801		0.00063		0.0034		0	
% of Total V in	33.54231	39.25368	27.20401	82.41593425		14.40141584		0.188979212		1.019887812		0	
Mean Discharge (m ³ /min)	0.04167125			0.034620333		0.005990333		8.23333E-05		0.000397333		0	

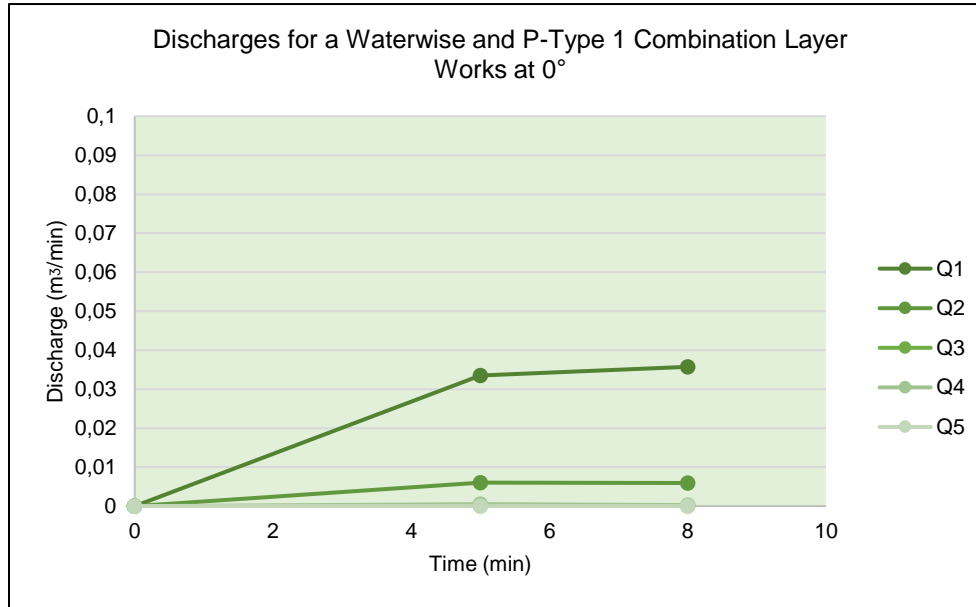


Fig. G-1: A graph of discharge per unit time for the Full-scale Model with a Waterwise and P-Type 1 surface combination layer works at 0° incline.

Table G-2: Full-scale Model test data for a Waterwise® and P-Type 1 combination layer works at 2.5° incline													
13-09-2018													
Incline 2.5° or 3.5%													
Time (min):	Inlet Meters (m ³)			Outlet Meters (m ³)									
	1	2	3	Q1	Discharge at Q ₁ (m ³ /min)	Q2	Discharge at Q ₂ (m ³ /min)	Q3	Discharge at Q ₃ (m ³ /min)	Q4	Discharge at Q ₄ (m ³ /min)	Q5	Discharge at Q ₅ (m ³ /min)
0	3.56676	4.69748	2.96575	1.17325	0	0.45931	0	0.25685	0	0.46336	0	1.07115	0
10	-	-	-	1.28573	0.011248	0.49835	0.003904	0.25685	0	0.46336	0	1.07115	0
15	-	-	-	1.39545	0.021944	0.52158	0.004646	0.25685	0	0.46336	0	1.07115	0
20	-	-	-	1.50805	0.02252	0.54548	0.00478	0.25685	0	0.46336	0	1.07115	0
25	-	-	-	1.61225	0.02084	0.57718	0.00634	0.25685	0	0.46336	0	1.07115	0
30	3.89019	5.06127	3.10019	1.71418	0.020386	0.58805	0.002174	0.25685	0	0.46336	0	1.07115	0
ΔV Total (m ³)	0.32343	0.36379	0.13444	0.54093		0.12874		0		0		0	
% of Total V in	39.363	44.275	16.362	65.83379987		15.66828128		0		0		0	
Mean Discharge (m ³ /min)	0.027388667			0.0193876		0.0043688		0		0		0	

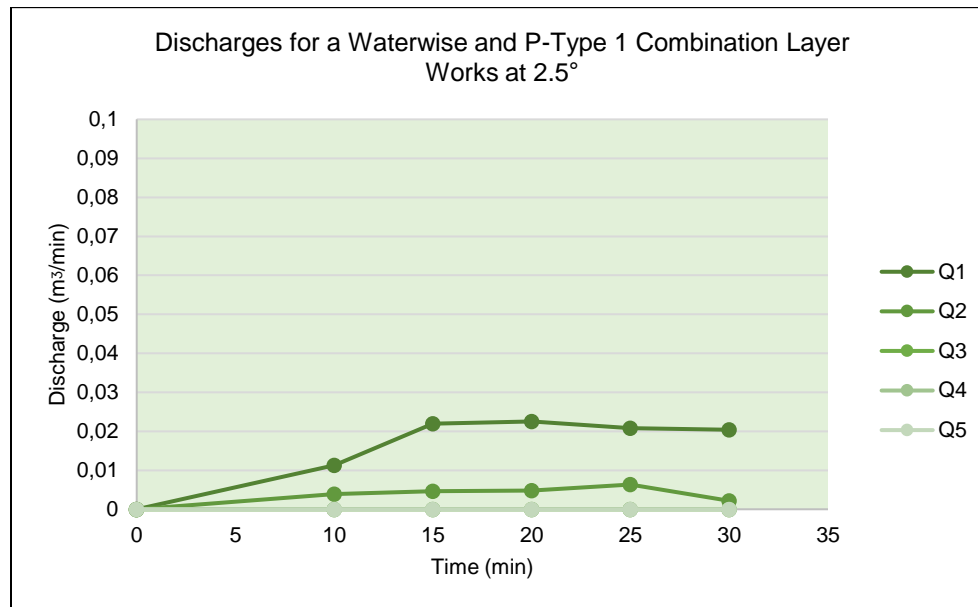


Fig. G-2: A graph of discharge per unit time for the Full-scale Model with a Waterwise and P-Type 1 surface combination layer works at 2.5° incline.

Table G-3: Full-scale Model test data for a Waterwise® and P-Type 1 combination layer works at 5° incline													
06-09-2018													
Incline 5° or 8.7%													
Time (min):	Inlet Meters (m ³)			Outlet Meters (m ³)									
	1	2	3	Q1	Discharge at Q1 (m ³ /min)	Q2	Discharge at Q2 (m ³ /min)	Q3	Discharge at Q3 (m ³ /min)	Q4	Discharge at Q4 (m ³ /min)	Q5	Discharge at Q5 (m ³ /min)
0	3.4205	4.52323	2.84195	0.88521	0	0.35992	0	0.2441	0	0.46075	0	1.07115	0
5				0.9792	0.018798	0.40098	0.008212	0.2451	0.0002	0.46075	0	1.07115	0
10	3.52165	4.64677	2.90092	1.07828	0.019816	0.44342	0.008488	0.24609	0.000198	0.46075	0	1.07115	0
ΔV Total (m ³)	0.10115	0.12354	0.05897	0.19307		0.0835		0.00199		0		0	
% of Total V in	35.65889	43.55214	20.78897	68.06387929		29.43664951		0.701544102		0		0	
Mean Discharge (m ³ /min)	0.028366			0.018798		0.008212		0.0002		0		0	

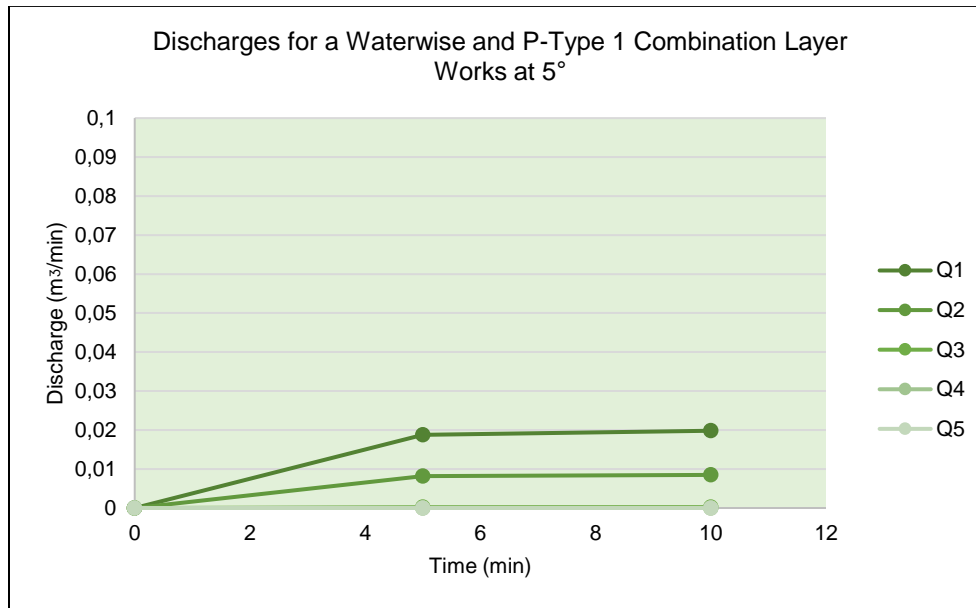


Fig. G-3: A graph of discharge per unit time for the Full-scale Model with a Waterwise and P-Type 1 surface combination layer works at 5° incline.

Table G-4: Full-scale Model test data for a Waterwise® and P-Type 2 combination layer works at 0° incline

05-02-2019

Incline 0° or 0%

Time (min):	Inlet Meters (m ³)			Outlet Meters (m ³)									
	1	2	3	Q1	Discharge at Q ₁ (m ³ /min)	Q2	Discharge at Q ₂ (m ³ /min)	Q3	Discharge at Q ₃ (m ³ /min)	Q4	Discharge at Q ₄ (m ³ /min)	Q5	Discharge at Q ₅ (m ³ /min)
0	8.82065	10.70095	6.43985	7.9316	0	2.0636	0	0.43918	0	1.02755	0	4.1351	0
10				8.04671	0.011511	2.07246	0.000886	0.43918	0	1.02755	0	4.1351	0
15				8.2252	0.035698	2.08765	0.003038	0.43918	0	1.02755	0	4.1351	0
20				8.4534	0.04564	2.0966	0.00179	0.43918	0	1.02755	0	4.1351	0
25	9.03865	11.03012	6.5377	8.49785	0.00889	2.10045	0.00256	0.43918	0	1.02755	0	4.1351	0
ΔV Total (m ³)	0.218	0.32917	0.09785	0.56625		0.03685		0		0		0	
% of Total V in	33.7974	51.03253	15.17007	87.78797557		5.713001147		0		0		0	
Mean Discharge (m ³ /min)	0.0258008			0.030949667		0.001904667		0		0		0	

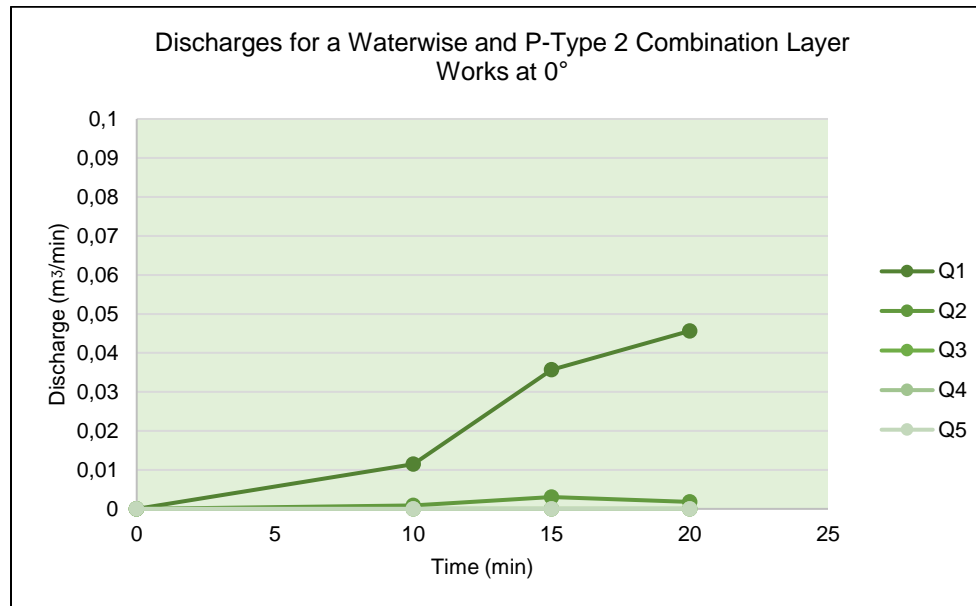


Fig. G-4: A graph of discharge per unit time for the Full-scale Model with a Waterwise and P-Type 2 surface combination layer works at 0° incline.

Table G-5: Full-scale Model test data for a Waterwise® and P-Type 2 combination layer works at 2.5° incline

05-02-2019

Incline 2.5° or 3.5%

Time (min):	Inlet Meters (m ³)			Outlet Meters (m ³)									
	1	2	3	Q1	Discharge at Q ₁ (m ³ /min)	Q2	Discharge at Q ₂ (m ³ /min)	Q3	Discharge at Q ₃ (m ³ /min)	Q4	Discharge at Q ₄ (m ³ /min)	Q5	Discharge at Q ₅ (m ³ /min)
0	9.03865	11.03012	6.5377	8.49785	0	2.10045	0	0.43918	0	1.02755	0	4.1351	0
10	-	-	-	8.57347	0.007562	2.13415	0.00337	0.43918	0	1.02755	0	4.1351	0
15	-	-	-	8.72785	0.030876	2.1615	0.00547	0.43918	0	1.02755	0	4.1351	0
20	9.18365	11.2534	6.5928	8.83005	0.02044	2.16545	0.00079	0.43918	0	1.02755	0	4.1351	0
ΔV Total (m ³)	0.145	0.22328	0.0551	0.3322		0.065		0		0		0	
% of Total V in	34.24819	52.73749	13.01431	78.46379139		15.35263829		0		0		0	
Mean Discharge (m ³ /min)	0.021169			0.019626		0.00321		0		0		0	

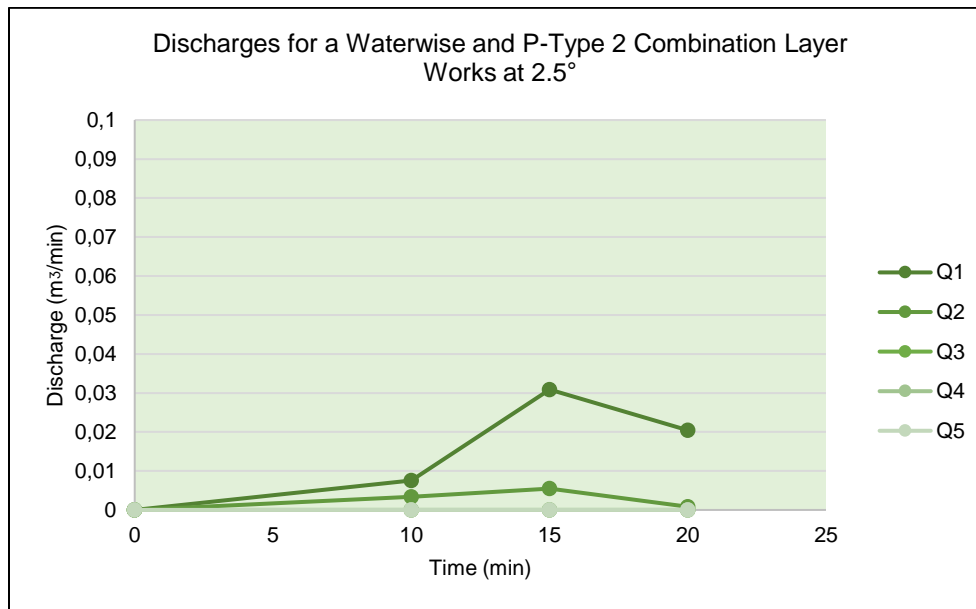


Fig. G-5: A graph of discharge per unit time for the Full-scale Model with a Waterwise and P-Type 2 surface combination layer works at 2.5° incline.

Table G-6: Full-scale Model test data for a Waterwise® and P-Type 2 combination layer works at 5° incline													
05-02-2019													
Incline 5° or 8.7%													
Time (min):	Inlet Meters (m ³)			Outlet Meters (m ³)									
	1	2	3	Q1	Discharge at Q ₁ (m ³ /min)	Q2	Discharge at Q ₂ (m ³ /min)	Q3	Discharge at Q ₃ (m ³ /min)	Q4	Discharge at Q ₄ (m ³ /min)	Q5	Discharge at Q ₅ (m ³ /min)
0	9.18365	11.2534	6.5928	8.83005	0	2.16545	0	0.43918	0	1.02755	0	4.1351	0
10				8.89251	0.006246	2.18602	0.002057	0.43918	0	1.02755	0	4.1351	0
15				9.01695	0.024888	2.2353	0.009856	0.43918	0	1.02755	0	4.1351	0
20	9.3482	11.3927	6.6429	9.08075	0.01276	2.2404	0.00102	0.44025	0.000214	1.02755	0	4.1351	0
ΔV Total (m ³)	0.16455	0.1393	0.0501	0.2507		0.07495		0.00107		0		0	
% of Total V in	46.48962	39.35584	14.15454	70.82921317		21.17530725		0.302302585		0		0	
Mean Discharge (m ³ /min)	0.0176975			0.014631333		0.004311		7.13333E-05		0		0	

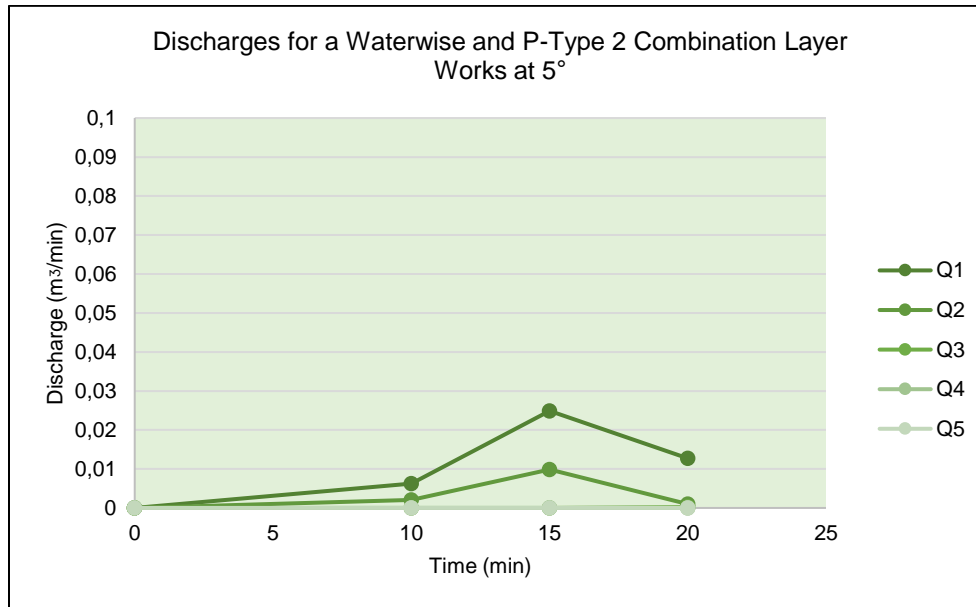


Fig. G-6: A graph of discharge per unit time for the Full-scale Model with a Waterwise and P-Type 2 surface combination layer works at 5° incline.

Table G-7: Full-scale Model test data for a Waterwise® and P-Type 3 combination layer works at 0° incline													
29-11-2018													
Incline 0° or 0%													
Time (min):	Inlet Meters (m ³)			Outlet Meters (m ³)									
	1	2	3	Q1	Discharge at Q ₁ (m ³ /min)	Q2	Discharge at Q ₂ (m ³ /min)	Q3	Discharge at Q ₃ (m ³ /min)	Q4	Discharge at Q ₄ (m ³ /min)	Q5	Discharge at Q ₅ (m ³ /min)
0	8.20238	9.73595	6.12985	6.5165	0	1.8072	0	0.40525	0	1.02525	0	4.1351	0
10				6.63014	0.011364	1.82125	0.001405	0.40525	0	1.02525	0	4.1351	0
15				6.7622	0.026412	1.84695	0.00514	0.40525	0	1.02525	0	4.1351	0
20				6.8839	0.02434	1.8645	0.00351	0.40525	0	1.02525	0	4.1351	0
25				7.03185	0.02959	1.8793	0.00296	0.40525	0	1.02525	0	4.1351	0
30	8.30342	10.1226	6.2571	7.0493	0.00349	1.88712	0.001564	0.40525	0	1.02525	0	4.1351	0
ΔV Total (m ³)	0.10104	0.38665	0.12725	0.5328		0.07992		0		0		0	
% of Total V in	16.43087	62.87605	20.69308	86.64259928		12.99638989		0		0		0	
Mean Discharge (m ³ /min)	0.020498			0.0229265		0.00325375		0		0		0	

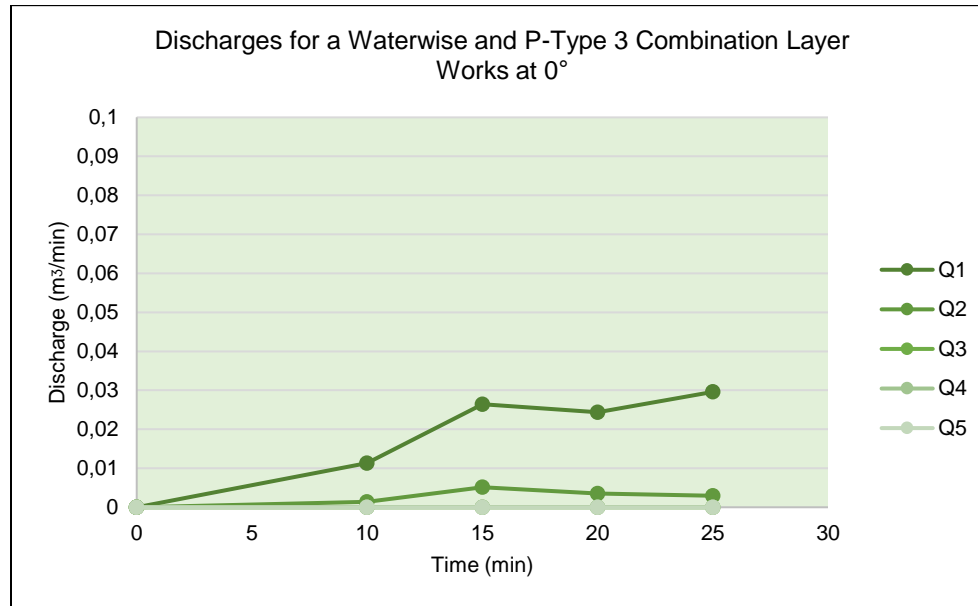


Fig. G-7: A graph of discharge per unit time for the Full-scale Model with a Waterwise and P-Type 3 surface combination layer works at 0° incline.

Table G-8: Full-scale Model test data for a Waterwise® and P-Type 3 combination layer works at 2.5° incline													
29-11-2018													
Incline 2.5° or 3.5%													
Time (min):	Inlet Meters (m ³)			Outlet Meters (m ³)									
	1	2	3	Q1	Discharge at Q ₁ (m ³ /min)	Q2	Discharge at Q ₂ (m ³ /min)	Q3	Discharge at Q ₃ (m ³ /min)	Q4	Discharge at Q ₄ (m ³ /min)	Q5	Discharge at Q ₅ (m ³ /min)
0	8.30342	10.1226	6.2571	7.1393	0	1.88712	0	0.40525	0	1.02525	0	4.1351	0
10	-	-	-	7.22545	0.008615	1.90775	0.002063	0.4071	0.000185	1.02525	0	4.1351	0
15	-	-	-	7.40525	0.03596	1.93855	0.00616	0.408	0.00018	1.02525	0	4.1351	0
20	-	-	-	7.48865	0.01668	1.9608	0.00445	0.4108	0.00056	1.02525	0	4.1351	0
25	-	-	-	7.58795	0.01986	1.98455	0.00475	0.41365	0.00057	1.02525	0	4.1351	0
30	8.57763	10.49343	6.36878	7.66725	0.01586	2.00565	0.00422	0.41635	0.00054	1.02525	0	4.1351	0
ΔV Total (m ³)	0.27421	0.37083	0.11168	0.52795		0.11853		0.0111		0		0	
% of Total V in	36.23665	49.00492	14.75843	69.76821017		15.66365366		1.466856962		0		0	
Mean Discharge (m ³ /min)	0.025224			0.019395		0.0043286		0.000407		0		0	

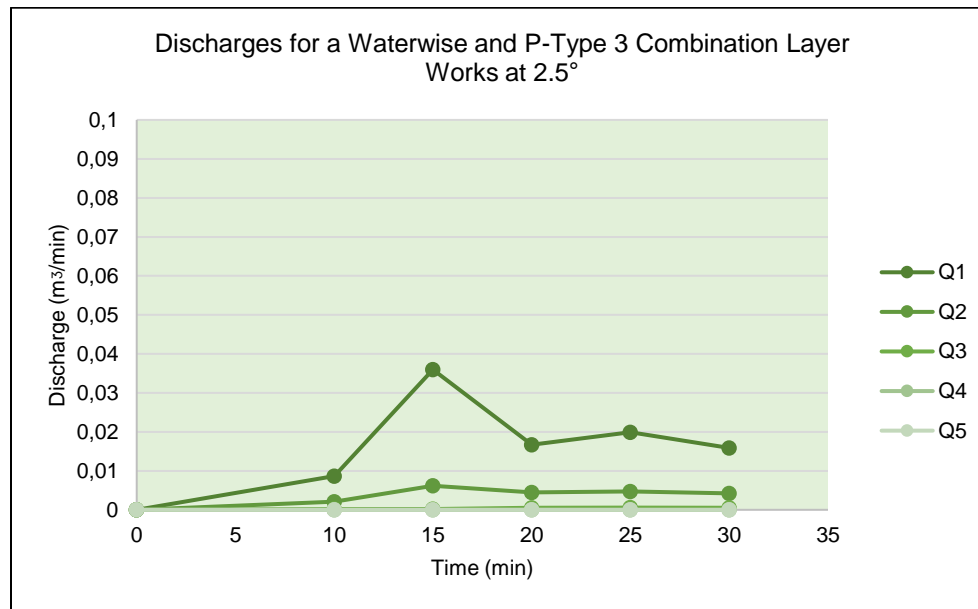


Fig. G-8: A graph of discharge per unit time for the Full-scale Model with a Waterwise and P-Type 3 surface combination layer works at 2.5° incline.

Table G-9: Full-scale Model test data for a Waterwise® and P-Type 3 combination layer works at 5° incline													
29-11-2018													
Incline 5° or 8.7													
Time (min):	Inlet Meters (m ³)			Outlet Meters (m ³)									
	1	2	3	Q1	Discharge at Q ₁ (m ³ /min)	Q2	Discharge at Q ₂ (m ³ /min)	Q3	Discharge at Q ₃ (m ³ /min)	Q4	Discharge at Q ₄ (m ³ /min)	Q5	Discharge at Q ₅ (m ³ /min)
0	8.57763	10.49343	6.36878	7.66725	0	2.00565	0	0.41635	0	1.02525	0	4.1351	0
10				7.70035	0.00331	2.0134	0.000775	0.42345	0.00071	1.02525	0	4.1351	0
15				7.8239	0.02471	2.0406	0.00544	0.42395	0.0001	1.02525	0	4.1351	0
20				7.9299	0.0212	2.05525	0.00293	0.42775	0.00076	1.02525	0	4.1351	0
25	8.77256	10.6365	6.41465	7.93135	0.00029	2.05772	0.000494	0.42865	0.00018	1.02525	0	4.1351	0
ΔV Total (m ³)	0.19493	0.14307	0.04587	0.2641		0.05207		0.0123		0		0	
% of Total V in	50.78021	37.27043	11.94936	68.79933311		13.56448798		3.204209759		0		0	
Mean Discharge (m ³ /min)	0.0153548			0.0123775		0.00240975		0.0004375		0		0	

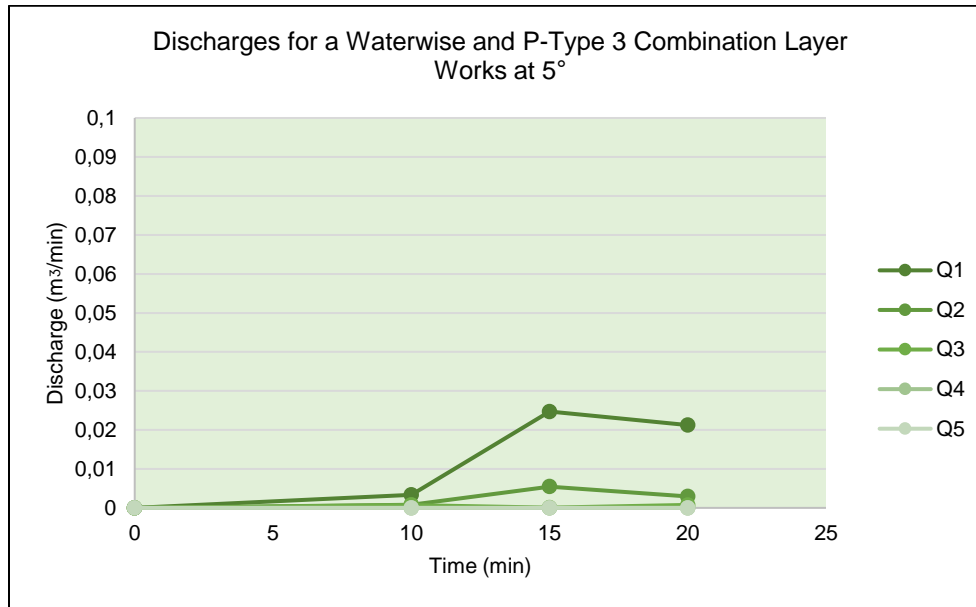


Fig. G-9: A graph of discharge per unit time for the Full-scale Model with a Waterwise and P-Type 3 surface combination layer works at 5° incline.

Table G-10: Full-scale Model test data for a Waterwise® and P-Type 4 combination layer works at 0° incline													
19-07-2018													
Incline 0° or 0%													
Time (min):	Inlet Meters (m ³)			Outlet Meters (m ³)									
	1	2	3	Q1	Discharge at Q ₁ (m ³ /min)	Q2	Discharge at Q ₂ (m ³ /min)	Q3	Discharge at Q ₃ (m ³ /min)	Q4	Discharge at Q ₄ (m ³ /min)	Q5	Discharge at Q ₅ (m ³ /min)
0	1.90917	2.77449	1.47114	0.7215	0	0.77062	0	1.20005	0	0.8206	0	0.68245	0
10				0.88872	0.016722	0.83297	0.006235	1.20602	0.000597	0.8206	0	0.74089	0.005844
15				0.97731	0.017718	0.86501	0.006408	1.20887	0.00057	0.8206	0	0.7709	0.006002
17	2.17996	3.06895	1.62161	1.00954	0.016115	0.87757	0.00628	1.21012	0.000625	0.8206	0	0.78307	0.006085
ΔV Total (m ³)	0.27079	0.29446	0.15047	0.28804		0.10695		0.01007		0		0.10062	
% of Total V in	37.83463	41.14179	21.02358	40.24478846		14.94299447		1.406974795		0		14.05857039	
Mean Discharge (m ³ /min)	0.042101176			0.016851667		0.006307667		0.000597333		0		0.005977	

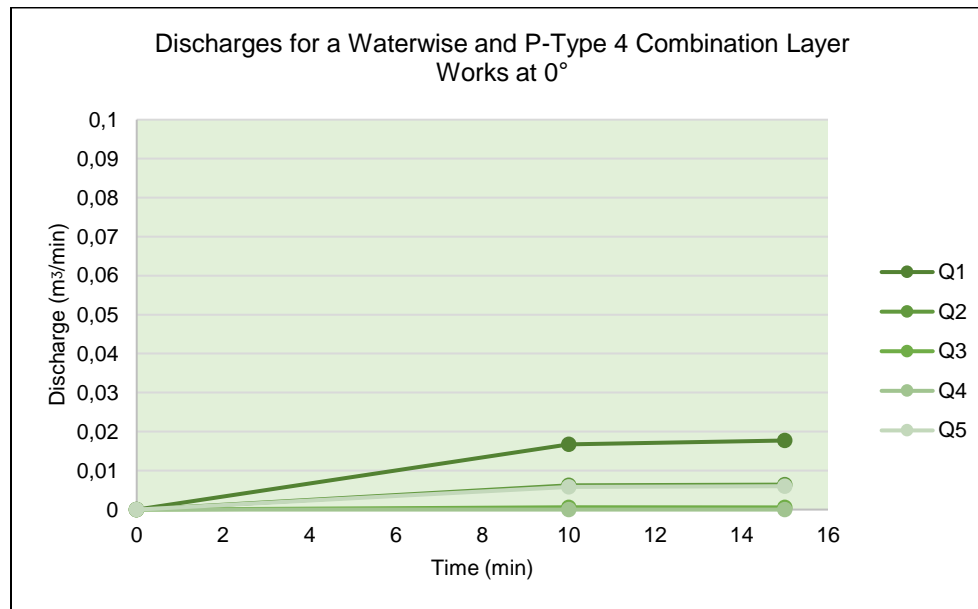


Fig. G-10: A graph of discharge per unit time for the Full-scale Model with a Waterwise and P-Type 4 surface combination layer works at 0° incline.

Table G-11: Full-scale Model test data for a Waterwise® and P-Type 4 combination layer works at 2.5° incline													
19-07-2018													
Incline 2.5° or 3.5%													
Time (min):	Inlet Meters (m³)			Outlet Meters (m³)									
	1	2	3	Q1	ΔQ1/min	Q2	ΔQ2/min	Q3	ΔQ3/min	Q4	ΔQ4/min	Q5	ΔQ5/min
0	2.177996	3.06895	1.62161	1.00954	0	0.87757	0	1.21012	0	0.82059	0	0.78309	0
10	-	-	-	1.07835	0.006881	0.94225	0.006468	1.2355	0.002538	0.85295	0.003236	0.80595	0.002286
15	-	-	-	1.1133	0.00699	0.98795	0.00914	1.24875	0.00265	0.87005	0.00342	0.81698	0.002206
20	2.42896	3.3595	1.87142	1.18411	0.014162	1.06216	0.014842	1.27524	0.005298	0.90181	0.006352	0.84057	0.004718
ΔV Total (m³)	0.250964	0.29055	0.24981	0.17457		0.18459		0.06512		0.08122		0.05748	
% of Total V in	31.71444	36.71695	31.56861	22.06049608		23.32672837		8.229246175		10.26381103		7.263775647	
Mean Discharge (m³/min)	0.0395662			0.009344333		0.01015		0.003495333		0.004336		0.00307	

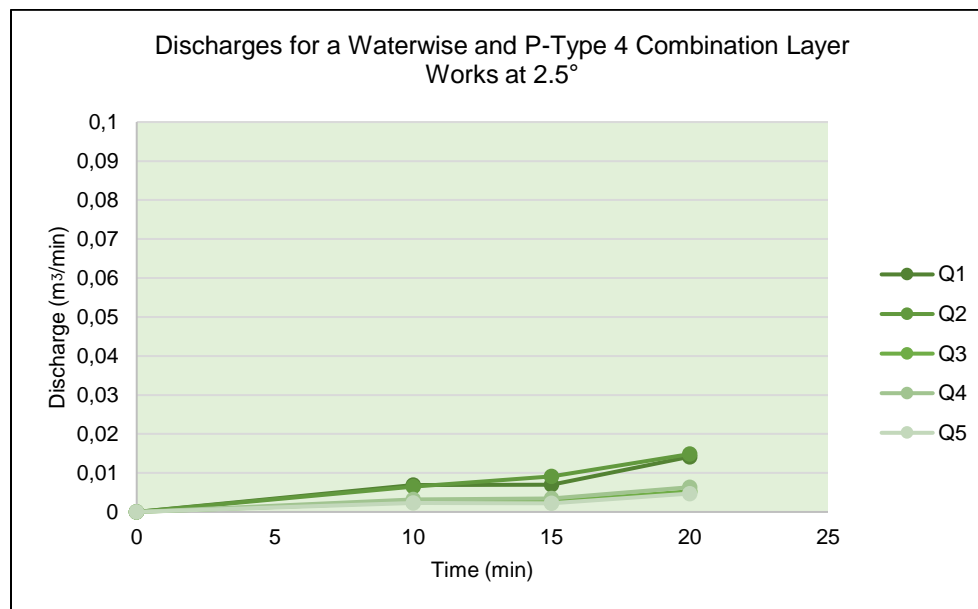


Fig. G-11 A graph of discharge per unit time for the Full-scale Model with a Waterwise and P-Type 4 surface combination layer works at 2.5° incline.

Table G-12: Full-scale Model test data for a Waterwise® and P-Type 4 combination layer works at 5° incline													
19-07-2018													
Incline 5° or 8.7													
Time (min):	Inlet Meters (m³)			Outlet Meters (m³)									
	1	2	3	Q1	Discharge at Q ₁ (m³/min)	Q2	Discharge at Q ₂ (m³/min)	Q3	Discharge at Q ₃ (m³/min)	Q4	Discharge at Q ₄ (m³/min)	Q5	Discharge at Q ₅ (m³/min)
0	2.42896	3.3595	1.87142	1.18411	0	1.06216	0	1.27524	0	0.90181	0	0.84057	0
10				1.1995	0.001539	1.0875	0.002534	1.2793	0.000406	0.92085	0.001904	0.88256	0.004199
15				1.25802	0.011704	1.09964	0.002428	1.29008	0.002156	0.93203	0.002236	0.90401	0.00429
20	2.65566	3.62346	2.11504	1.29057	0.00651	1.11791	0.003654	1.29511	0.001006	0.94086	0.001766	0.92505	0.004208
ΔV Total (m³)	0.2267	0.26396	0.24362	0.10646		0.05575		0.01987		0.03905		0.08448	
% of Total V in	30.87378	35.94814	33.17808	14.49855641		7.592471537		2.706052187		5.318134771		11.5051479	
Mean Discharge (m³/min)	0.036714			0.006584333		0.002872		0.001189333		0.001968667		0.004232333	

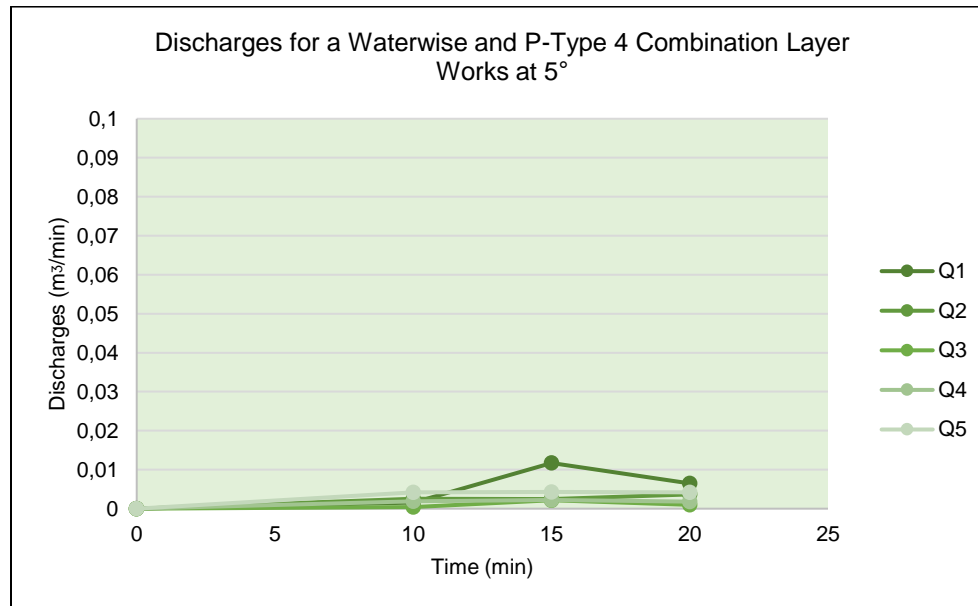


Fig. G-12: A graph of discharge per unit time for the Full-scale Model with a Waterwise and P-Type 4 surface combination layer works at 5° incline.

Table G-13: Full-scale Model test data for a Waterwise® and P-Type 5 combination layer works at 0° incline													
18-10-2018													
Incline 0° or 0													
Time (min):	Inlet Meters (m ³)			Outlet Meters (m ³)									
	1	2	3	Q1	Discharge at Q ₁ (m ³ /min)	Q2	Discharge at Q ₂ (m ³ /min)	Q3	Discharge at Q ₃ (m ³ /min)	Q4	Discharge at Q ₄ (m ³ /min)	Q5	Discharge at Q ₅ (m ³ /min)
0	6.81472	8.46868	5.43556	5.8493	0	1.62127	0	0.37295	0	0.82991	0	2.91545	0
10				5.85675	0.000745	1.62127	0	0.37495	0.0002	0.8549	0.002499	2.9962	0.008075
15				5.86555	0.00176	1.62127	0	0.37535	8E-05	0.9074	0.0105	3.1559	0.03194
20				5.87075	0.00104	1.6274	0.001226	0.37965	0.00086	0.93905	0.00633	3.24765	0.01835
25				5.878	0.00145	1.6342	0.00136	0.3844	0.00095	0.96855	0.0059	3.3312	0.01671
30	7.09875	8.80405	5.7436	5.88398	0.001196	1.63813	0.000786	0.38721	0.000562	0.98052	0.002394	3.36678	0.007116
ΔV Total (m ³)	0.28403	0.33537	0.30804	0.03468			0.01686		0.01426		0.15061		0.45133
% of Total V in	30.62516	36.16083	33.21401	3.739325455			1.817907358		1.537565772		16.23932546		48.66406452
Mean Discharge (m ³ /min)	0.030914667			0.0012382		0.0006744		0.0005304		0.0055246		0.0164382	

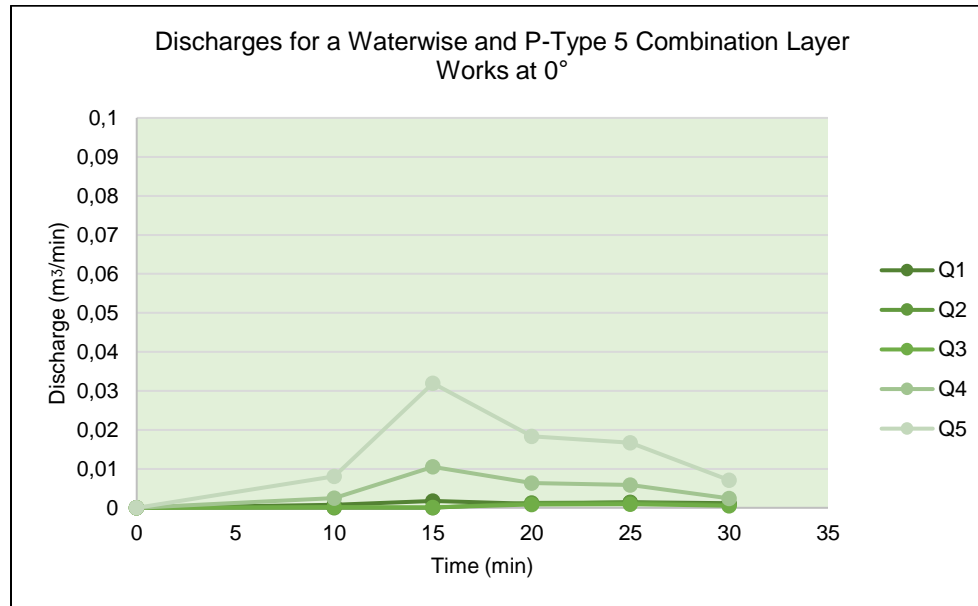


Fig. G-13: A graph of discharge per unit time for the Full-scale Model with a Waterwise and P-Type 5 surface combination layer works at 0° incline.

Table G-14: Full-scale Model test data for a Waterwise® and P-Type 5 combination layer works at 2.5° incline													
18-10-2018													
Incline 2.5° or 3.5%													
Time (min):	Inlet Meters (m ³)			Outlet Meters (m ³)									
	1	2	3	Q1	Discharge at Q1 (m ³ /min)	Q2	Discharge at Q2 (m ³ /min)	Q3	Discharge at Q3 (m ³ /min)	Q4	Discharge at Q4 (m ³ /min)	Q5	Discharge at Q5 (m ³ /min)
0	7.319	9.00655	5.82635	5.88396	0	1.63812	0	0.38721	0	0.98624	0	3.72948	0
10	-	-	-	5.88398	2E-06	1.6455	0.000738	0.38721	0	0.99185	0.000561	3.79825	0.006877
15	-	-	-	5.88405	1.4E-05	1.65905	0.00271	0.38721	0	1.005	0.00263	3.95745	0.03184
20	-	-	-	5.88405	0	1.6693	0.00205	0.38721	0	1.01185	0.00137	4.03185	0.01488
25	-	-	-	5.88405	0	1.6796	0.00206	0.38721	0	1.01975	0.00158	4.11665	0.01696
30	7.57128	9.3211	5.90069	5.88405	0	1.68476	0.001032	0.38721	0	1.021	0.00025	4.13494	0.003658
ΔV Total (m ³)	0.25228	0.31455	0.07434	9E-05		0.04664		0		0.03476		0.40546	
% of Total V in	39.34682	49.05875	11.59443	0.014036839		7.27420185		0		5.421339114		63.23751891	
Mean Discharge (m ³ /min)	0.021372333			3.2E-06		0.001718		0		0.0012782		0.014843	

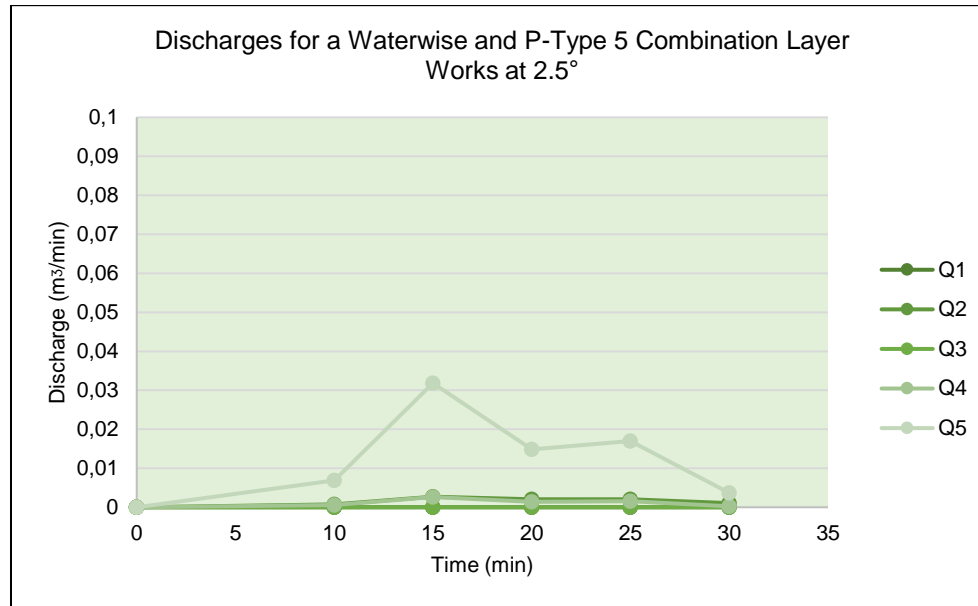


Fig. G-14: A graph of discharge per unit time for the Full-scale Model with a Waterwise and P-Type 5 surface combination layer works at 2.5° incline.

Table G-15: Full-scale Model test data for a Waterwise® and P-Type 5 combination layer works at 5° incline													
18-10-2018													
Incline 5° or 8.7													
Time (min):	Inlet Meters (m ³)			Outlet Meters (m ³)									
	1	2	3	Q1	Discharge at Q ₁ (m ³ /min)	Q2	Discharge at Q ₂ (m ³ /min)	Q3	Discharge at Q ₃ (m ³ /min)	Q4	Discharge at Q ₄ (m ³ /min)	Q5	Discharge at Q ₅ (m ³ /min)
0	7.09875	8.80405	5.7436	5.88398	0	1.63813	0	0.38721	0	0.98052	0	3.36678	0
10				5.88398	0	1.63813	0	0.38721	0	0.98625	0.000573	3.43125	0.006447
15				5.88398	0	1.63813	0	0.38721	0	0.98625	0	3.57775	0.0293
20				5.88398	0	1.63813	0	0.38721	0	0.98625	0	3.64985	0.01442
25				5.88398	0	1.63813	0	0.38721	0	0.98625	0	3.71435	0.0129
30	7.319	9.00655	5.82635	5.88398	0	1.63813	0	0.38721	0	0.98625	0	3.72948	0.015926
ΔV Total (m ³)	0.22025	0.2025	0.08275	0			0			0.00573		0.3627	
% of Total V in	43.57072	40.05935	16.36993	0			0			1.133531157		71.75074184	
Mean Discharge (m ³ /min)	0.01685			0			0			0.0001146		0.0157986	

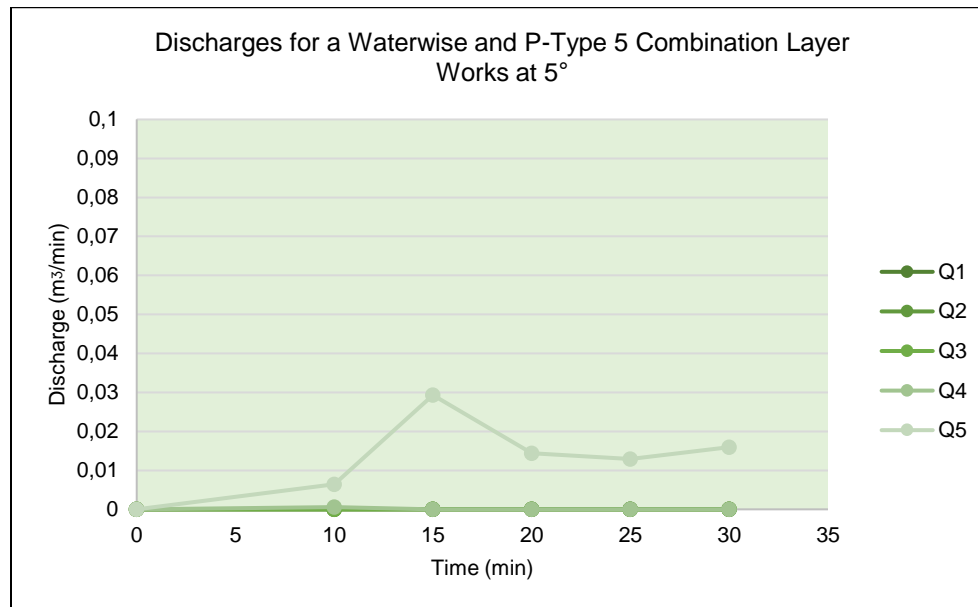


Fig. G-15: A graph of discharge per unit time for the Full-scale Model with a Waterwise and P-Type 5 surface combination layer works at 5° incline.

Table G-16: Full-scale Model test data for a Citylock® and P-Type 1 combination layer works at 0° incline													
20-09-2018													
Incline 0° or 0%													
Time (min):	Inlet Meters (m ³)			Outlet Meters (m ³)									
	1	2	3	Q1	Discharge at Q ₁ (m ³ /min)	Q2	Discharge at Q ₂ (m ³ /min)	Q3	Discharge at Q ₃ (m ³ /min)	Q4	Discharge at Q ₄ (m ³ /min)	Q5	Discharge at Q ₅ (m ³ /min)
0	3.89018	5.06128	3.26235	1.72336	0	0.59132	0	0.25685	0	0.46336	0	1.07116	0
10	-	-	-	2.041	0.031764	0.6132	0.002188	0.25685	0	0.46336	0	1.07116	0
15	-	-	-	2.2306	0.03792	0.65775	0.00891	0.25685	0	0.46336	0	1.07116	0
20	-	-	-	2.40615	0.03511	0.68275	0.005	0.25685	0	0.46336	0	1.07116	0
25	-	-	-	2.5912	0.03701	0.71055	0.00556	0.25685	0	0.46336	0	1.07116	0
30	-	-	-	2.7678	0.03532	0.7379	0.00547	0.25685	0	0.46336	0	1.07116	0
35	4.37268	5.5765	3.68592	2.92775	0.06731	0.74896	0.007682	0.25685	0	0.46336	0	1.07116	0
ΔV Total (m ³)	0.4825	0.51522	0.42357	1.20439		0.15764		0		0		0	
% of Total V in	33.94803	36.25017	29.8018	84.73921578		11.09133252		0		0		0	
Mean Discharge (m ³ /min)	0.040608286			0.040739		0.005801667		0		0		0	

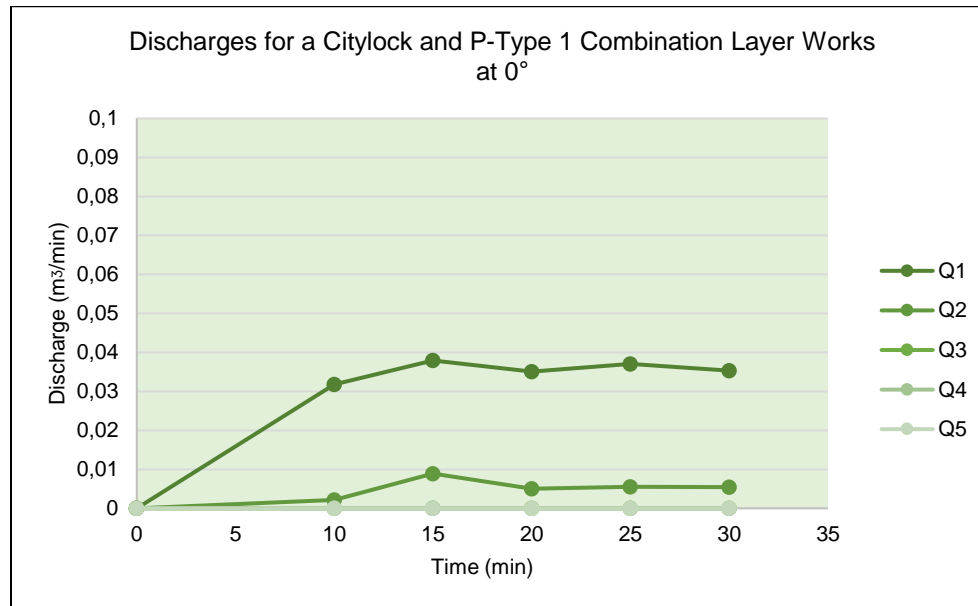


Fig. G-16: A graph of discharge per unit time for the Full-scale Model with a Citylock and P-Type 1 surface combination layer works at 0° incline.

Table G-17: Full-scale Model test data for a Citylock® and P-Type 1 combination layer works at 2.5° incline

20-09-2018

Incline 2.5° or 3.5%

Time (min):	Inlet Meters (m ³)			Outlet Meters (m ³)									
	1	2	3	Q ₁	Discharge at Q ₁ (m ³ /min)	Q ₂	Discharge at Q ₂ (m ³ /min)	Q ₃	Discharge at Q ₃ (m ³ /min)	Q ₄	Discharge at Q ₄ (m ³ /min)	Q ₅	Discharge at Q ₅ (m ³ /min)
0	4.37268	5.5765	3.68592	2.92775	0	0.74896	0	0.25685	0	0.46336	0	1.07116	0
10	-	-	-	3.17805	0.02503	0.78695	0.003799	0.25685	0	0.46336	0	1.07116	0
15	-	-	-	3.4067	0.04573	0.87205	0.01702	0.25685	0	0.46336	0	1.07116	0
20	-	-	-	3.5576	0.03018	0.9135	0.00829	0.25685	0	0.46336	0	1.07116	0
25	-	-	-	3.6193	0.01234	0.95865	0.00903	0.25685	0	0.46336	0	1.07116	0
30	-	-	-	3.77045	0.03023	1.00015	0.0083	0.25685	0	0.46336	0	1.07116	0
35	4.83943	6.11112	3.97886	3.81125	0.00816	1.01611	0.003192	0.25685	0	0.46336	0	1.07116	0
ΔV Total (m ³)	0.46675	0.53462	0.29294	0.8835		0.26715		0		0		0	
% of Total V in	36.06169	41.30541	22.63291	68.26030858		20.64034119		0		0		0	
Mean Discharge (m ³ /min)	0.036980286			0.028702		0.0092878		0		0		0	

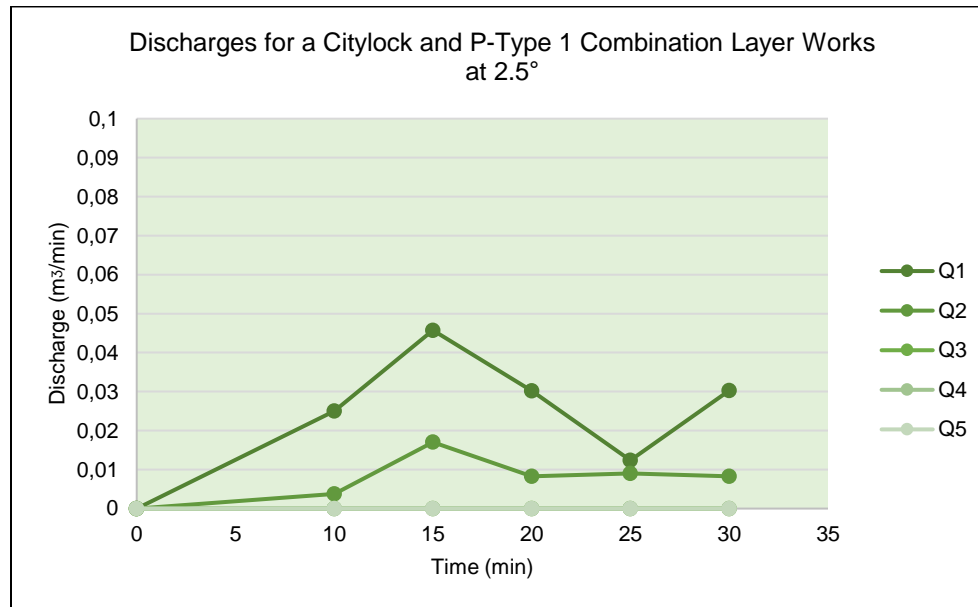


Fig. G-17: A graph of discharge per unit time for the Full-scale Model with a Citylock and P-Type 1 surface combination layer works at 2.5° incline.

Table G-18: Full-scale Model test data for a Citylock® and P-Type 1 combination layer works at 5° incline														
20-09-2018														
Incline 5° or 8.7														
Time (min):	Inlet Meters (m³)			Outlet Meters (m³)										
	1	2	3	Q1	Discharge at Q1 (m³/min)	Q2	Discharge at Q2 (m³/min)	Q3	Discharge at Q3 (m³/min)	Q4	Discharge at Q4 (m³/min)	Q5	Discharge at Q5 (m³/min)	
0	4.83943	6.11112	3.97886	3.81125	0	1.01611	0	0.25685	0	0.46336	0	1.07116	0	
10				3.92995	0.01187	1.04915	0.003304	0.25705	2E-05	0.46336	0	1.07116	0	
15				4.131	0.04021	1.1268	0.01553	0.2571	1E-05	0.46336	0	1.07116	0	
20				4.2726	0.02832	1.16565	0.00777	0.2571	0	0.46336	0	1.07116	0	
25				4.4335	0.03218	1.20185	0.00724	0.2571	0	0.46336	0	1.07116	0	
30				4.58515	0.03033	1.23545	0.00672	0.2571	0	0.46336	0	1.07116	0	
35	5.15482	6.6374	4.14188	4.64495	0.01196	1.24805	0.00252	0.2571	0	0.46336	0	1.07116	0	
ΔV Total (m³)	0.31539	0.52628	0.16302	0.8337			0.23194			0.00025			0	0
% of Total V in	31.39177	52.38233	16.2259	82.98081995			23.08572794			0.024883297			0	0
Mean Discharge (m³/min)	0.028705429			0.028582			0.0081128			6E-06			0	0

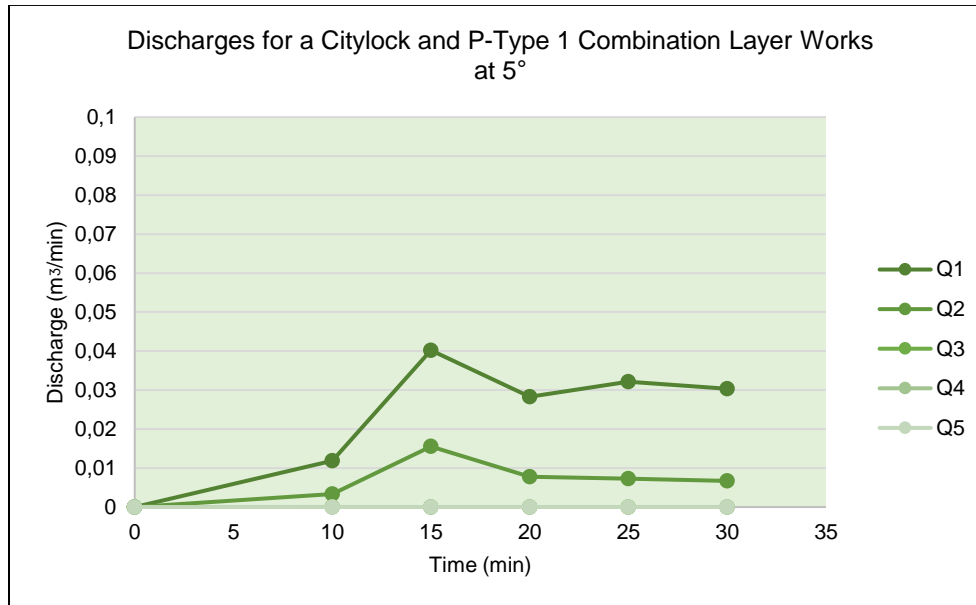


Fig. G-18: A graph of discharge per unit time for the Full-scale Model with a Citylock and P-Type 1 surface combination layer works at 5° incline.

Table G-19: Full-scale Model test data for a Citylock® and P-Type 2 combination layer works at 0° incline													
14-02-2019													
Incline 0° or 0%													
Time (min):	Inlet Meters (m ³)			Outlet Meters (m ³)									
	1	2	3	Q1	Discharge at Q1 (m ³ /min)	Q2	Discharge at Q2 (m ³ /min)	Q3	Discharge at Q3 (m ³ /min)	Q4	Discharge at Q4 (m ³ /min)	Q5	Discharge at Q5 (m ³ /min)
0	9.37155	11.43875	6.6514	9.08498	0	2.24624	0	0.44752	0	1.02839	0	4.1351	0
10				9.15395	0.006897	2.25331	0.000707	0.44752	0	1.02839	0	4.1351	0
15	9.4591	11.577	6.6926	9.2949	0.02819	2.2667	0.002678	0.44752	0	1.02839	0	4.1351	0
ΔV Total (m ³)	0.08755	0.13825	0.0412	0.20992		0.02046		0		0		0	
% of Total V in	32.79026	51.77903	15.43071	78.62172285		7.662921348		0		0		0	
Mean Discharge (m ³ /min)	0.0178			0.0175435		0.0016925		0		0		0	

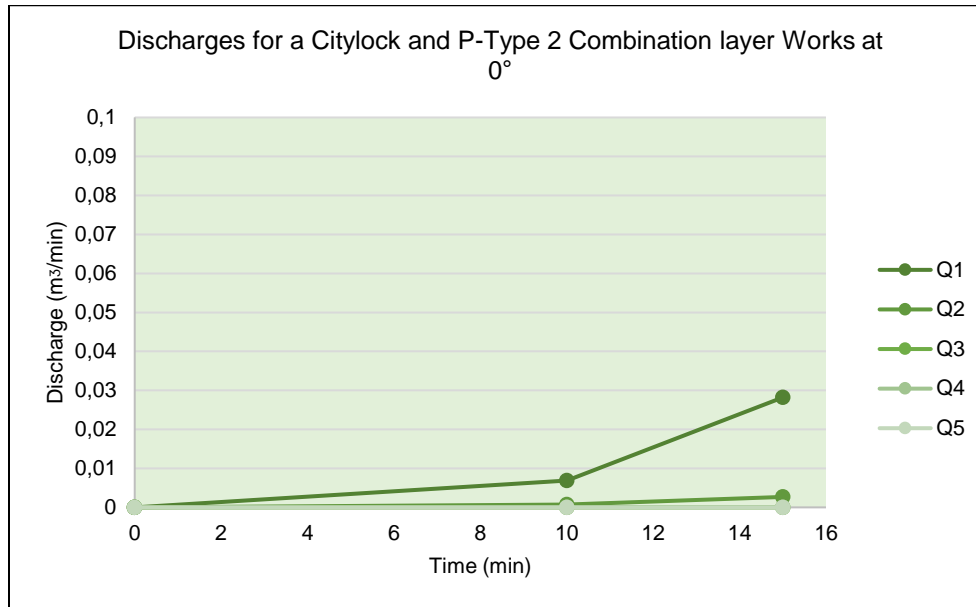


Fig. G-19: A graph of discharge per unit time for the Full-scale Model with a Citylock and P-Type 2 surface combination layer works at 0° incline.

Table G-20: Full-scale Model test data for a Citylock® and P-Type 2 combination layer works at 2.5° incline													
18-02-2019													
Incline 2.5° or 3.5%													
Time (min):	Inlet Meters (m ³)			Outlet Meters (m ³)									
	1	2	3	Q1	Discharge at Q1 (m ³ /min)	Q2	Discharge at Q2 (m ³ /min)	Q3	Discharge at Q3 (m ³ /min)	Q4	Discharge at Q4 (m ³ /min)	Q5	Discharge at Q5 (m ³ /min)
0	9.7907	12.1512	6.8404	10.12735	0	2.36505	0	0.44755	0	1.0284	0	4.1351	0
10	-	-	-	10.32485	0.01975	2.38395	0.00189	0.44765	1E-05	1.0284	0	4.1351	0
15	-	-	-	10.3877	0.01257	2.4331	0.00983	0.4486	0.00019	1.0284	0	4.1351	0
20	-	-	-	10.49955	0.02237	2.45765	0.00491	0.4489	6E-05	1.0284	0	4.1351	0
25	9.9993	12.5139	6.9148	10.6264	0.02537	2.4645	0.00137	0.4489	0	1.0284	0	4.1351	0
ΔV Total (m ³)	0.2086	0.3627	0.0744	0.49905		0.09945		0.00135		0		0	
% of Total V in	32.30602	56.1716	11.52238	77.28821434		15.40188942		0.209075422		0		0	
Mean Discharge (m ³ /min)	0.025828			0.020015		0.0045		6.5E-05		0		0	

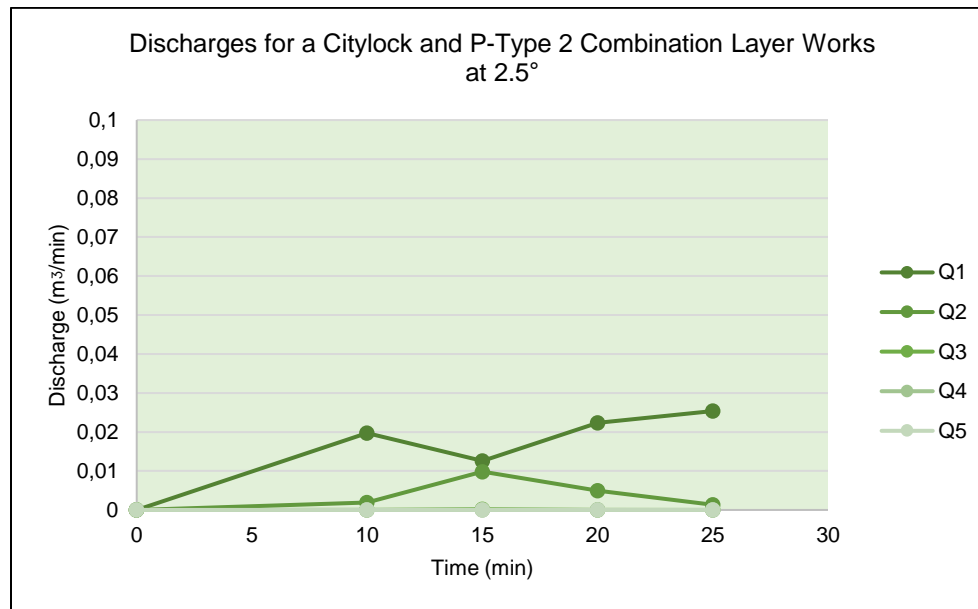


Fig. G-20: A graph of discharge per unit time for the Full-scale Model with a Citylock and P-Type 2 surface combination layer works at 2.5° incline.

Table G-21: Full-scale Model test data for a Citylock® and P-Type 2 combination layer works at 2.5° incline													
14-02-2019													
Incline 5° or 8.7													
Time (min):	Inlet Meters (m ³)			Outlet Meters (m ³)									
	1	2	3	Q1	Discharge at Q1 (m ³ /min)	Q2	Discharge at Q2 (m ³ /min)	Q3	Discharge at Q3 (m ³ /min)	Q4	Discharge at Q4 (m ³ /min)	Q5	Discharge at Q5 (m ³ /min)
0	9.53665	11.7122	6.7232	9.47475	0	2.30105	0	0.44752	0	1.02839	0	4.1351	0
10				9.56415	0.00894	2.32254	0.002149	0.44752	0	1.02839	0	4.1351	0
15	9.6793	11.85225	6.77193	9.73315	0.0338	2.36866	0.009224	0.44752	0	1.02839	0	4.1351	0
ΔV Total (m ³)	0.14265	0.14005	0.04873	0.2584		0.06761		0		0		0	
% of Total V in	43.04076	42.25628	14.70295	77.96518118		20.39948104		0		0		0	
Mean Discharge (m ³ /min)	0.022095333			0.02137		0.0056865		0		0		0	

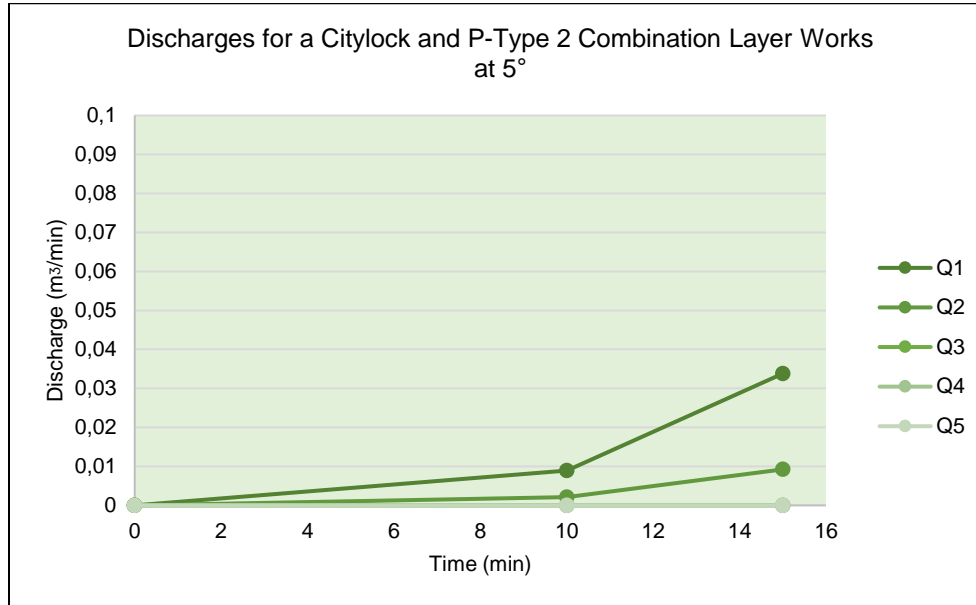


Fig. G-21: A graph of discharge per unit time for the Full-scale Model with a Citylock and P-Type 2 surface combination layer works at 5° incline

Table G-22: Full-scale Model test data for a Citylock® and P-Type 3 combination layer works at 0° incline													
22-11-2018													
Incline 0° or 0%													
Time (min):	Inlet Meters (m ³)			Outlet Meters (m ³)									
	1	2	3	Q1	Discharge at Q1 (m ³ /min)	Q2	Discharge at Q2 (m ³ /min)	Q3	Discharge at Q3 (m ³ /min)	Q4	Discharge at Q4 (m ³ /min)	Q5	Discharge at Q5 (m ³ /min)
0	7.65562	9.3211	5.99009	5.8895	0	1.69185	0	0.39478	0	1.02525	0	4.1351	0
10				5.9802	0.00907	1.6972	0.000535	0.39478	0	1.02525	0	4.1351	0
15	7.778	9.49216	5.9946	6.15295	0.03455	1.71195	0.00295	0.39478	0	1.02525	0	4.1351	0
ΔV Total (m ³)	0.12238	0.17106	0.00451	0.26345		0.0201		0		0		0	
% of Total V in	41.07401	57.41232	1.513677	88.42087599		6.746098339		0		0		0	
Mean Discharge (m ³ /min)	0.019863333			0.02181		0.0017425		0		0		0	

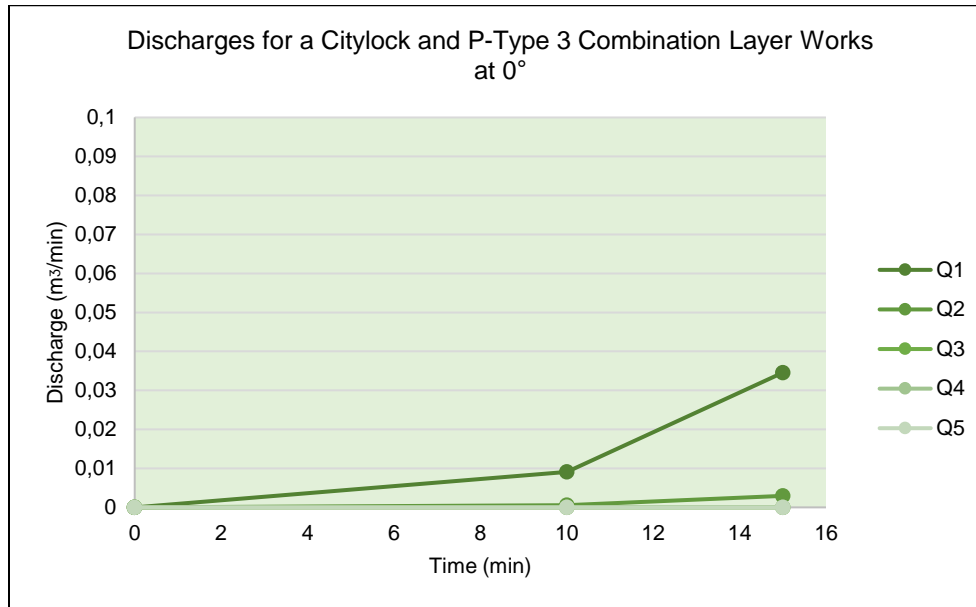


Fig. G-22: A graph of discharge per unit time for the Full-scale Model with a Citylock and P-Type 3 surface combination layer works at 0° incline

Table G-23: Full-scale Model test data for a Citylock® and P-Type 3 combination layer works at 2.5° incline													
22-11-2018													
Incline 2.5° or 3.5%													
Time (min):	Inlet Meters (m ³)			Outlet Meters (m ³)									
	1	2	3	Q1	Discharge at Q1 (m ³ /min)	Q2	Discharge at Q2 (m ³ /min)	Q3	Discharge at Q3 (m ³ /min)	Q4	Discharge at Q4 (m ³ /min)	Q5	Discharge at Q5 (m ³ /min)
0	7.778	9.49216	5.9946	6.15295	0	1.71195	0	0.39478	0	1.02525	0	4.1351	0
10	-	-	-	6.22975	0.00768	1.72895	0.0017	0.3959	0.000112	1.02525	0	4.1351	0
15	7.91218	9.66205	6.00618	6.3932	0.03269	1.76687	0.007584	0.39854	0.000528	1.02525	0	4.1351	0
ΔV Total (m ³)	0.13418	0.16989	0.01158	0.24025		0.05492		0.00376		0		0	
% of Total V in	42.50911	53.82227	3.66862	76.11278315		17.3990179		1.191192777		0		0	
Mean Discharge (m ³ /min)	0.021043333			0.020185		0.004642		0.00032		0		0	

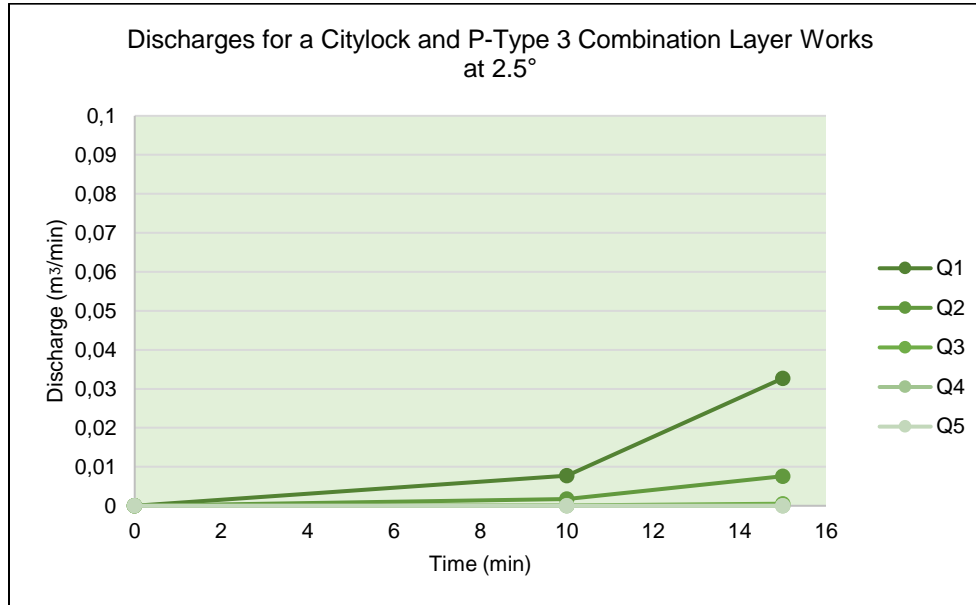


Fig. G-23: A graph of discharge per unit time for the Full-scale Model with a Citylock and P-Type 3 surface combination layer works at 2.5° incline

Table G-24: Full-scale Model test data for a Citylock® and P-Type 3 combination layer works at 5° incline													
22-11-2018													
Incline 5° or 8.7													
Time (min):	Inlet Meters (m ³)			Outlet Meters (m ³)									
	1	2	3	Q1	Discharge at Q1 (m ³ /min)	Q2	Discharge at Q2 (m ³ /min)	Q3	Discharge at Q3 (m ³ /min)	Q4	Discharge at Q4 (m ³ /min)	Q5	Discharge at Q5 (m ³ /min)
0	7.91218	9.66205	6.00618	6.3932	0	1.76687	0	0.39854	0	1.02525	0	4.1351	0
10				6.4281	0.00349	1.77845	0.001158	0.40025	0.000171	1.02525	0	4.1351	0
15	8.0238	9.73592	6.12985	6.5165	0.01768	1.8072	0.00575	0.40525	0.001	1.02525	0	4.1351	0
ΔV Total (m ³)	0.11162	0.07387	0.12367	0.1233		0.04033		0.00671		0		0	
% of Total V in	36.10428	23.89378	40.00194	39.88226161		13.04502523		2.170397205		0		0	
Mean Discharge (m ³ /min)	0.020610667			0.010585		0.003454		0.0005855		0		0	

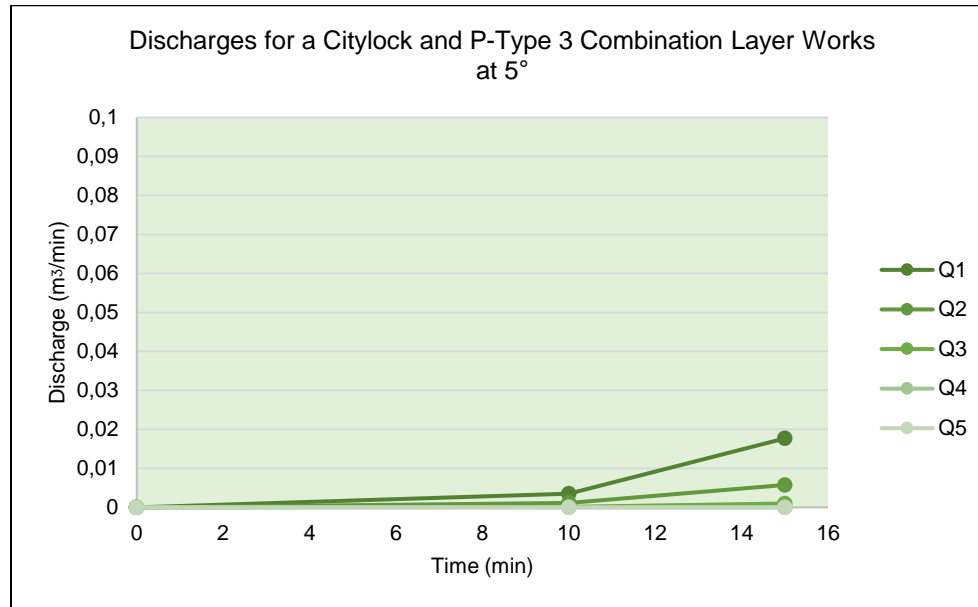


Fig. G-24: A graph of discharge per unit time for the Full-scale Model with a Citylock and P-Type 3 surface combination layer works at 5° incline

Table G-25: Full-scale Model test data for a Citylock® and P-Type 5 combination layer works at 0° incline														
04-10-2018														
Incline 0° or 0%														
Time (min):	Inlet Meters (m ³)			Outlet Meters (m ³)										
	1	2	3	Q1	Discharge at Q1 (m ³ /min)	Q2	Discharge at Q2 (m ³ /min)	Q3	Discharge at Q3 (m ³ /min)	Q4	Discharge at Q4 (m ³ /min)	Q5	Discharge at Q5 (m ³ /min)	
0	5.94912	7.47535	4.62426	5.72987	0	1.62124	0	0.37295	0	0.61471	0	1.12616	0	
10				5.74765	0.001778	1.62124	0	0.37295	0	0.6422	0.002749	1.24135	0.011519	
15				5.779	0.00627	1.62124	0	0.37295	0	0.69075	0.00971	1.42975	0.03768	
20				5.7954	0.00328	1.62124	0	0.37295	0	0.71865	0.00558	1.537	0.02145	
25				5.8229	0.0055	1.62124	0	0.37295	0	0.7484	0.00595	1.6516	0.02292	
30	6.33915	7.91512	5.03062	5.84929	0.005278	1.62124	0	0.37295	0	0.77954	0.006228	1.83514	0.036708	
ΔV Total (m ³)	0.39003	0.43977	0.40636	0.11942			0			0.16483			0.70898	
% of Total V in	31.55174	35.57549	32.87277	9.66056174			0			13.33403443			57.35341703	
Mean Discharge (m ³ /min)	0.041205333			0.0044212			0			0.0060434			0.0260554	

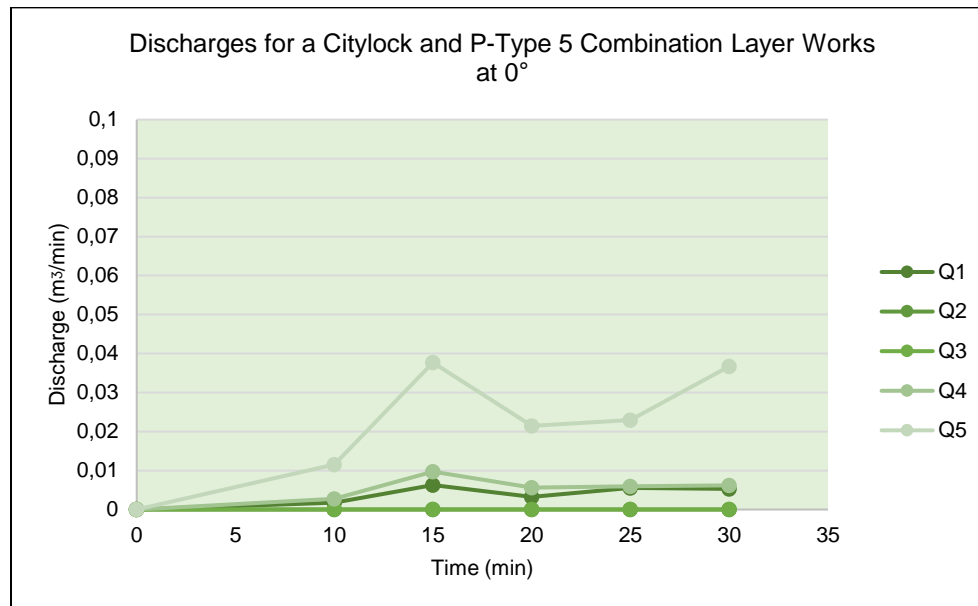


Fig. G-25: A graph of discharge per unit time for the Full-scale Model with a Citylock and P-Type 5 surface combination layer works at 0° incline

Table G-26: Full-scale Model test data for a Citylock® and P-Type 5 combination layer works at 2.5° incline														
04-10-2018														
Incline 2.5° or 3.5%														
Time (min):	Inlet Meters (m ³)			Outlet Meters (m ³)										
	1	2	3	Q1	Discharge at Q1 (m ³ /min)	Q2	Discharge at Q2 (m ³ /min)	Q3	Discharge at Q3 (m ³ /min)	Q4	Discharge at Q4 (m ³ /min)	Q5	Discharge at Q5 (m ³ /min)	
0	6.33915	7.91512	5.03062	5.84929	0	1.62124	0	0.37295	0	0.77954	0	1.83514	0	
10	-	-	-	5.84929	0	1.62124	0	0.37295	0	0.7973	0.001776	2.07635	0.024121	
15	-	-	-	5.84929	0	1.62124	0	0.37295	0	0.80875	0.00229	2.1957	0.02387	
20	-	-	-	5.84929	0	1.62124	0	0.37295	0	0.8208	0.00241	2.3197	0.0248	
25	6.60109	8.22091	5.1787	5.84929	0	1.62124	0	0.37295	0	0.82457	0.000754	2.4123	0.01852	
ΔV Total (m ³)	0.26194	0.30579	0.14808	0			0			0.04503			0.57716	
% of Total V in	36.59351	42.71944	20.68705	0			0			6.290775485			80.63033487	
Mean Discharge (m ³ /min)	0.0286324			0			0			0.0018075			0.02282775	

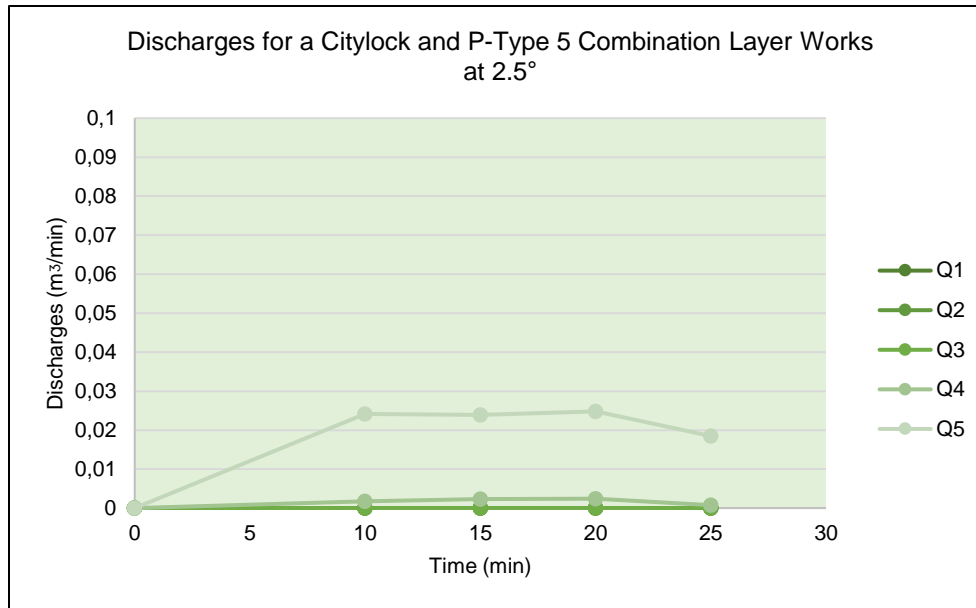


Fig. G-26: A graph of discharge per unit time for the Full-scale Model with a Citylock and P-Type 5 surface combination layer works at 2.5° incline.

Table G-27: Full-scale Model test data for a Citylock® and P-Type 5 combination layer works at 5° incline														
04-10-2018														
Incline 5° or 8.7														
Time (min):	Inlet Meters (m ³)			Outlet Meters (m ³)										
	1	2	3	Q1	ΔQ1/min	Q2	ΔQ2/min	Q3	ΔQ3/min	Q4	ΔQ4/min	Q5	ΔQ5/min	
0	6.60109	8.22091	5.1787	5.84929	0	1.62124	0	0.37295	0	0.82457	0	2.4123	0	
10				5.84929	0	1.62124	0	0.37295	0	0.82645	0.000188	2.6138	0.02015	
15				5.84929	0	1.62124	0	0.37295	0	0.82835	0.00038	2.74015	0.02527	
20				5.84929	0	1.62124	0	0.37295	0	0.8299	0.00031	2.843	0.02057	
25	6.81472	8.46866	5.30669	5.84929	0	1.62124	0	0.37295	0	0.8309	0.0002	2.91272	0.013944	
ΔV Total (m ³)	0.21363	0.24775	0.12799	0			0			0.00633			0.50042	
% of Total V in	36.24718	42.03641	21.71641	0			0			1.0740282			84.90761321	
Mean Discharge (m ³ /min)	0.0235748			0			0			0.0002695			0.0199835	

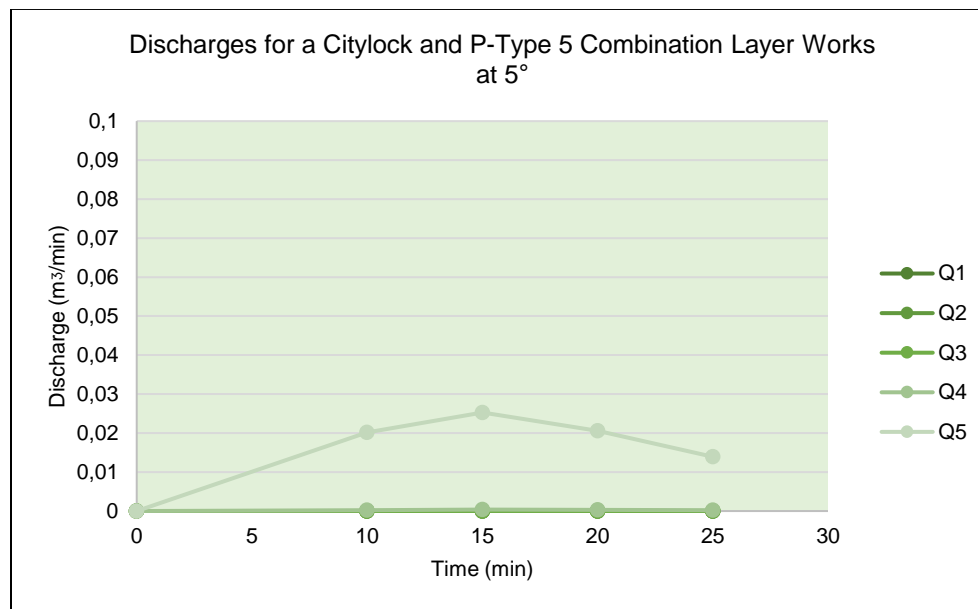


Fig. G-27: A graph of discharge per unit time for the Full-scale Model with a Citylock and P-Type 5 surface combination layer works at 5° incline.

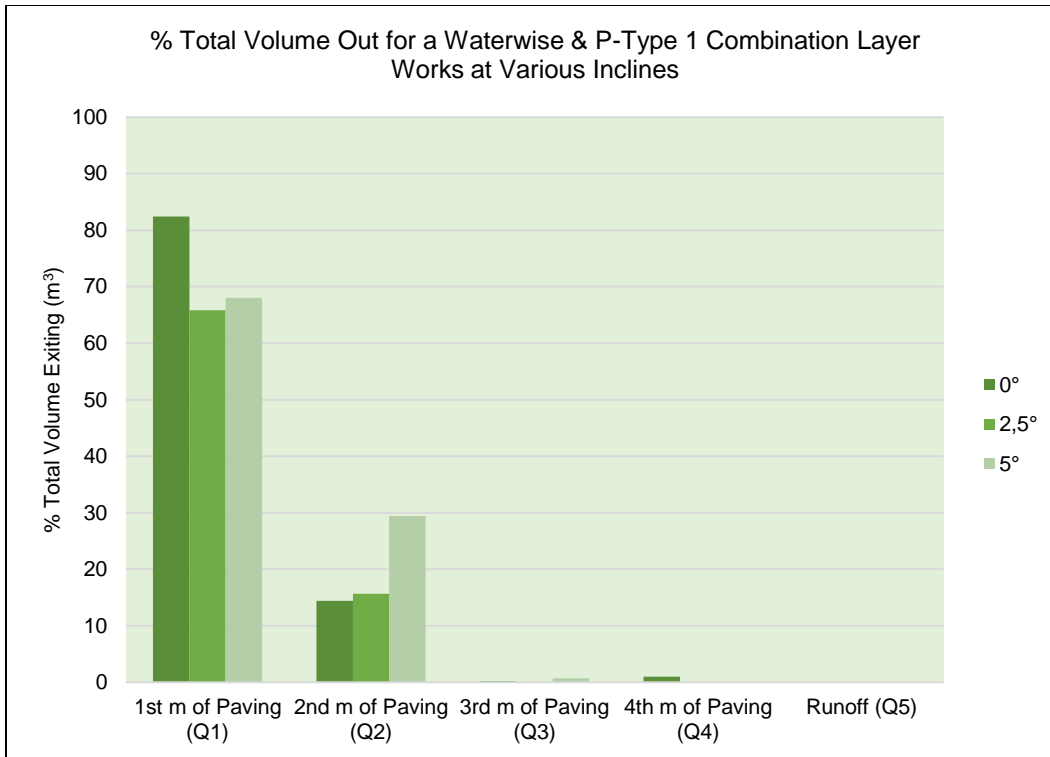


Fig. G-28: A column graph of volume percentages exiting the Full-scale Model with a Waterwise and P-Type 1 surface combination layer works, at various points and various inclines.

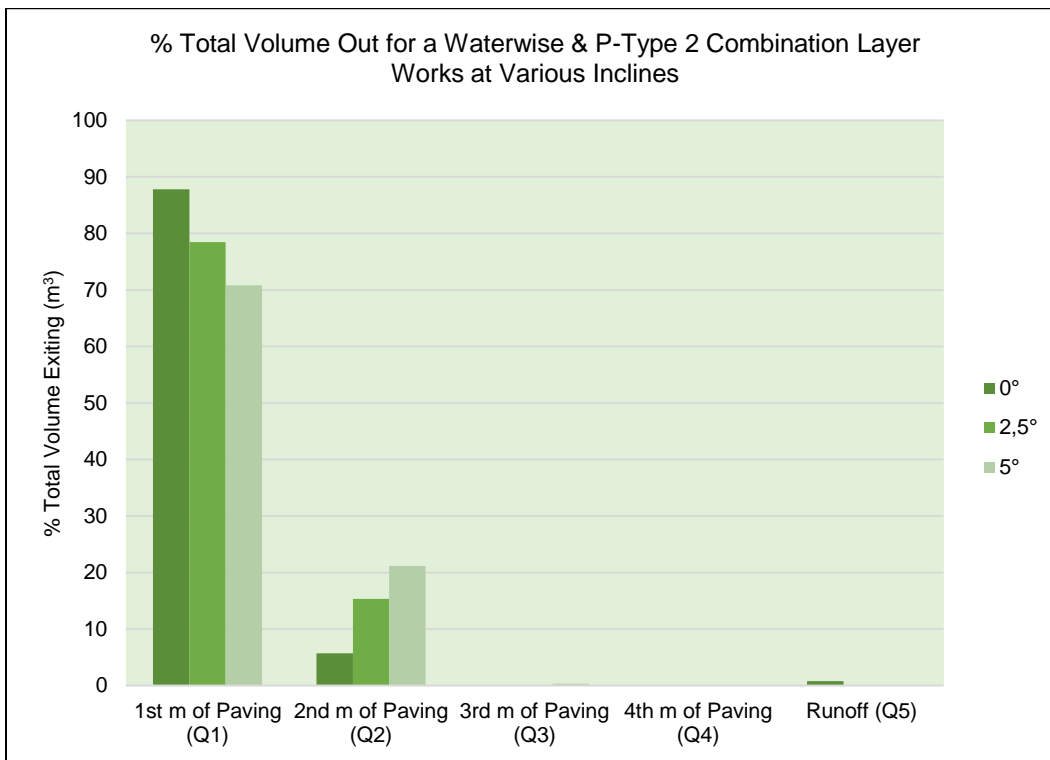


Fig. G-29: A column graph of volume percentages exiting the Full-scale Model with a Waterwise and P-Type 2 surface combination layer works, at various points and various inclines.

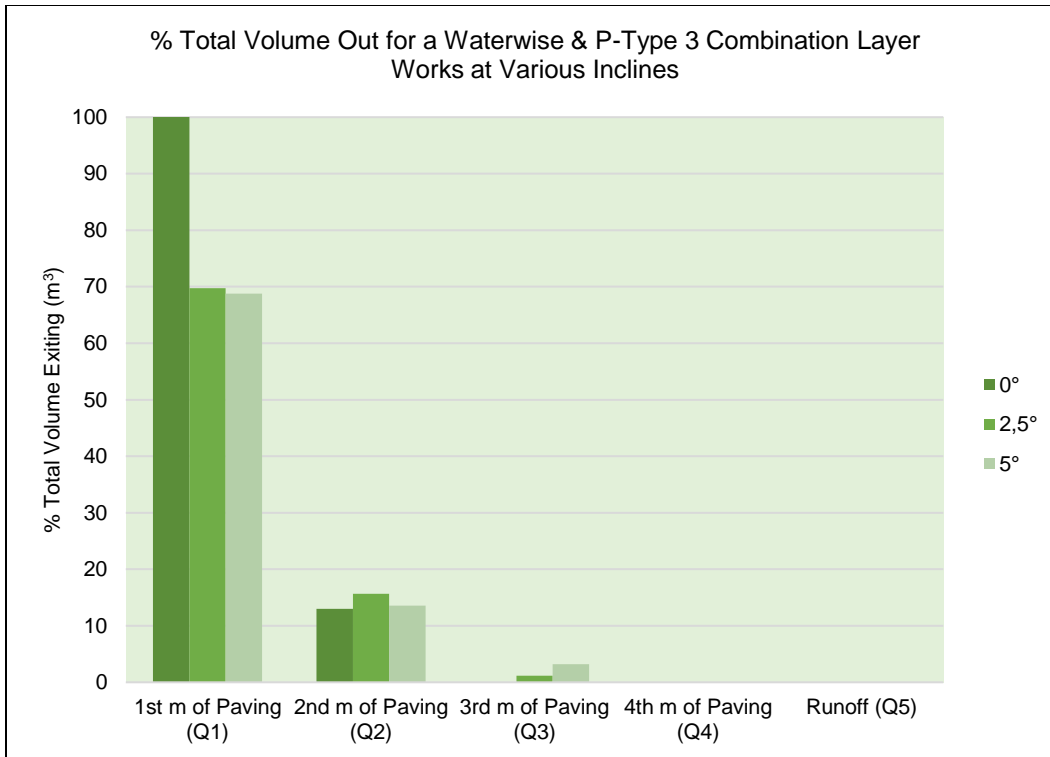


Fig. G-30: A column graph of volume percentages exiting the Full-scale Model with a Waterwise and P-Type 3 surface combination layer works, at various points and various inclines.

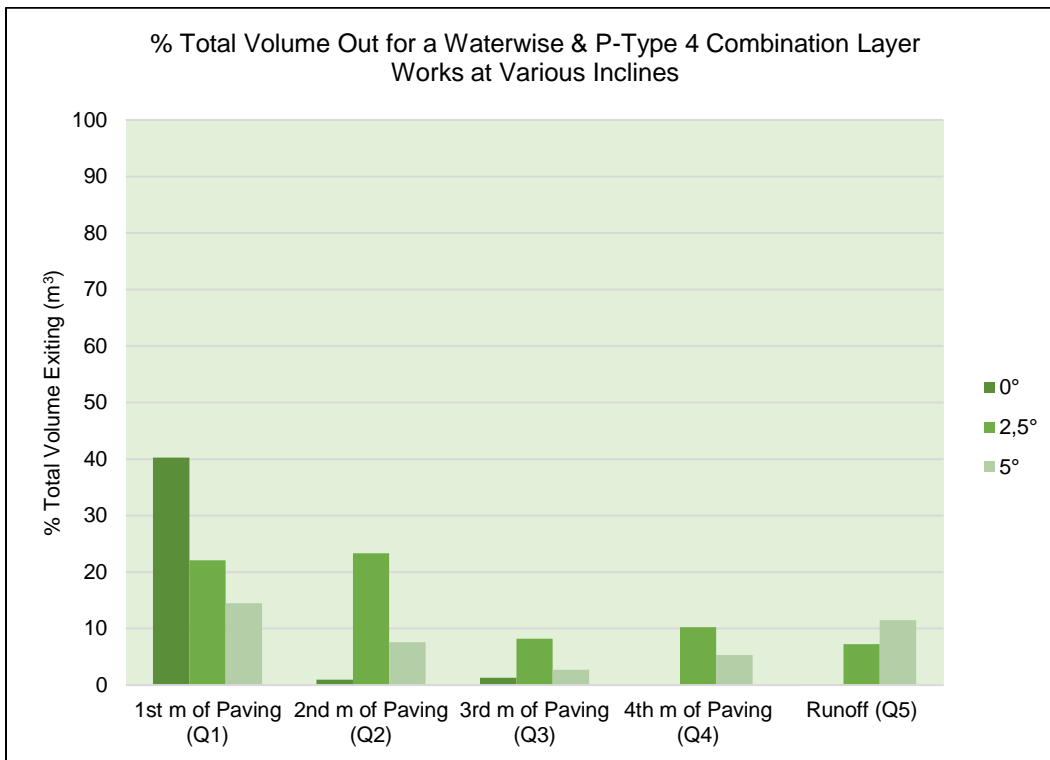


Fig. G-31: A column graph of volume percentages exiting the Full-scale Model with a Waterwise and P-Type 4 surface combination layer works, at various points and various inclines.

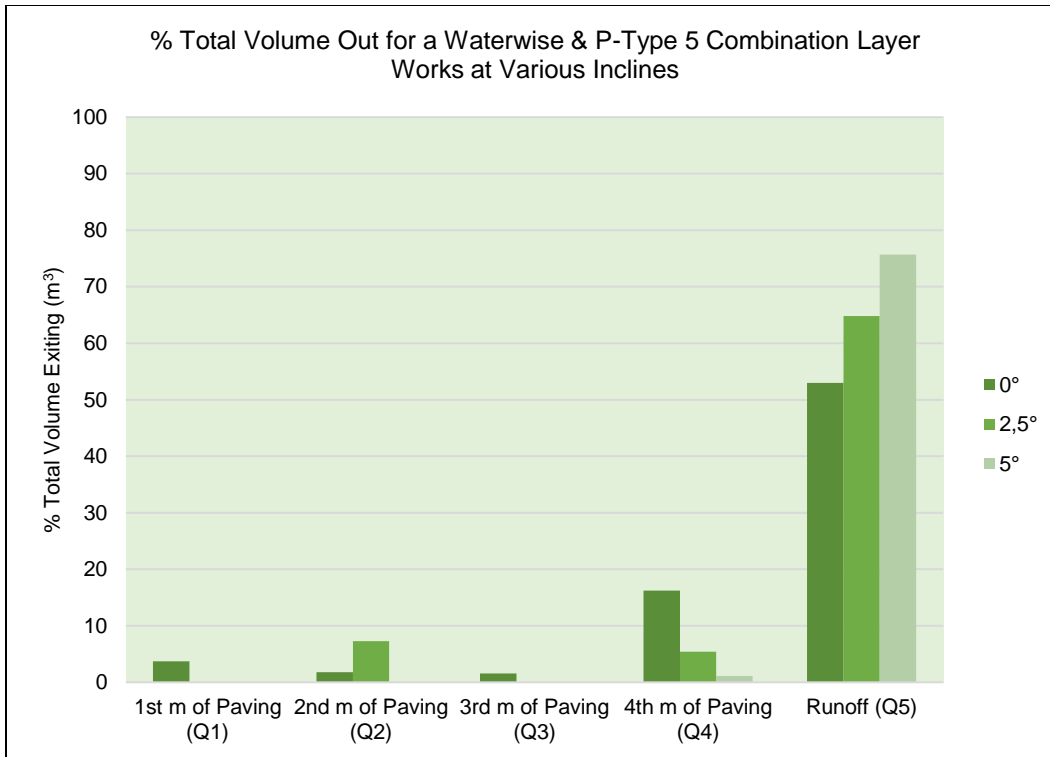


Fig. G-32: A column graph of volume percentages exiting the Full-scale Model with a Waterwise and P-Type 5 surface combination layer works, at various points and various inclines.

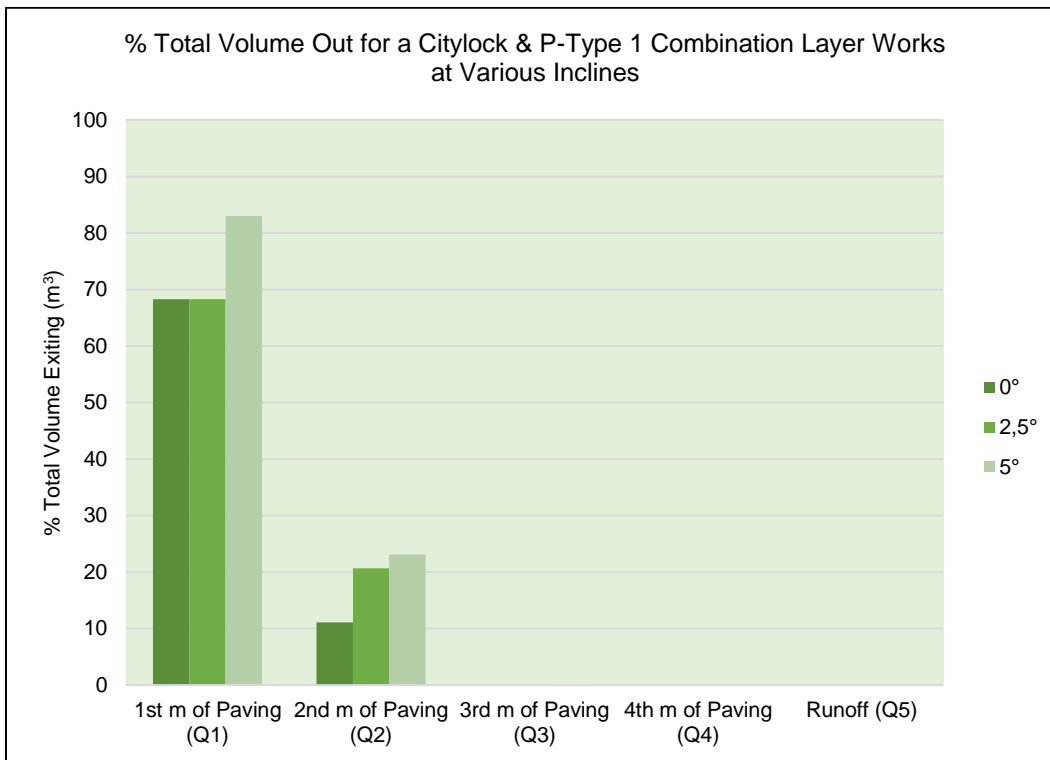


Fig. G-33: A column graph of volume percentages exiting the Full-scale Model with a Citylock and P-Type 1 surface combination layer works, at various points and various inclines.

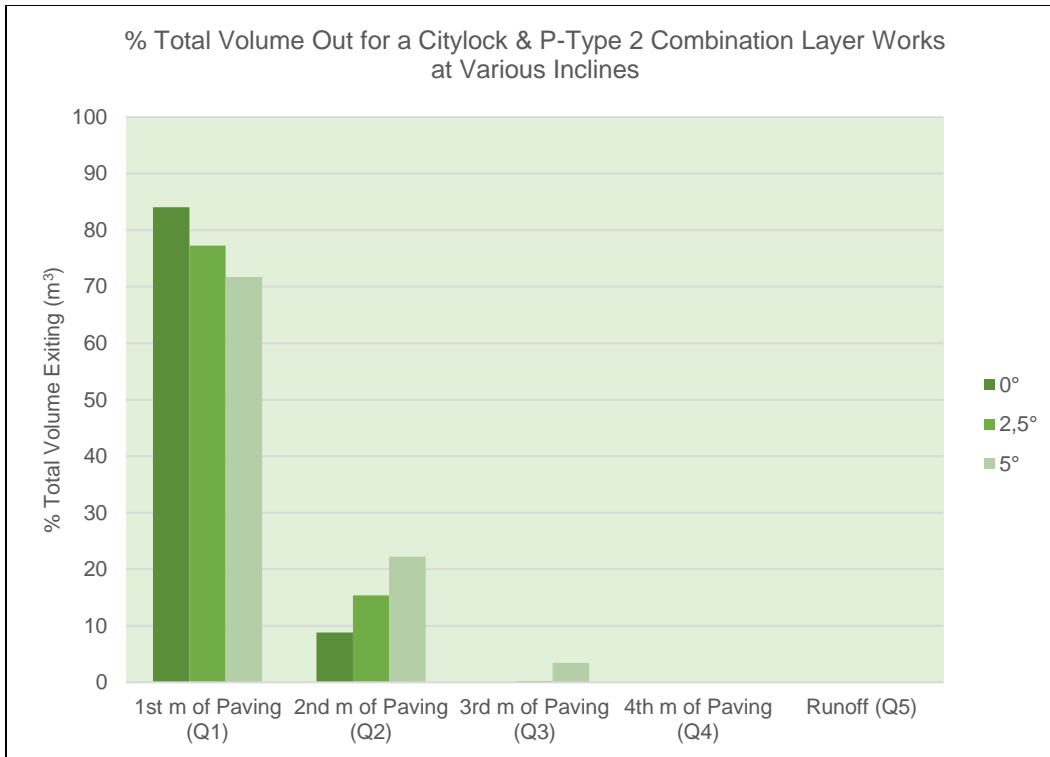


Fig. G-34: A column graph of volume percentages exiting the Full-scale Model with a Citylock and P-Type 2 surface combination layer works, at various points and various inclines.

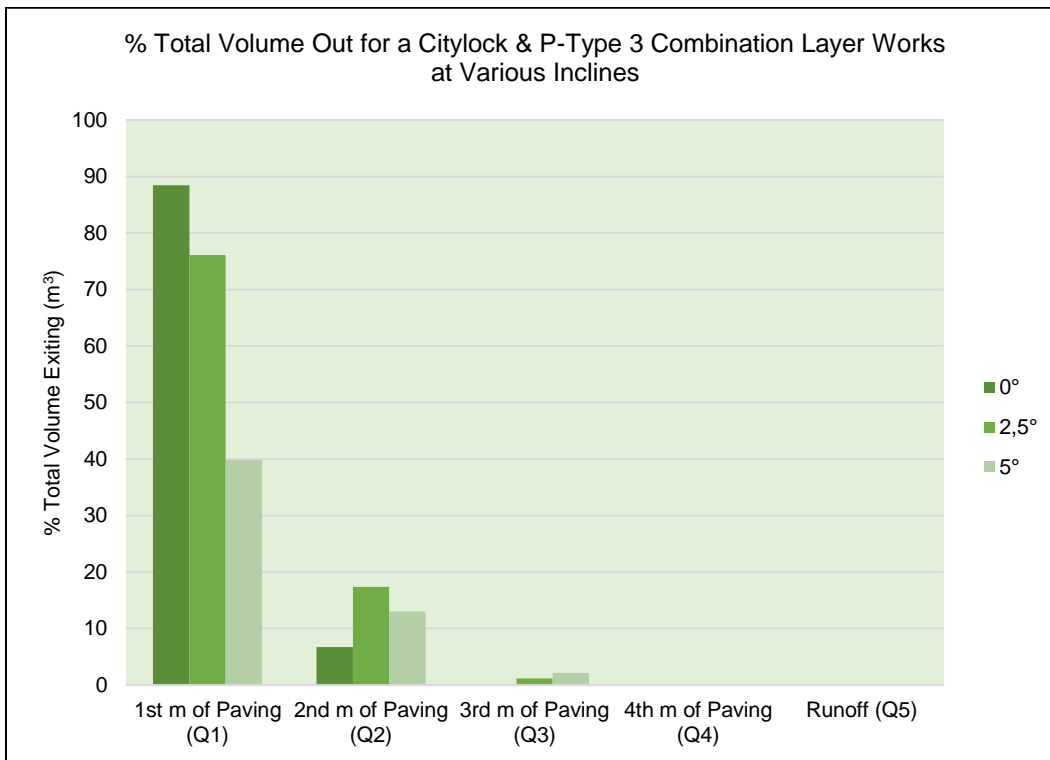


Fig. G-35: A column graph of volume percentages exiting the Full-scale Model with a Citylock and P-Type 3 surface combination layer works, at various points and various inclines.

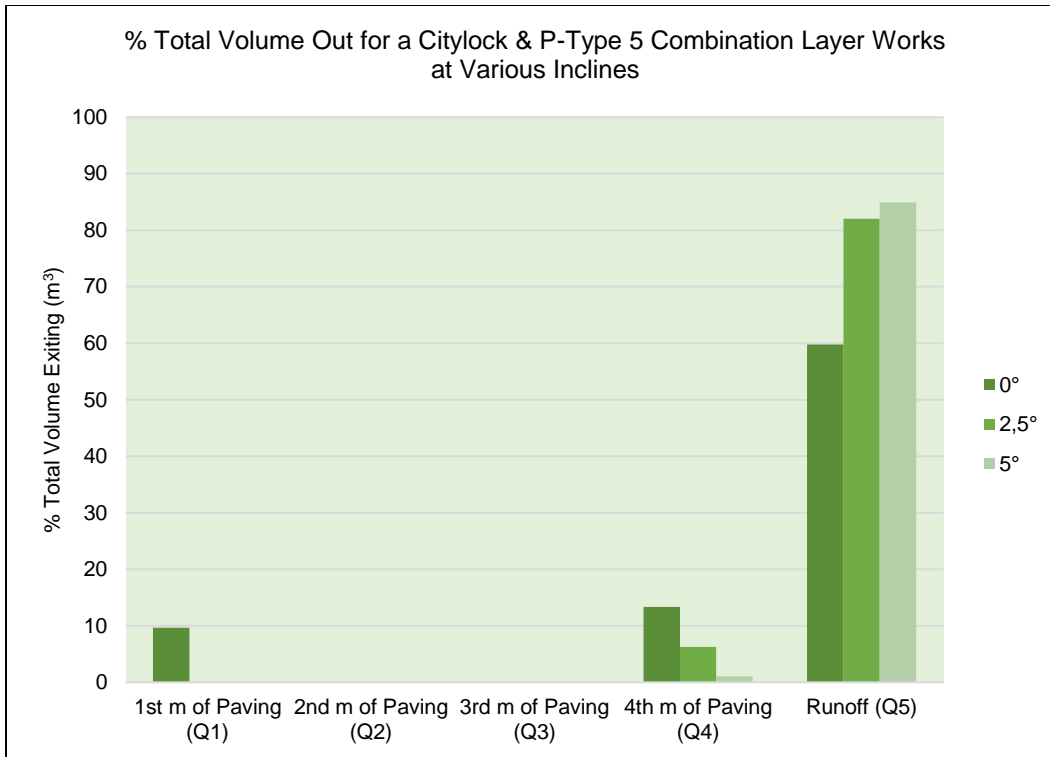


Fig. G-36: A column graph of volume percentages exiting the Full-scale Model with a Citylock and P-Type 5 surface combination layer works, at various points and various inclines.